

الجمهورية الجزائرية الديمقراطية الشعبية
Democratic and Popular Republic of Algeria
وزارة التعليم العالي والبحث العلمي
Ministry of Higher Education and Scientific Research

University Mohamed Khider– BISKRA
Faculty of Exact Sciences and Science of
Nature and Life.
Department of Material Sciences
Réf:



جامعة محمد خيضر بسكرة
كلية العلوم الدقيقة وعلوم
الطبيعة والحياة
قسم علوم المادة
المرجع:

Thesis
Presented to obtain the degree of
Doctorate

Specialty: Photonic physics

Entitled:

**ELABORATION ET ETUDES DES VERRES
ANTIMOINO-PHOSPHATE POUR APPLICATION
DANS L'AMPLIFICATION OPTIQUE**

Presented by:

Agti Fatima Zohra

Jury:

Toufik Tibermacine	Professor	U.M.K. Biskra	President
Med Toufik Soltani	Professor	U.M.K. Biskra	Supervisor
Derradji Bahloul	Professor	ENS-EREDD Batna	Examiner
Omar Bentouila	MCA	Univ- Ouargla	Examiner
Mourad Baazouzi	MCA	U.M.K. Biskra	Examiner

Thanks

Most of the work presented in this manuscript was carried out at the Laboratory of Photonic Physics and Multifunctional Nanomaterials of the University of Biskra and Centro de Química Estrutural, Av. Rovisco Pais 1, Instituto Superior Técnico, University of Lisbon-Portugal.

I would like to thank in particular the director of my thesis, Mr Mohamed Toufik Soltani, a Professor at Biskra University who offered me the subject provided me with wading in the field of glasses and optics-photonics and laser, for his instructions, help and his corrections.

I would like to thank in particular Mr Luis Filipe da Silva dos Santos Professor at the Department of Chemical Engineering and Centro de Química Estrutural, Av. Rovisco Pais 1, Instituto Superior Técnico, University of Lisbon, Lisboa, 1049-001, Portugal for welcoming me to his laboratory, for his help and advice.

I would particularly like to thank Mr Toufik Tibermacine Professor at the University of Biskra for having accepted the presidency of the jury. I would like to express my thanks and gratitude to the other members of the jury for the special attention paid to my work by agreeing to read and judge this thesis:

- Mr. Derradji Bahloul, Professor at ENS-EREDD Batna.
- Mr Omar Bentouila, MCA at the University kasedi Merbah Ouergla.
- Mr Mourad Baazouzi, MCA at the University Mohamed Khieder Biskra.

I would also like to thank all those who have contributed, from near or far, for their advice, suggestions and encouragement to carry out this work.

Dedication

To All my families

To all those who are dear to me.

Table of Contents

Contents	I
List of Figures	II
List of tables.....	III
General Introduction	01
Chapter I: Lens monograph and considerations theoretical	
I-Introduction	07
I.1 Definition of glass and glass transition	07
I.2 Oxide glasses	08
I.3 Antimony Oxide and Antimony Glass	08
I.4 the Phosphate oxide and phosphate Glass	09
I. 5Tungsten Oxide and the Glasses continent tungsten	12
I.6 Rare earth ions	13
I.7 Electronic energy levels of the praseodymium Pr^{+3} ions	13
I.8 Ytterbium Yb^{+3} ions	15
I.9 Co-doping	16
I.10 JUDD-OFELT Theory	17
I.11 Electrical dipole transitions	17
IV.3 Quality of adjustment	20
IV.4. Probability of emission	21
IV.5. Calculation of lifetimes and connection ratios	21
IV.6. Effective section of emission	22
The "McCumber" method	23
The "Füchtbauer-Ladenburg" method	23
IV.7. Quantum efficiency	24

Chapter II: Preparation of samples and experimental techniques of characterisation

Introduction	32
II.2 Experimental strategies	32
II.2.1 Choice of the matrix	32
II.2.2 Synthesis method	33
II.2.3 The stages of synthesis	33
II.2.4 starting materials	35
II.3 Characterization techniques	36
II.3.1 Thermal properties (Differential scanning calorimetric (DSC)	36
II.3.2 Mechanical properties	37
II.3.2.1 Density measurement	37
Elastic Properties (Ultrasonic Method)	37
II.3.8 Vickers hardness (Duramin struers)	38
II.3.3 Optical properties	39
II.3.3.1 UV-Visible spectroscopy	39
II.3.3.2 Determination of absorption coefficients	41
II.3.3.3 Optical gap and disorder	41
II.3.7 Refractive index (HORIBA Jobin Yvon)	42
II.3.4 Infrared spectroscopy	44
II.3.4.1 Fourier Transform Spectrometers (FT-IR)	46
II.3.4.2 UATR technique	46
II.3.5 Raman spectroscopy	47
II.3.6 Luminescence	48

**Chapter III Structural, thermal, mechanical, and optical study
antimony oxides (Sb₂O₃) glass.**

Introduction	52
III.1 Structural study	52
III.1.1 FTIR spectroscopy	52
III.1.2 Raman spectra	56
III.2 Thermal properties	57
III.2.1 Differential scanning calorimetric results	57
III.2.2 Characteristic temperatures	58
III.3 Mechanical Properties	60
III.3.1 The molar volume (V _m), oxygen molar volume (V _o) and density (d)	60
III.3.2 Elastic Properties (Ultrasonic Method)	64
III.4 Optical properties	68
III.4.1 UV-Visible transmission (Transmittance spectra)	68
III.4.2 Optical Gap and Urbach energy	69
Refractive index (HORIBA Jobin Yvon)	72

**Chapter IV: Spectroscopic study of the Pr⁺³ ion in glasses Sb₂O₃-WO₃-
NaPO₃ and Sb₂O₃-WO₃-NaPO₃-Yb₂O₃.**

Introduction	80
IV. Spectroscopic properties	80
IV. 1. Absorption spectroscopy	80
Case of 47.5 Sb ₂ O ₃ 47.5 NaPO ₃ 5 WO ₃ - x Pr ₂ O ₃ glasses	82
IV. 1.1. Determination of Judd-Ofelt parameters	85
IV. 1.1.1. Oscillator strengths and Judd-Ofelt intensity parameters	85
IV. 1.1.2. Calculation of the radiative parameters	89

Case of Sb_2O_3 47.5 NaPO_3 5 WO_3 0.1 Pr_2O_3 $x\text{Yb}_2\text{O}_3$ co-doping praseodymium / ytterbium glasses	92
IV. 1.2. Judd-Ofelt Analysis	93
IV. 2. Excitation spectrum and visible-NIR emission spectra and calculation of emission cross sections	98
Case of 47.5 Sb_2O_3 47.5 NaPO_3 5 WO_3 - x Pr_2O_3 glasses	98
IV. 2.1. Absorption, emission cross-section characteristics of 1.74 μm band	103
IV. 3. Fluorescence decay	105
Case of 47.5 Sb_2O_3 47.5 NaPO_3 5 WO_3 0.1 Pr_2O_3 $x\text{Yb}_2\text{O}_3$, ($x= 0.25, 0.5, 0.75, 1$) glasses	107
IV. 2. 1. Fluorescence decay	110
IV. 4. CIE chromaticity coordinates	112
Case of 47.5 Sb_2O_3 47.5 NaPO_3 5 WO_3 - x Pr_2O_3 glasses	112
Case of 47.5 Sb_2O_3 47.5 NaPO_3 5 WO_3 0.1 Pr_2O_3 $x\text{Yb}_2\text{O}_3$, ($x= 0.25, 0.5, 0.75, 1$) glasses	113
Conclusion	115

Conclusion General

LIST OF FIGURES

Figure I.1: sites of tetrahedral phosphates and Schematic representation of phosphate groups and their denomination in terms of Q^n ; the bridging oxygen atoms being linked to PO_4 groups and the non-bridging oxygen atoms have their negative charge neutralized by a cation. The red arrows indicate the creation of non-bridging links..	12
Figure I.2: Praseodymium ion energy diagram Pr^{+3} .	14
Figure I.3: Energy diagram of the Yb^{+3} ions (transition).	16
Figure I.4: Co-doping Ytterbium - Praseodymium.	17
Figure II.1: Balance.	34
Figure II.2: Benzene spout.	34
Figure II.3: heated plate	34
Figure II.4: Nabertherm oven.	34
Figure II.5: type polisher Minitch 233 Megapol Pressi	34
Figure II.6: Glass	34
Figure II.7: Differential scanning calorimetric (DSC).	36
Figure II.8: Balance equipped with a hydrostatic weighing device (type OHAUS Adventurer AX).	37
Figure (II.9): Pulse-Echo set up: Immersion transducer with Olympus Panametrics-NDT Model 5800 generator, coupled with an oscilloscope 20GHz (type HAMEG).	38
Figure II.10: Duramin struers of Vickers hardness.	39
Figure II.11: Perkin Elmer Lambda 35 UV-Vis spectrophotometer.	40
Figure II.12: a) determination of the energy gap by extrapolation from $(\alpha hv)^2$ as a function of (hv) and b) Variation of $\ln \alpha$ as a function of hv .	42
Figure II.13: Uvisel ellipsometer from HORIBA Jobin Yvon.	44
Figure II.14: Perkin Elmer Spectrum Two FTIR spectrophotometer.	45
Figure II.15: a) UATR techniques of the Perkin Elmer spectrophotometer.	47
Spectrum Two. b) Spectrum Two spectrometer (FT-IR).	47

Figure II.16: Horiba Yvon FluoroMax®-4 spectrofluorimeter.	49
Figure III.1: Infrared spectrum of glasses.....	54
Figure III.2: Raman spectra of 60Sb ₂ O ₃ - (40-x) NaPO ₃ -xWO ₃ glass system.....	56
Figure III.3: System DSC Curves of glasses.	57
Figure III.4: variation of glass temperature T _g and thermal stability DT.....	59
Figure III.5: Compositional dependence of density and molar volume of SNW _x glasses.	62
Figure III. 6. Longitudinal and transverse sound velocity of SNW _x glasses, lines are drawn as guides for the eyes.....	66
Figure III. 7. Elastic moduli and micro hardness of SNW glasses.	67
Figure III.8: Transmittance spectra in the UV, visible ranges.....	69
Figure III.9: (αhν) ² vs. (hν) plot of glass.....	70
Figure III. 10: (Ln α) vs. (hν) plot of glass.	70
Figure III. 11: The optical band gap (E _g) and Urbach energy (ΔE) of SNW glasses.....	71
Figure III. 12: Dispersion curve of SNW25 glass in the visible region.....	73
Figure III. 13: Refractive index of SNW _x glasses at selective wavelengths.....	73
Figure III. 14: Compositional dependence of the Abbe number in the SNW _x glasses, line is drawn as guide for the eyes.	74
Figure III.15: The results of refractive index of the glasses.	75
Figure IV.1: Absorption spectrum in visible, NIR of SNW glasses doped xPr ⁺³ (x = 0.05, 0.1, 0.25, 0.3 mol.%).....	84
Figure (IV.2): Energy diagram of praseodymium ion in the SNW glasses.	85
Figure IV.3: Absorption spectrum visible and NIR of 47.5 Sb ₂ O ₃ 47.5 NaPO ₃ 5 WO ₃ 0.1 Pr ₂ O ₃ xYb ₂ O ₃ , (x= 0.25, 0.5, 0.75, 1) glasses.....	92
Figure IV.4: Excitation spectrum of SNW glasses doped xPr ⁺³ (x = 0.05, 0.1, 0.25, 0.3 mol. %).	98
Figure IV.5: Emission spectrum in visible, NIR of SNW glasses doped xPr ⁺³ (x = 0.05, 0.1, 0.25, 0.3 mol. %).	99

Figure IV.6: The absorption (σ_{abs}) and emission cross-sections (σ_{em}) of $^1D_4 \leftrightarrow ^1G_4$ transitions of SNW0.25Pr⁺³ glass. 104

Figure IV.7: Fluorescence decay time of $^3P_0 \rightarrow ^3H_6$ transition of SNW Pr⁺³ glasses. 106

Figure IV.8: Emission spectrum in visible, NIR of SNWPr glasses co doped xYb⁺³ (x = 0.25, 0.5, 0.75, 1 mol. %). 108

Figure IV.9: Fluorescence decay time of $^3P_0 \rightarrow ^3H_6$ transition of Yb⁺³ co doped SNWPr glasses. 111

Figure IV.10: Chromaticity Diagram of Pr⁺³ doped SNW glasses. 112

Figure IV.11: Chromaticity Diagram of Yb⁺³ co doped SNW glasses. 114

LIST OF TABLES

Table I.1: Electronic configurations of the rare earth ions used.	13
Table II.1: Physicochemical characteristics of the starting materials.....	35
Table II.2: Nomenclature of processed glasses.	35
Table III.1: Summary of DSC data of glasses.	35
Table III.2: results of density, hardness, molar volume, oxygen molar volume and thickness ..	58
Table III.3: sound velocities, elastic modules.....	61
Table III.4 illustrates the values of the optical gap and disorder of the different samples.	65
Table IV.1: Transition, oscillator forces and RMS of 47.5 Sb ₂ O ₃ 47.5 NaPO ₃ 5 WO ₃ - x Pr ₆ O ₁₁ (x= 0.05, 0.1, 0.25, 0.3) glasses.....	70
Table IV.2: Judd-Ofelt parameters and spectroscopic quality factor of 47.5 Sb ₂ O ₃ 47.5 NaPO ₃ 5 WO ₃ - x Pr ₆ O ₁₁ (x= 0.05, 0.1, 0.25, 0.3) glasses compared with other glass systems reported in the literature.....	87
Table IV.3: The radiative parameters of 47.5 Sb ₂ O ₃ 47.5 NaPO ₃ 5 WO ₃ - x Pr ₆ O ₁₁ (x= 0.05, 0.1, 0.25, 0.3) glasses.	88
Table IV.4: the integrated emission efficiency section (Σ) values.....	90
Table IV.5: Transition, oscillator forces and RMS of 47.5 Sb ₂ O ₃ 47.5 NaPO ₃ 5 WO ₃ - 0.1 Pr ₆ O ₁₁ xYb ₂ O ₃ (x= 0.25, 0.5, 0.75, 1) glasses.	91
Table IV.6: Judd-Ofelt parameters and spectroscopic quality factor of 47.5 Sb ₂ O ₃ 47.5 NaPO ₃ 5 WO ₃ - 0.1 Pr ₆ O ₁₁ xYb ₂ O ₃ (x= 0.25, 0.5, 0.75, 1) glasses compared with other glass.	94
Table IV.7: The radiative parameters of 47.5 Sb ₂ O ₃ 47.5 NaPO ₃ 5 WO ₃ - 0.1 Pr ₆ O ₁₁ xYb ₂ O ₃ (x= 0.25, 0.5, 0.75, 1) glasses	94
Table IV.8: The integrated emission efficiency section (Σ) values of 47.5 Sb ₂ O ₃ 47.5 NaPO ₃ 5 WO ₃ - 0.1 Pr ₆ O ₁₁ xYb ₂ O ₃ (x= 0.25, 0.5, 0.75, 1) glasses.	96
Table IV.9: Emission band position (λ_{max} , nm), radiative transition probability (A_{rad} , s ⁻¹), full width at half maximum (FWHM, nm), effective bandwidth ($\Delta\lambda_{eff}$, nm), peak stimulated emission cross-section ($\sigma_{em}^{F-L} \times 10^{-21}$, cm ²), Optical gain ($\sigma_{em}^{F-L} \times \tau_{rad} 10^{-23}$ cm ³) and the gain bandwidth ($\sigma_{em}^{F-L} \times \Delta\lambda_{eff} \times 10^{-28}$ cm ³), of the Pr ⁺³ doped SNW glasses.	101
Table IV.10: The radiative lifetimes (τ_{rad} , ms), experimental lifetime (τ_{exp} , ms) and quantum efficiency η (%) of Pr ³⁺ doped antimony based glasses (SNW).	105
Table IV.11: Emission band position (λ_{max} , nm), radiative transition probability (A_{rad} , s ⁻¹), full width at half maximum (FWHM, nm), effective bandwidth ($\Delta\lambda_{eff}$, nm), peak stimulated	

emission cross-section ($\sigma_{em}^{F-L} \times 10^{-21}$, cm^2), Optical gain ($\sigma_{em}^{F-L} \times \tau_{rad} 10^{-23}$ cm^3) and the gain bandwidth ($\sigma_{em}^{F-L} \times \Delta\lambda_{eff} \times 10^{-28}$ cm^3), of the Pr^{+3}/Yb^{+3} co doped SNW glasses. 108

Table IV.12: The radiative lifetimes (τ_{rad} , ms), experimental lifetime (τ_{exp} , ms) and quantum efficiency η (%) of Yb^{+3} co doped antimony based glasses (SNWPr)..... 111

Table IV.13: Excitation calorimetric parameters of Pr^{+3} doped antimony based glasses (SNW).
..... 112

Table IV.14: Excitation calorimetric parameters of Yb^{+3} co doped antimony based glasses (SNWPr). 113

INTRODUCTION

Introduction

Among heavy metal oxide glasses (HMOG), antimony oxide glasses possess low phonon energy ($\sim 600 \text{ cm}^{-1}$) [1, 2], high refractive index [3, 4], high chemical durability and good corrosion resistance, which makes them suitable for laser sources and optical amplification in telecommunications. Antimony oxide glasses, free from traditional glass formers such as SiO_2 , P_2O_5 or B_2O_3 , have shown an extended near infrared transmission cutoff up to $8 \mu\text{m}$ [4, 5].

Antimony oxide has been incorporated into several combinations of glasses for various usages. In silicate glasses, it is used as a refining agent to remove gas bubbles [6]. The combination of antimony borate or antimony phosphate glasses has proven their high third-order non-linearity, making these glasses very promising for all-optical switching, 3D optical storage as well as holographic data storage [7-12]. Antimony phosphate glasses with ZnO , PbO , WO_3 or MoO_3 , have been studied for various purposes [13-16]. A Sb_2O_3 content greater than 30 (mol%) considerably improves the water durability of phosphate glasses [14]. It has also shown that the incorporation of WO_3 in Sb_2O_3 - SbPO_4 - WO_3 glasses improves thermal stability and increases the glass transition temperature (T_g) [17], and a photosensitive response under laser irradiation [18] by affecting the redox behavior of the different oxidation states of tungsten W^{+6} , W^{+5} or W^{+4} . So the why tungsten oxide has been widely used in smart windows, anti-glare mirrors for automobiles, non-emissive displays, optical recording devices, semiconductor gas sensors, and non-linear optics [19]. We also point out that in addition to its application in optical devices, phosphate glasses can also be used for biomedical applications [20].

The structure of vitreous Sb_2O_3 is an infinite double chain identical to the valentinite crystalline form of Sb_2O_3 , Sb^{3+} cation has bonded to 3 oxygens, and the free pair of electrons at the fourth corner forms a triangular pyramid SbO_3 unit [8, 21, 22]. Crystalline WO_3 forms a three-dimensional arrangement of WO_6 octahedral shared by their corners. However, in WO_3 containing glasses, the main structural units are tetragonal WO_4 (four-fold coordinated W^{+4}) or octahedral WO_6 units (six-fold coordinated W^{+6}) [23]. NaPO_3 glasses have structuring from an arrangement of tetrahedral PO_4 forming linear chains [23].

Glasses with the mixture of antimony, phosphate or WO_3 oxides have been reported in different cases in binary or ternary glasses NaPO_3 - WO_3 , Sb_2O_3 - SbPO_4 , Sb_2O_3 - SbPO_3 - WO_3 or Na_2O - WO_3 - SbPO_4 . [17, 18, 24-26]. The main investigations are focused on thermal properties and structural organization in these glasses. Furthermore, glasses containing a large amount of

WO₃ enhance the connectivity of the network by forming W-O-W linkages and exhibit large polarizable clusters of WO₆.

In the other hand, over the past few decades, great attention has been given to the development of rare-earth (RE) doped glasses used as functional material in visible and infrared lasers, color displays, amplifiers for telecommunications, switching and the wavelength converting devices, etc. [27, 28] The praseodymium (Pr⁺³) ion exhibits efficient fluorescence from the visible to infrared region. These glasses have found wide applications in many optical devices such as solid-state lasers, up conversion lasers and optical fibers [29, 30]. Praseodymium (Pr⁺³) doped materials can easily achieve simultaneous emissions in blue, green, orange, red and infrared regions. Due to the rich energy level diagram of Pr⁺³, the emission lines of the metastable states ³P_{0,1,2}, ¹D₂ and ¹G₄ provide an intense visible laser [31]. Pr⁺³ ions possess three-level laser action associated with the transitions from the ³P₀ state in certain activated host systems which are potentially useable for visible laser generation. Yb⁺³ ion is commonly used as a sensitizer because of the large absorption cross-section around 980 nm (²F_{7/2}/²F_{5/2}) which lead to efficient absorption of pump photons resulting in a large enhancement of up-conversion luminescence in RE doped materials. It has been observed that the fluorescence intensity of rare earth (RE) ions are increased several folds when a glass host has low phonon energy due to the reduction of the non-radiative relaxation mechanisms.

Glasses within Sb₂O₃-NaPO₃-WO₃ system are selected in this work as hosts for Pr³⁺ or Pr³⁺/Yb³⁺ couple [32, 33]. We report the advantage of SNW host glass and the impact of its structure on the radiative properties and the efficiency of energy transfer from Yb⁺³ to Pr⁺³ ions. Emphasis was placed on the calculation of the visible emission and NIR laser properties of the different radiative transitions of Yb⁺³ and Pr⁺³ ions. [34].

Since these new glasses are made for the first time, a systematic study of influence of the substitution of NaPO₃ by WO₃ on the physical properties of these glasses. It includes the structural, thermal, mechanical, physical, optical properties, including the dispersion of refractive index of the different glasses synthesized. In the structural investigation, the possible structural role of WO₃ is taken into account.

As a new glass host for rare earth element, Sb₂O₃-NaPO₃-WO₃ glasses doped with Pr₆O₁₁ or co-doped with Pr⁺³/Yb⁺³ couple are fabricated to investigate the luminescence properties supported by the study of judd ofelt formalism. The different studied glasses as follow (in molar concentrations):

Host glasses: 60Sb₂O₃-(40-x) NaPO₃-xWO₃, where x = 0 to 25 (mol.%),

Doped glasses:

- $60 \text{ Sb}_2\text{O}_3 (40-x) \text{ NaPO}_3 x \text{ WO}_3 0.1 \text{ Pr}_2\text{O}_3 (x=0,5,10,15,20,25)$,
- $47.5 \text{ Sb}_2\text{O}_3 47.5 \text{ NaPO}_3 5 \text{ WO}_3 - x \text{ Pr}_6\text{O}_{11} (x= 0.05, 0.1, 0.25, 0.3)$,
- $47.5 \text{ Sb}_2\text{O}_3 47.5 \text{ NaPO}_3 5 \text{ WO}_3 0.1 \text{ Pr}_6\text{O}_{11} x \text{ Yb}_2\text{O}_3, (x= 0.25, 0.5, 0.75, 1)$.

The thesis is structured in four chapters, starting with a general introduction and ending with a general conclusion.

The first chapter is reserved for the study of bibliographic searches of antimony-based glasses and the systems chosen. Afterwards will be dedicated to the spectroscopic study of rare earth ions and the optical transitions studied using the theory of Judd-Ofelt, which also contains the different methods for calculating the basic spectroscopic quantities.

The second chapter presents the chosen systems and details of the experimental procedures used in this work.

The third chapter presents the experimental results and analysis of the different characterizations Raman, FTIR, DSC, density, some physical properties, Vickers hardness, UV-visible and infrared transmission, the optical gap, disorder, elastic, Refractive index.

The fourth chapter is dedicated to the study of spectroscopic characterizations and results of the analysis made by Judd-Ofelt theory, for SNW doped Pr^{+3} and SNW co doped $\text{Pr}^{+3} / \text{Yb}^{+3}$ glasses a detailed study is carried out to calculate the various parameters. radiative properties such as spontaneous emission probabilities (A_{rad}), radiative lifetimes (τ_{rad}), branch rate (β), the values of the integrated effective section (Σ), the effective sections stimulated emission (σ_{se}), Optical gain ($\sigma_{\text{em}}^{\text{F-L}} \times \tau_{\text{rad}}$) and the gain bandwidth ($\sigma_{\text{em}}^{\text{F-L}} \times \Delta\lambda_{\text{eff}}$), in the other hand, the experimental study of photoluminescence and also performed as well as the calculation of the chromaticity coordinates CIE and CCT for these glasses.

Finally, this study is summarized by a general conclusion of all the different results obtained.

References

- [1] T. Som, B. Karmakar, *Opt. Mater.*, 31 (2009) 609-618. <https://doi:10.1016/j.optmat.2008.06.018>.
- [2] M. T. Soltani, A. Boutarfaia, R. Makhloufi, and M. Poulain, *J. Phys. Chem. Solids*. 64 (2003) 2307–2312. [https://doi:10.1016/S0022-3697\(03\)00220-8](https://doi:10.1016/S0022-3697(03)00220-8).
- [3] M. Hamzaoui, M. T. Soltani, M. Baazouzi, B. Tioua, Z. G. Ivanova, R. Lebullenger, M. Poulain, and J. Zavadil, *Phys. Status Solidi B* (2012) 2213-2221. <https://doi.org/10.1002/pssb.201248271>.
- [4] M. Baazouzi, M.T. Soltani, M. Hamzaoui, M., J. Troles, *Opt. Mater.*, 36 (2013) 500-504. <https://doi.org/10.1016/j.optmat.2013.10.017>.
- [5] B. Dubois, H. Aomi, J.J. Videau, J. Pottier and P. Hagenmuller, *Mat. Res. Bull.* 19(1984)1317-1323. [https://doi.org/10.1016/0025-5408\(84\)90194-6](https://doi.org/10.1016/0025-5408(84)90194-6)
- [6] L.-Grund and B. Jonson, *Glass Tech.* 50 (2009) 62-64.
- [7] E. L. Falcão Filho, C.A.C. Bosco, G. S. Maciel, C. B. Araujo, M. Nalin, Y. Messaddeq, *Appl. Phys. Lett.*, 83 (2003) 1292-1294. <https://doi.org/10.1063/1.1828216>.
- [8] K. Terashima, T. Hashimoto, T. Uchino, S.-H. Kim, T. Yoko, *J. Ceram. Soc. Jpn.*, 104 (2011) 1008–1014. <https://doi.org/10.2109/jcersj.104.1008>.
- [9] D. Psaltis, G. W. Burr, *Computer* 31 (1998) 52-60. <https://doi.org/10.1109/2.652917>.
- [10] M. Nalin, G. Poirier, Y. Messaddeq, S. J. L. Ribeiro, E. J. Carvalho, L. Cescato, *J. Non-Cryst. Solids*, 352 (2006) 3535-3539. <https://doi.org/10.1016/j.jnoncrysol.2006.03.087>.
- [11] G.I. Sincerbox, *Opt. Mat.*, 4 (1995) 370-375. [https://doi.org/10.1016/0925-3467\(94\)00089-1](https://doi.org/10.1016/0925-3467(94)00089-1).
- [12] D. Strand, *J. Optoelectron. Adv. Mater.*, 7 (2005) 1679-1690. https://joam.inoe.ro/arhiva/pdf7_4/Strand.
- [13] G. Sahaya Baskaran, G. Little Flower, D. Krishna Raob, N. Veeraiyah, *J. Alloys Compd.*, 431 (2007) 303–312. <https://doi.org/10.1016/j.jallcom.2006.05.077>.
- [14] B. Zhang, Qi Chen, Li Song, H. Li, F. Hou, J. Zhang, *J. Non-Cryst. Solids*, 354 (2008) 1948–1954. <https://doi.org/10.1016/j.jnoncrysol.2007.11.007>.
- [15] J. J. Rothermel, K. H. Sun, A. Silverman, *J. Am. Ceram. Soc.*, Westerville. 32 (1949)153-162.
- [16] M. Nalin, M. Poulain, M. Poulain, S. J. L. Ribeiro and Y. Messaddeq, *J. Non-Cryst. Solids*. 284 (2001) 110-116. [http://dx.doi.org/10.1016/S0022-3093\(01\)00388-X](http://dx.doi.org/10.1016/S0022-3093(01)00388-X)

- [17] D. F. Franco, H. Fares, A. E. de Souza, S. H. Santagneli, M. Nalin, *Ecletica Quim. J.* 42(2017) 51. <https://doi.org/10.26850/1678-4618eqj.v42.1.2017.p51-59>
- [18] G. Poirier, F. S. Ottoboni, C. Cassanjes, A. Remonte, Y. Messaddeq, and S.L Ribeiro, *J. Phys. Chem. B.* 112 (2008) 4481-4487. <https://doi.org/10.1021/jp711709r>.
- [19] M. Ataalla, A. S. Afify, M. Hassan, M. Abdallah, M. Milanova, H. Y. Aboul-Enein, A. Mohamed, *J. Non-Cryst. Solids*, 491 (2018) 43–54. <https://doi.org/10.1016/j.jnoncrysol.2018.03.050>
- [20] J.C. Knowles, *J. Mater. Chem.*, 13 (2003) 2395–2401. <https://doi.org/10.1039/B307119G>.
- [21] M. Çelikbilek Ersundu, A.E. Ersundu, M.T. Soltani and M. Baazouzi, *Ceram. Int.*, 43 (2017) 491-497. <http://dx.doi.org/10.1016/j.ceramint.2016.09.184>
- [22] C. A. Cody, L. Dicarlo, and R. K. Darlington, *Inorg. Chem.*, 18 (1979). <https://doi.org/10.1021/ic50196a036>.
- [23] D. Manzani, C. B. de Araújo, G. Boudebs, Y. Messaddeq, and S. J. L. Ribeiro, *J. Phys. Chem. B*, 117 (2013) 408–414. <https://doi.org/10.1021/jp3097296>.
- [24] M. Nalin, Y. Messaddeq, S. J. L. Ribeiro, M. Poulain, V. Briois, G. Brunklus, C. Rosenhahn, B. D. Mosel and H. Eckert, *J. Mater. Chem.*, 14(2004) 3398-3405. <https://doi.org/10.1039/B406075J>.
- [25] M. Nalin , G. Poirier , S.J.L. Ribeiro , Y. Messaddeq , L. Cescato, *J. Non-Cryst. Solids*, 353(2007) 1592-1597. <https://doi.org/10.1016/j.jnoncrysol.2007.01.031>.
- [26] C. C. de Araujo, W. Strojek, L. Zhang, H. Eckert, G. Poirier, S. J. L. Ribeiro and Y. Messaddeq, *J. Mater. Chem.*, 32 (2006). <https://doi.org/10.1039/B605971F>.
- [27] F. Ondracek, J. Agerska, L. Salavcova, M. Míka, J. Spirkova, J. Ctyroky. *IEEE J Quantum Electron* 44 (2008) 536.
- [28] A. Balakrishna, S. Babu, Vinod Kumar, O. M. Ntwaeaborwa, Y. C. Ratnakaram, *Spectrochimica Acta Part A: Molecular and Biomolecular Spectroscopy* 170 (2017) 167-173.
- [29] Li JP, TT. Zhang, GQ.Zhu, HR.Zheng, *J Rare earths.* 35-7 (2017) 645.
- [30] C. Pan, Z. Yaxun, S. Xiue, Z. Minghan, Z. Zizhong, *Journal of Luminescence* 197 (2018) 31-37.
- [31] DD. Ramteke, HC. Swart, RS. Gedam. *Physica B.* 480 (2016) 111.
- [32] B. Afef, H. H. Hegazy, H. Algarni, Y. Yang, K. Damak, E. Yousef, R. Maâlej, *Journal of rare earths*, 35- 4 (2017) 361.

[33] Sk .Mahamuda, K.Swapna, A.Srinivasa Rao, T.Sasikala, L. Rama Moorthy Physica B. 428 (2013) 36.

[34] D. Rajesh, M. Reza Dousti, J. Amjad Raja, J Non-Cryst Solids. 450 (2016) 149.

Chapter I: Glass, generalities and theoretical considerations

Introduction:

A glass has an unlimited number of chemical compositions. They include oxides, halides, chalcogenides, metallic or organics.

We are interested in the mixed former antimony and phosphate oxides with the addition of tungsten oxide WO_3 as a network modifier in the system $60\text{Sb}_2\text{O}_3-(40-x)\text{NaPO}_3-x\text{WO}_3$. Antimony oxide as a family of heavy metal oxide glasses has better properties compared to traditional glasses silicate, borate or phosphate [1].

In this study, undoped glasses and doped with ion Pr^{3+} are investigated to obtain new luminescent materials emitting in the visible and the near infrared range. The characteristics expected of this type of glass have made it a material of choice for many recent applications such as optical amplification; fibers and lasers [2]. The investigation of spectroscopic properties of Pr^{3+} ions are related to energy phonon; the transitions between the different energy levels of the dopant [3]. Judd-Ofelt theory is used to study the spectroscopic properties of rare-earth elements by the evaluation of the phenomenological intensity parameters Ω_t ($t = 2, 4, 6$) and other related spectroscopic properties [4].

This chapter is devoted to a general presentation of antimony glasses and glasses containing phosphates and tungsten oxides. The general concepts on the spectroscopy of rare earth ions (TR) in particular Pr^{3+} are presented. The formalism of Judd-Ofelt theory is set out in detail.

I.1 Definition of glass and glass transition:

According to the definition proposed by Zarzycki, the glass is a non-crystalline solid without periodic arrangement at long distances. All glasses exhibit the glass transition phenomenon. It can be explained by the change in enthalpy as a function of the temperature which occurs during the passage from the liquid to the glassy solid. This change in enthalpy occurs at lower temperatures. The transition temperature (T_g) varies depending on the cooling rate during the formation of glassy state. So if the cooling is faster, the T_g is a little higher than the slower cooling speed [5, 6].

I.2 Oxide glasses:

For a long time, glass has been formed from oxides of silica, germanium, boron or phosphates). These glasses are called: traditional glasses. Apart from these oxides, several families of heavy oxide glasses have emerged. They are known by the abbreviation HMOG (Heavy Metal Oxide Glasses). Glasses based on antimony oxide were one of them.

The synthesis of heavy metal oxide glasses is made from the air melting of the mixture of oxides in crucibles: Pt, Au, SiO_2 or Al_2O_3 [7]. The synthesis is carried out at temperatures below 1000°C . Lower than in silica glasses.

Due to the high atomic mass and high polarizability, HMOGs are of great interest for specific applications such as optoelectronics [8, 9]. Their high infrared transmittance and high refractive index allows HMOG to be potential candidates in several applications in telecommunications devices, sensors and nonlinear optics [10]. They are very efficient in optical amplification in infrared and lasers when doped with rare earths [11].

In addition to their optical transmission in the visible and excellent transmission in the infrared range, heavy metals oxide glasses has low phonon energy, high refractive indices [12-15], low glass transition temperature, high thermal expansion, high density and high solubility of rare earth ions [16].

I.3 Antimony oxide and antimony Glass:

The crystallographic study shows that antimony oxide appears either in cubic or orthorhombic form, which are called senarmontite or valentinite respectively consisting SbO_3 chains and Sb_4O_6 units [17]. While Sb_2O_4 can be monoclinic (clinocervantite) or often orthorhombic (cervantite); antimony tetra oxide [Sb_2O_4] is a mixture of enter-valence components containing the ions: Sb^{+3} , Sb^{+5} in its crystal lattice and it is stable up to 1000°C [18, 19].

Antimony trioxide Sb_2O_3 comes in the form of a very fine, odorless white powder, which when heated takes on a yellow color but turns white again on cooling. Antimony oxide is toxic, especially in the form of vapors [20,21].

The main physical and chemical characteristics are:

Chapter I: Glass, generalities and theoretical considerations

The melting point is located after the transition from senarmontite to valentinite phase that can be between 640 ° C and 655 ° C depending on the rate of heating, the Molar mass: 291.52g / mol, Boiling point: 1425C ° (it sublimes partially before reaching this temperature), Density: 5.2 (cubic); 5.67 (orthorhombic), Vapor pressure: 133 Pa at 574 °C, Vapor density (air = 1): 19.8 at 1560 °C, the atomic weight of antimony is 122. [22-23]

Antimony oxide is insoluble in organic solvents and very slightly soluble in water; it dissolves easily in hydrochloric acid, tartaric acid and caustic alkalis, in acid solutions it dissolves, giving complex poly-antimoniate acids, in basic solutions, it dissolves with the formation of antimonates. It is however easily reducible in antimony and in antimony tri-hydride SbH_3 , too toxic gas [24, 25].

Antimony oxide glasses deteriorate on contact with an aqueous solution. The alteration depends on the composition of the glasses and the alternating solution. This mechanism is slow at room temperature [26].

Antimony oxide glasses have high density, phonon energy close to 600 cm^{-1} , high refractive index, low softening temperature and high infrared transmission. moderate attenuation in the visible and near infrared as well as a refractive index, which can be easily modified, high linear thermal expansion, [27] low melting and glass transition temperature. The addition such as of B_2O_3 [28], SiO_2 , P_2O_5 [29,30], or transitional oxides [31,32] give stabilization of the Sb_2O_3 network [33,34]. The applications of antimony glasses are in optical recording media [35] and NLO appliances due to their photosensitivity, non-centrosymmetric structure and fast response times as a consequence of the high polarisable Sb^{3+} ions with strongly localized stereochemically active lone pair of electrons ($5s^2$) [36,37] and in optics and Photonics applications [38].

I.4 Phosphate oxide and phosphate Glass:

Phosphate glasses constitute materials of choice for the development of new analysis techniques. Thus, the structural characterizations were able to develop and multiply under good conditions. Techniques such as infrared spectroscopy and Raman and liquid chromatography have been widely used to study local order. Before approaching the phosphate glasses, it is essential to ask the question of the nature of the glass itself. From the user's perspective, it is possible to introduce the

Chapter I: Glass, generalities and theoretical considerations

thermodynamic and structural definitions of the vitreous state. The important notions of vitrification and vitreous state raise a number of problems such as the nature of the glass transition, the structure of glass and its thermodynamic properties. It is then that the place of glass can be determined in the context of the other states of condensed matter [39,40].

The description of phosphate glasses begins by dealing with their structure and their vitrification. Successively described:

- ✓ the consequences of the pentavalent of phosphorus on the specific nature of the phosphate glass network,
- ✓ the structural entities forming the phosphate network and their nomenclature,
- ✓ the evolution of this network concerning the nature and concentration of the cations and anions incorporated,
- ✓ The description of structural models involving the formation of mixed networks, both anionic and cationic.

Finally, it is important to mention the problem of chemical durability, which is an imperative condition for the development of this type of material. To obtain stable glasses, in particular with respect to water, their composition can be optimized by playing on the modification of the phosphate network by the introduction of acid oxides or even amphoteric or on the partial replacement of oxygen by other ligands. [41,42]

Phosphate compounds have very variable structures. They can form three-dimensional or linear networks. In all cases, these networks are based on the arrangement of PO_4 tetrahedra. In fact, phosphorus when combined with oxygen forms 5 covalent bonds with 4 oxygen (3 single bonds and a double bond). Oxygen having a single bond with phosphorus can then be terminals (P-O-) or linked to another atom of phosphorus (P-O-P). It is the number of terminal and bridging oxygen that will determine the nature of the phosphorus site. There is a nomenclature to describe the PO_4 tetrahedron [43]. This tetrahedron is called Q^n , n being the number of bridging oxygen atoms. There are therefore 4 possible types of Q^n tetrahedra:

Phosphate compounds have very variable structures. They can form three-dimensional or linear networks. In all cases, these networks are based on the arrangement of PO_4

Chapter I: Glass, generalities and theoretical considerations

tetrahedra. In fact, phosphorus when combined with oxygen, it forms 5 covalent bonds with 4 oxygen (3 single bonds and a double bond). The oxygen having a simple bond with phosphorus can then be terminal (PO-) or linked to another phosphorus atom (P-O-P), this is the number of terminal oxygen and bridging which will determine the nature of the phosphorus site.

There is a nomenclature to describe the PO₄ tetrahedron [44]. This tetrahedron is called Qⁿ: n is the number of bridging oxygen atoms. There are therefore 4 possible types of Qⁿ tetrahedra [45]. Phosphates can be classified in the following categories, see fig I.1:

a) Mono phosphates (ortho phosphates): is phosphorus compounds made up of PO₄ grouping 3- isolated.

b) Poly phosphates: are linear sequences formed from PO₄ tetrahedra, formula [P_nO_{3n}+ 1] (n + 2) -. Depending on the value of n we can cite:

- Pyrophosphate or di phosphate [P₂O₇]⁻⁴ for n = 2.
- Poly phosphate or triphosphate [P₃O₁₀]⁻⁵ for n = 3.
- Tetra poly phosphate or tetra phosphate [P₄O₁₃]⁶⁻ for n = 4. If n tends to infinity we define meta phosphate (long chain poly phosphate) described by the formula [P_nO₃]ⁿ [46].

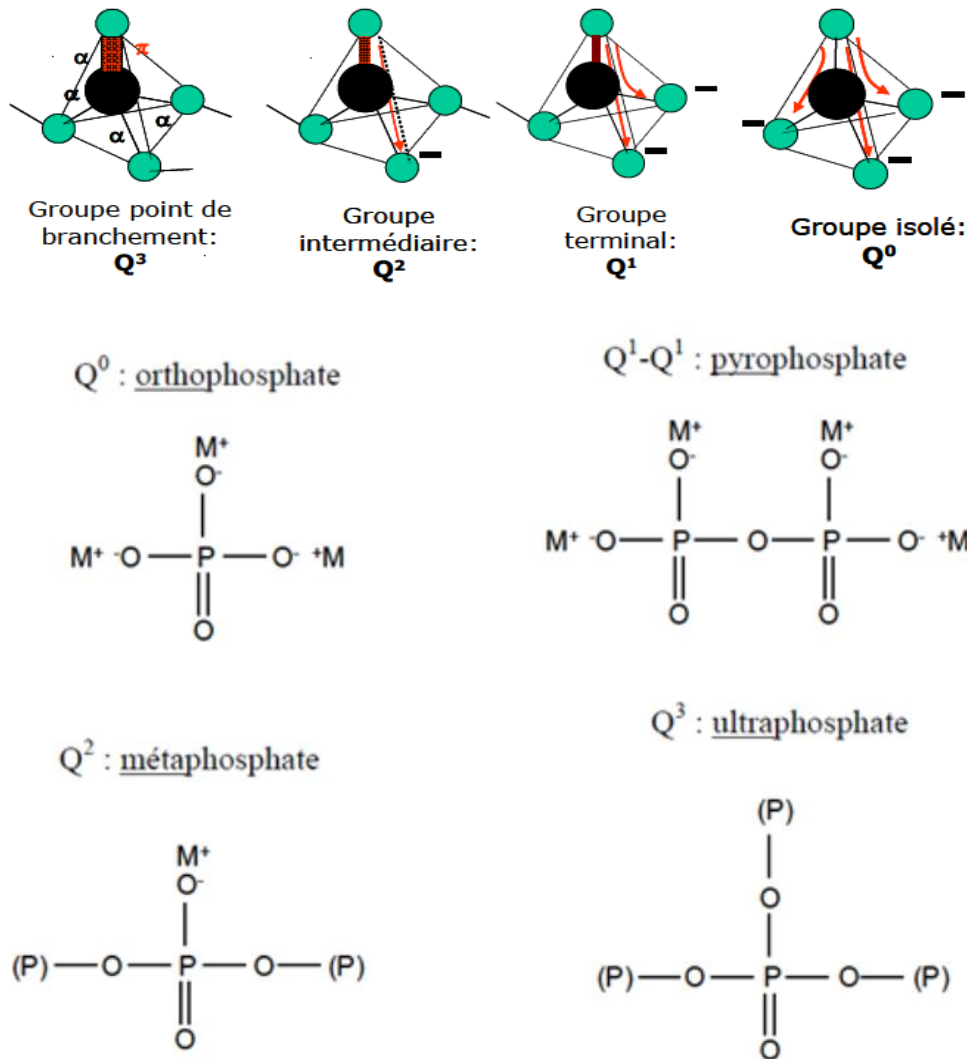


Figure I.1: sites of tetrahedral phosphates and Schematic representation of phosphate groups and their denomination in terms of Qⁿ; the bridging oxygen atoms being linked to PO₄ groups and the non-bridging oxygen atoms have their negative charge neutralized by a cation. The red arrows indicate the creation of non-bridging links. [47, 48].

I. 5 Glass and Oxide of tungsten:

Tungsten oxide belongs to the intermediate oxides. It cannot form a glass but on the other hand he can play the role of second glass former in binary or ternary glasses.

WO₃ undergoes many phase changes depending on the temperature. WO₃ tungsten trioxides are characterized by a more or less significant distortion of the WO₆ octahedron so by a more or less high symmetry, the glasses that incorporation

Chapter I: Glass, generalities and theoretical considerations

tungsten oxide have an extremely high thermal stability specially in the binary of $\text{WO}_3\text{-NaPO}_3$ and the heating of glasses do not have the phenomenon of crystallization generally due to intermediate nature of WO_3 in the network of some composition of glasses in the form of WO_6 . It has high resistance to heat, corrosion and strong bonds.

The Increasing of tungsten in the antimony glasses and phosphate glasses lead to an increase in the absorption and the transition to IR [49-51] thus increasing the connectivity of the vitreous network. Also the polarizable WO_6 unites present non-linear optical and photosensitive properties; tungsten trioxide (WO_3) is used as a base material for sensors chemicals. It is well studied because of its electrical, catalytic and photochromic properties. Among the photocatalysts declared sensitive to visible light corrosion resistivity [52].

I.6 Rare earth ions:

Rare earth ions are also called lanthanide ions. The properties of these ions come mainly from the shielding of the 4f orbitals which are, for the most part, completely filled, by the 5S^2 and 5P^6 orbitals. Thus, the valence electrons are little disturbed by the external environment and their electronic transitions produce fine and intense lines, [53] The electronic configurations of the rare earth ions used are shown in Table I-1 [54]:

Table I-1: Electronic configurations of the rare earth ions used.

Trivalent rare earth ion	Electronic configurations
Praséodyme, Pr^{+3}	$1\text{S}^2 2\text{S}^2 2\text{P}^6 3\text{S}^2 3\text{P}^6 3\text{d}^{10} 4\text{S}^2 4\text{P}^6 4\text{d}^{10} 5\text{S}^2 5\text{P}^6 4\text{F}^2$
Ytterbium, Yb^{+3}	$1\text{S}^2 2\text{S}^2 2\text{P}^6 3\text{S}^2 3\text{P}^6 3\text{d}^{10} 4\text{S}^2 4\text{P}^6 4\text{d}^{10} 5\text{S}^2 5\text{P}^6 4\text{F}^{13}$

I.7 Electronic energy levels of the praseodymium Pr^{+3} ions:

The energy diagram of praseodymium ion (Figure I.2) [55] is made up of 13 multiplets corresponding to three triplets ($^3\text{H}_4, 5, 6, ^3\text{F}_2, 3, 4, ^3\text{P}_{0,1,2}$) and 4 singlets ($^1\text{G}_4, ^1\text{D}_2, ^1\text{I}_6, ^1\text{S}_0$). The praseodymium has two active electrons, Hund's rule determines the fundamental spectral term; it is that of multiplicity $(2\text{S} + 1)$ maximum and having the

Chapter I: Glass, generalities and theoretical considerations

maximum orbital quantum number L . in the case of praseodymium is 3H_4 . [56] The energy distribution of the LS terms of the two ions is identical. The essential difference appears due to the spin-orbit interaction, the coupling constant b is positive for the praseodymium, $b(\text{Pr}^{3+}) = 700 \text{ cm}^{-1}$. [57] As part of the spin-orbit coupling; these energy levels of the same spectral term are classified in increasing order of J for the praseodymium ion when the energy increases (the fine structure constant b being positive when the layer $4f$ is less than half full) where the 13 bytes or 6 bytes appear to correspond to optical transitions located in the infrared range and 5 in the visible range [58].

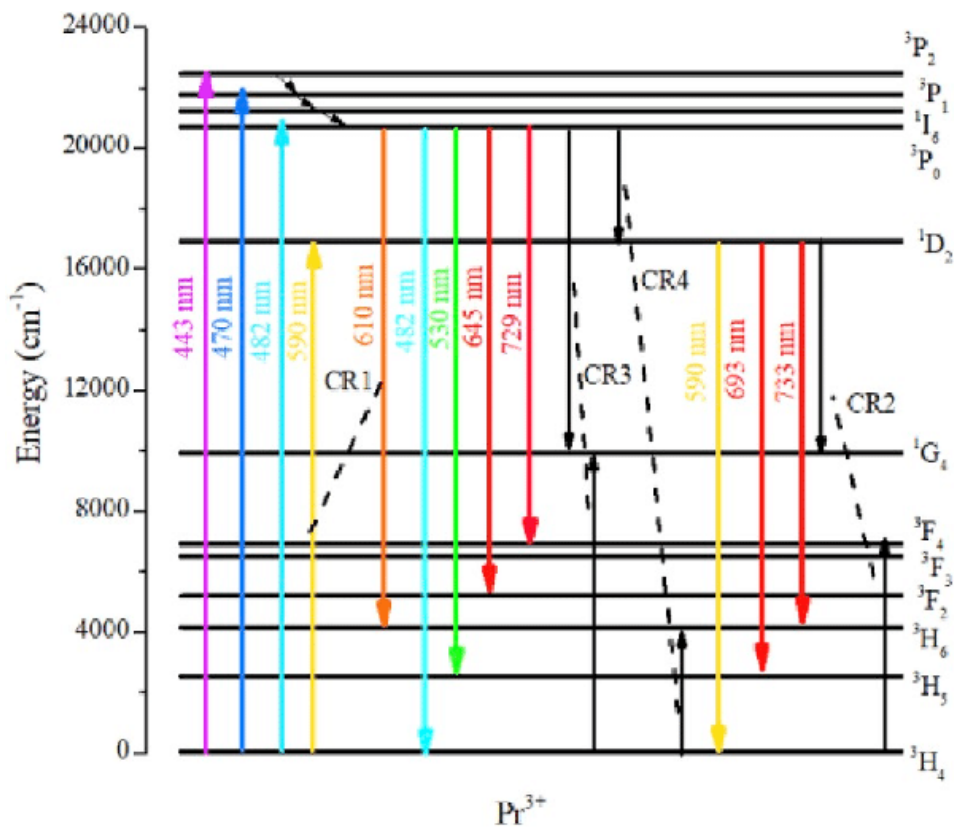


Figure I-2: Praseodymium ion energy diagram Pr^{3+} .

The 1S_0 level located at 47000 cm^{-1} from the fundamental level corresponds to an optical transition at a wavelength of 213 nm (ultra-violet). The Intraconfigurational $4f$ - $4f$ transitions of the Pr^{3+} ion have aroused great interest because of the 16 laser transitions observed in the visible and the infrared domain from the 3P_j , 1D_2 , 1G_4 , 3F_3 levels [59]. The $^3P_0 \rightarrow ^3H_4$ transition corresponds to the shortest wavelength in the blue, while the $^3F_3 \rightarrow ^3F_2$ transition corresponds to the longest wavelength in the far

infrared at 7.24 μm [60]. In emission in a broad spectral range, many studies have been carried out for the Pr^{3+} ion due to the blue (${}^3\text{P}_0 \text{S}^3\text{H}_4$), green (${}^3\text{P}_0 \text{S}^3\text{H}_5$), yellow (${}^3\text{P}_0 \text{S}^3\text{H}_6$) and red (${}^3\text{P}_0\text{S}^3\text{F}_2$) emissions in fluorinated matrices [61, 62].

In summary, a low Pr^{3+} content in glasses presents a large and intense emission in the near infrared. In addition, trivalent praseodymium is a well-known active ion exhibiting the phenomenon of quantum cutting (QC) and a good up-conversion emission alone or co-doped with other rare earth ions [63].

I.8 Ytterbium Yb^{+3} ions:

The Ytterbium ion offers several advantages in the following literature. The disadvantage is that the Yb^{+3} lasers are at almost 3 levels, which increases the laser threshold by reabsorbing the emission [64]. In the phosphate glass host, Yb^{+3} ions act as sensitizers that absorb strongly at 980 nm, a length wavelength that corresponds to the emission wavelength of diode lasers at present available. The Yb^{+3} ions have very attractive characteristics for laser emission in the ~ 1 range μm . Optical spectra correspond to the transitions between the Stark sublevels of the two bytes [65,66]: ${}^2\text{F}_{7/2} \leftrightarrow {}^2\text{F}_{5/2}$ (figure I.3). The Emission Levels of Pr^{+3} , Yb^{+3} are ${}^3\text{P}_0$ (21800 cm^{-1}), ${}^2\text{F}_{5/2}$ (10000 cm^{-1}) and the Final Levels are ${}^3\text{H}_J$ ($J=4.5.6$) ${}^3\text{F}_J$ ($J=2.3.4$), ${}^2\text{F}_{7/2}$ respectively and Emission Wavelength (nm) are 490, 540, 600, 650, 705, 730 of Pr^{+3} and 980 of Yb^{+3} [67].

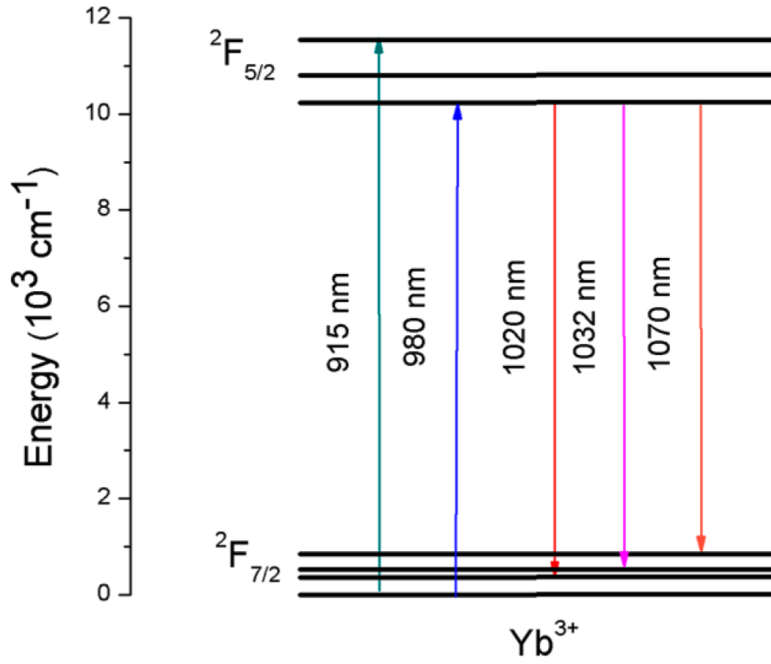


Figure (I.3): Energy diagram of the Yb³⁺ ions (transition) [68].

I.9 Co-doping:

The term co-doping is associated with doping ions added to the main doping ion, the doping Ytterbium – Praseodymium in figure I.4. [69] In energy transfer processes rare earth ions can be different. One donor or sensitizer, mean this ion allows the pump's energy to be better harnessed before transmits it to the acceptor or activator ion. The co-doping interests: Performing a wavelength match when the accepting rare earth would only present no absorption lines at laser diode wavelengths [70].

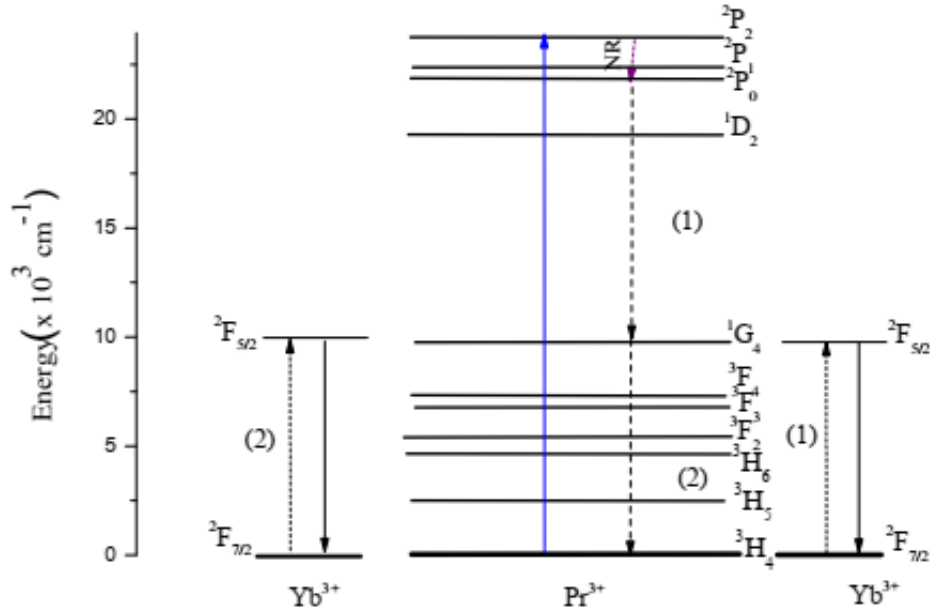


Figure (I.4): Co-doping Ytterbium - Praseodymium.

I.10 JUDD-OFELT Theory:

The theory developed by Judd and Ofelt makes it possible to calculate the probabilities of transitions radiative dipoles between 4fn levels of a rare earth ion from parameters reflecting the interaction of this ion with the local field created by the atoms of the host matrix [71, 72]. Indeed, these transitions prohibited by the Laporte rule, can only occur when they are "forced" by a non-centro-symmetrical field allowing a mixture between states of two configurations 4fn and 4fn-1 5d. Judd-Ofelt theory, resides in the ability to predict the forces of oscillators, via the determination of parameters phenomenological Ω (-) ($\lambda = 2, 4, 6$) [73].

I.11 Electrical dipole transitions:

In the case of an electric dipole transition, the calculation of the intensities of the transitions is very difficult. Judd and Ofelt's approximations have solved this problem at the price of these approximations:

Chapter I: Glass, generalities and theoretical considerations

- The burst of an electronic configuration is negligible compared to the deviation between two configurations. The resulting results are no longer valid for intraconfigurational transitions that involve close to the other configurations.

- The population of each electronic level is assumed to be equally distributed over all the Stark components.

- The absorption spectrum required for these calculations should generally be recorded at room temperature. [74]

The theory is based on the study of the absorption bands of the rare earth ion to determining the oscillator forces of the transitions from the fundamental level. These oscillator forces characterize, as their name suggests, the strength of a transition between two levels. These forces are dimensionless magnitudes of the order of 10⁻⁸ to 10⁻⁶ for rare earth ions in solid matrices [75]. The f_{exp} oscillator forces and the measured transition forces S_{meas} , for all the transitions from the fundamental level is given by the relation: [76].

$$f_{\text{exp}} = \frac{mc^2}{\pi e^2} \int \sigma_{\text{abs}}(\lambda) d\lambda \quad \text{I.1}$$

$$S_{\text{meas}} = \frac{3hc(2J+1)}{8\pi^3 e^2 \bar{\lambda}} n \left[\frac{3}{n^2+2} \right]^2 \int \sigma_{\text{abs}}(\lambda) d\lambda \quad \text{I.2}$$

m: Mass of the electron (9.109382×10⁻²⁸ g).

e: Charge of the electron (4.8032×10⁻¹⁰ e.u.).

c: Speed of light in vacuum (3×10¹⁰ cm.s⁻¹).

h: Planck's constant (h=6.62×10⁻²⁷ erg.s).

J: The total angular momentum of the ground state is from the designation 2S+1LJ.

n: Refractive index of the matrix.

$\bar{\lambda}$: Wavelength barycentres (nm).

$\sigma_{\text{abs}}(\lambda)$: Absorption efficiency section as a function of wavelength.

Chapter I: Glass, generalities and theoretical considerations

$\int \sigma_{\text{abs}}(\lambda) d\lambda$: The integrated area of the line considered (cm^2) is determined by the calculation of the peak areas attributed to the different transitions.

λ : Mean wavelength of the transition (nm).

Intra f^n transitions are known to have one or the other electric dipole ($\sim 10^{-6}$). Magnetic ($\sim 10^{-9}$) or electric quadrupole ($\sim 10^{-11}$) dipole, character or a contribution in more than one of these modes. The order of the contributions shows that the transitions are mainly electric dipole in character [77, 78].

This last approximation eliminates odd terms and limits the calculation of to even t parameters. This is why, in the expression of the transition force electric dipolar, t only takes the values 2, 4, and 6 [79, 80]:

$$S_{\text{ED}} = \sum_{t=2,4,6} \Omega_t |\langle f^n \alpha [\text{SL}] J || U^t || f^n \alpha' [\text{S}'\text{L}'] J' \rangle|^2 \quad \text{I.3}$$

$|\langle 4f^n \alpha [\text{SL}] J || U^t || 4f^n \alpha' [\text{S}'\text{L}'] J' \rangle|$ The reduced matrix elements of the tensor operator U^t of rank t . They depend mainly on the TR considered and have been calculated for different TRs by Nielson and Koster [81], Carnall [82], Weber and Kaminskii [83]. Later, we will use the matrix elements computed by Weber for Praseodymium [84]. The three phenomenological intensity parameters $\Omega_{t=2,4,6}$, called "Judd-Ofelt parameters", are characteristic of the couple formed by the TR ion and the host matrix. They describe the intensity and symmetry of the electrostatic field created by the ligands (closest neighbors of the TR), as well as the interconfigurational radial overlap [85].

Since there are only three Judd-Ofelt parameters, N must be greater than 3. For example, since Ytterbium (Yb) has only one absorption level, the theory

$$f_{\text{cal}} = \frac{8\pi^2 mc}{3h(2J+1)\lambda} [X_{\text{DE}} S_{\text{DE}} + X_{\text{DM}} S_{\text{DM}}] \quad \text{I.4}$$

$X_{\text{DE}} = \frac{(n^2+2)^2}{9n}$ and $X_{\text{DM}} = n^3$ Are the effective field corrections associated with electric dipole and magnetic dipole components, respectively [86, 87].

Chapter I: Glass, generalities and theoretical considerations

The magnetic dipole transition force is expressed as follows: [88, 89]

$$S_{DM} = U_B^2 \left| \langle 4f^n \alpha [SL]J || L + 2S || 4f^n \alpha' [S'L'] J' \rangle \right|^2 \quad \text{I.5}$$

$$U_B = \left[\frac{h}{4\pi mc} \right] \text{ and } \left| \langle 4f^n \alpha [SL]J || L + 2S || 4f^n \alpha' [S'L'] J' \rangle \right|^2 \quad \text{I.6}$$

Represents the reduced matrix elements of the L+2S operator between two Eigen states of the coupled ion intermediary. The method for calculating reduced matrix elements is described in the literature [90]. For example, the Eigen states of the Pr³⁺ ion are tabulated by Weber [91] and Nielson and Koster [92], these reduced matrix elements do not depend on the rare-earth host medium but only on the doping ion and the transition under consideration, the same applies to the magnetic dipole transition forces. The strongest DM transitions will generally be in the infrared for Pr³⁺ is the ³H₄→³H₅ transition, but exceptions may be expected. All other absorption transitions have a magnetic dipole contribution [93].

IV.3 Quality of adjustment:

The quality of fit, characterized by the value of r.m.s "Root Mean Square error", between the experimental and theoretical values of the electric dipole transition and oscillator force intensities is determined by the following equation [94]

$$r. m. s = \sqrt{\frac{\sum_i^q (x_i^{exp} - x_i^{cal})^2}{q-p}} \quad \text{I.7}$$

With

q: Number of transitions considered experimentally.

p: Number of unknowns, in this case p=3.

$x_{exp} = f_{exp}$ or S_{meas} and $x_{cal} = f_{cal}$ or S_{cal}

Error percentage [95]:

$$erreur\% = \frac{r. m. s}{r. m. s(S)} \rightarrow \sqrt{\frac{\sum X_{cal}^2}{q}} \quad \text{I.8}$$

With the standardized method, for each transition, the transition forces calculated are normalized by the effective absorption cross section. In the case of the standard, an

adjustment on transition forces gives greater weight to transitions long wavelengths, a problem that does not occur with the standard method [96].

IV.4. Probability of emission:

The theory of Judd-Ofelt allows determining the probabilities of transitions radiative radiation between these two bytes can be broken down into two terms: [97,98]

$$A(J' - J) = A_{DE}(J' - J) + A_{DM}(J' - J) \quad \text{I. 9}$$

The probabilities of electric (ADE) and magnetic (ADM) dipole transitions are expressed as follows as a function of the forces of electric and magnetic dipole transitions, SDE and SDM respectively, according to equation (I.19). The magnetic dipole transition forces are most of the time much lower than the forces of electrical dipole transitions. [99]

$$A(J' - J) = \frac{64\pi^4 e^2}{3h(2J'+1) \lambda^3} \left[n \left(\frac{n^2+2}{3} \right)^2 S_{DE} + n^3 S_{DM} \right] \quad \text{I. 10}$$

The transitions from level 5d to level 4f are transitions between different parity levels and are therefore allowed by the selection rules. They have so a short life span of a few dozen to a few hundred years is possible. Nanoseconds, and have high luminescence intensity. Similarly, in this case, the effective direct excitation cross section is much larger (of the order of 10-18 cm² [100]. The integrated emission efficiency section (Σ) becomes [101]:

$$\Sigma = \frac{\lambda^2}{8\pi^2 c} A_{rad} \quad \text{I. 11}$$

IV.5. Calculation of lifetimes and connection ratios:

Indeed, the radiative lifetime of a given rare earth ion emitting level can be calculated according to the relationships:

$$\tau_{rad} = \frac{1}{\sum_J A(J'-J)} \quad \text{I.12}$$

Chapter I: Glass, generalities and theoretical considerations

Another important radiative parameter characterizing the excited state is the ratio of connection, which accounts for the probability of a level de-energize to a level of lower energy in particular. It is expressed as a % and the sum of the connection ratios calculated for a level is equal to 1. For a de-excitation from J' to J: [102]

$$\beta = \frac{A(J' - J)}{\sum_J A(J' - J)} = \tau_{rad} \times A(J' - J) \quad \text{I. 13}$$

The connection report is directly accessible through the experiment, from a photoluminescence spectrum. The transition with $\beta > 0.5$ is a potential candidate for the laser. All the tools have been developed, and it is now just a matter of finding the radiative lifetime τ_{rad} , and the connection report β . This is the purpose of the Judd-Ofelt program. In conclusion, the Judd-Ofelt technique appears as a predictive tool allowing the determination of the different spectroscopic properties of a rare earth ion in a given material. However, it does not give access to the spectra of effective cross-sections of stimulated emission, which are necessary for any laser system modeling. [103]

IV.6. Effective cross-section of emission:

To determine these cross sections, we combined the results obtained by Judd-Ofelt analysis using so-called spectroscopic methods:

- The McCumber method, also called reciprocity [104]

- The Füchtbauer-Ladenburg (FL) method [105]

- The “laser” methods, ie the “small signal gain”, gain saturation, threshold and yield measurements [106].The first two methods are the most common and are the ones developed and used later:

The "McCumber" method:

The reciprocity method, therefore, does not use the fluorescence spectrum but the spectrum absorption. This method proposed by McCumber [107] and reformulated by Payne [108], is calculated at the following equation:

$$\sigma_{emMC}(\lambda) = \sigma_{abs}(\lambda) \frac{Z_l}{Z_u} \exp\left[\frac{E_{ZL} - \frac{hc}{\lambda}}{K_B T}\right] \quad \text{I. 14}$$

Z_l and Z_u: are respectively the partition functions of the bytes.

g_i and g_j: are the respective degenerations of the Stark sublevels i and j.

E_i and E_j: are respectively, the energies of the sub-levels of the fundamental state and of the state excites.

E_{ZL}: Zero-line energy (E_{ZL}= hc / λ_{ZL})

The constants used here are hc=1×10⁷ nmcm⁻¹, and kT=208 cm⁻¹ at temperature ambient. This method gives accurate results, but can only be used when the lower

level of the transition is the fundamental level. This disadvantage may be circumvented by using the Füchtbauer-Ladenburg method. For the study of sections stimulated emission between two excited bytes, it is necessary to exceed by the Füchtbauer-Ladenburg method. [109]

The "Füchtbauer-Ladenburg" method:

To calculate the stimulated emission cross section of a given transition by the Füchtbauer-Ladenburg method, it is necessary to have knowledge of the spectrum of the fluorescence I(λ) of the TR ion in the matrix, the refractive index n of this matrix, the lifetime of the transmitter level τ_{rad} and the connection report β of the transition concerned. The stimulated emission rms section σ_{em} calculated, for each transition, from the following relation: [110]

$$\sigma_{em}(\lambda) = \frac{\beta}{8\pi n^2 c \tau_{rad}} \frac{\lambda^5 I(\lambda)}{\int \frac{\lambda^5 I(\lambda)}{\lambda I(\lambda)} d\lambda} \quad \text{I. 15}$$

This method of calculating the stimulated emission RMS cross section is relevant when the emission spectrum is not altered. This method is therefore complementary to

This is a very different approach than the previous one since it is mainly valid for transitions leading to sparsely populated levels, i.e. the low-energy part of the emission spectrum [111]

Experimentally the branching ratio of a transition $m \rightarrow i$ is given by the ratio between the area under the band corresponding to this transition in the spectrum of quantum fluorescence $I(\lambda)$ and the surface of the whole spectrum [112]:

$$\beta = \frac{\int_{bandem} I(\lambda) d\lambda}{\int_{spectre} I(\lambda) d\lambda} \quad \text{I. 16}$$

Three MATLAB programs have been developed: one for Judd-Ofelt's theory, the two for the reciprocity method and the other for the Füchtbauer-Ladenburg relationship.

IV.7. Quantum efficiency:

The luminescence quantum efficiency noted η is defined as the ratio between the number of emitted photons corresponding to the laser wavelength on ions in the excited state of the laser transition. This performance is written:

$$\eta = \frac{\tau_{exp}}{\tau_{rad}} \quad \text{I. 17}$$

τ_{exp} : The fluorescence lifetime of the emitter level is determined. Experimentally by studying the decline in luminescence from this level in function of time.

τ_{rad} : The theoretical lifetime calculated using Judd Ofelt's theory. The higher the quantum efficiency, the more thermal energy deposited on the laser is limited promotes good performance (reduction of non-radiative radiation) [113].

References:

- [1].T. Som and B. Karmakar, *Optical Materials*, 31 (2009) 609-618.
- [2].L.Jiao, L. Xinyuhuang, J.Tang, S.Dai, G. Wang, T. Xu, and Q.Jiao, *Optical Materials Express*, 6 (2016) 12 – 1.
- [3].Taylor, R. Elizabeth, *Journal of applied physics* 92.1 (2002) 112-117.
- [4].P. Němec, J. Jedelsky, M. Frumar, *Journal of Non-Crystalline Solids*, 326 & 327 (2003) 325-329.
- [5].C.Jun Sun, Xu. Zhiha, Hu. Bin, G.M Chow, J.Shen, *Applied Physics Letters*, 91 (2007) 191-113.
- [6].J. Zarzycki, *Glasses and the Vitreous State*, Cambridge University Press, Cambridge, UK, 1991.
- [7].Dumbaugh, H.William, and C.Josef, Lapp, *Journal of the American Ceramic Society*, 75.9 (1992) 2315-2326.
- [8].E.M. Vogel, M.J. Weber, D.M. Krol, *Phys. Chem. Glasses*, 32 (1991) 231
- [9].S. L. Meena and B. Bhatia, *Journal of Pure Applied and Industrial Physics*, 6.6 (2016) 89-96.
- [10]. I.D. Aggarwal, G. Lu.Fluoride,GlassFiberOptics, Academic Press, Boston (1991).
- [11]. P. Petkova, A. Ghamri, P. Vasilev, I. Ismailov and M. T. Soltani, *Phys. Scr*, 162 (2014) 014-028.
- [12]. W.H. Dumbaugh, J.C. Lapp, *J. Am. Ceram. Soc*, 75 (1992) 2315.
- [13]. A. Winter, *J. Am. Ceram. Soc*, 40 (1957) 54.
- [14]. A. Winter, *Verres Refract*, 36 (1982) 353.
- [15]. B. Dubois, H. Aomi, J.J. Videau, J. Portier, P. Hagenmuller, *Mater. Res. Bull*, 19 (1984) 1317.
- [16]. J. Zavadil, Z. G. Ivanova, P. Kostka, M. Hamzaoui, M. T. Soltani, *Journal of Alloys and Compounds*, 611 (2014) 111-116.
- [17]. R.G. Orman, D. Holland, *J. Solid State Chem*. 180 (2007) 2587.
- [18]. I.Charef.khodja, doctoral thesis, Université Mohamed Khider Biskra, (2010).

Chapter I: Glass, generalities and theoretical considerations

- [19]. H. Masuda, Y. Ohta and K. Morinaga, *J. Japan Inst. Metals* 59 .1 (1995), 31-36.
- [20]. S.E. Golunski, T.G. Nevell and M.I. Pope, *Thermochim. Acta* 51 (1981), 153-168.
- [21]. S.E. Golunski and D. Jackson, *Appl. Catal.* 48 (1989), 123-135.
- [22]. K.OTHMER- *Encyclopedia of chemical technology*, 3e éd. 3. New York, John Willey, 107-108.
- [23]. J. W. Menary, *J. Acta. 865 Cryst*, 11, (1958), 742 - 743.
- [24]. P. PACAL, *Nouveau traité de chimie minérale*. Paris, Masson et Cie, 1958, 592.
- [25]. F.Montserrat, N.Belzile, and Y.W. Chen, *Earth-Science Reviews* 59.1-4 (2002) 265-285.
- [26]. P. J. Miller, C. A. Cody, *J. Spectrochimica Acta*, 38.5 (1982), 555-559.
- [27]. H. Hasegawa, M. Sone, M. Imoaka, *Phys. Chem. Glasses* 19 (1978) 28.
- [28]. A. J. G. Ellison, and S. Sen, *Physical Review B* 67.5 (2003) 052-203.
- [29]. M. Nalin, Y. Messaddeq, S.J.L. Ribeiro, M. Poulain, V. Briois, G. Brunlkaus, C. Rosenhahn, B.D. Mosel, H. Eckert, *J. Mater. Chem.* 14 (2004) 3398.
- [30]. B. Zhang, Q. Chen, L. Song, H. Li, F. Hou, J. Zhang, *J. Non-Cryst. Solids* 354 (2008) 1948.
- [31]. M.T. Soltani, A. Boutarfaia, R. Makhloufi, M. Poulain, *J. Phys. Chem. Solids* 64 (2003) 2307.
- [32]. M. Nalin, M. Poulain, M. Poulain, S. J. L. Ribeiro, and Y. Messaddeq, *J. Non-Cryst. Solids* 284 (2001) 110.
- [33]. R. Makhloufi, A. Boutarfaia, M. Poulain, *J. Alloys Compd.* 398 (2005) 249.
- [34]. R.G. Orman, D. Holland, *J. Solid State Chem.* 180 (2007) 2587.
- [35]. M.Hamzaoui, M. T.Soltani, M. Baazouzi, B.Tioua, Z. G. Ivanova, R.Lebullenger, J. Zavadil, *physica status solidi (b)*, 249.11 (2012) 2213-2221.
- [36]. S. B. Kolavekar, N. H.Ayachit, G.Jagannath, K.NagaKrishnakanth, S. V.Rao, *Optical Materials*, 83 (2018) 34-42.
- [37]. M. T.Soltani, T.Djouama, A.Boutarfaia, M. Poulain, In J.

Chapter I: Glass, generalities and theoretical considerations

- Optoelectron. Adv. Mater. Symp, 1 (2009) 339-342.
- [38]. T. Som, B. Karmakar, J. Alloys Compd. 476 (2009) 389.
- [39]. M. T.Soltani, M.Hamzaoui, S. Houhou, H.Touiri, L.Bediar, A. M.Ghemri, P. Petkova, Acta Phys. Pol. A, 123 (2013) 227-229.
- [40]. W. Vogel and W. Höland, Angewandte Chemie, 26 (1987) 527–544.
- [41]. U. Hoppe, Journal of Non-Crystalline Solids, 195, 1-2 (1996) 138–147.
- [42]. R. K. BROW, Journal of Non-Crystalline Solids, 263-264 (2000) 1-28.
- [43]. L. Bih, L. Abbas, S. Mohdachi, and A. Nadiri, Journal of Molecular Structure, 891, 1–3 (2008) 173–177.
- [44]. A.Boulegroun, Doctoral thesis, University Mohamed Khider–Biskra, 2019.
- [45]. M. P. Hehlen, M. G. Brik, K. W. Kramer, Journal of Luminescence 136 (2013) 221–239.
- [46]. R. Makhloufi, Doctoral thesis, University of Mohamed Khieder Biskra, 2017.
- [47]. L.Olivier, X.Yuan, A. N.Cormack, C. Jäger, Journal of non-crystalline solids, 293 (2001) 53-66.
- [48]. O.Bentouila, doctoral thesis, university kasdi merbah – Ouargla, 2016.
- [49]. S. H.Santagneli, Journal of Non-Crystalline Solids, 357 (2011) 2126 – 2131.
- [50]. N.I. Fernandes, Solid State Ionics, 181 (2010) 1125–1130.
- [51]. P.Gael, doctoral thesis, University of Rennes 1, (2003).
- [52]. N. Bondarenko, O. Eriksson, and N. V. Skorodumova, Physical review B 92, 165119 (2015).
- [53]. S.Joly, doctoral thesis, University National Polytechnique of Grenoble-INPG, 2009.
- [54]. O. Bentouila, doctoral thesis, University Kasdi Merbah Ouargla, 2016.
- [55]. L. Kassab, D.M.d. Silva, C. Araujo, journal of applied physics, 102 (2007)103-515.
- [56]. Y.Sun, F.Yu, M.Liao, X.Wang, Y.Li, L.Hu, J.Knight, Journal of Luminescence, 220 (2020) 117013.

Chapter I: Glass, generalities and theoretical considerations

- [57]. B.Tortech, doctoral thesis, University Jean Monnet of Saint- Etienne, 2008.
- [58]. J. Bonhoure, doctoral thesis, Université Nancy, 2007.
- [59]. G.H. Dieke, H.M. Crosswhite, *Applied Optics*, 2.7 (1963) 675.
- [60]. S.R. Bowmann, L.S. Shaw, B.J. Feldmann, J.Ganem, Addendum and Postdeadline, *Papers of Advanced Solid State Lasers (Washington)*, PD-1, 1995.
- [61]. E.Osiac, E.Heumann, G.Huber, S.Kuck, E.Sani, A.Toncelli, M.Tonelli, *Applied Physics*, 82.22 (2001)3832.
- [62]. T.Sandrock, E.Heumann, G.Huber, *OSA TOPS on Advanced Solid State Lasers*, 1(1996) 550
- [63]. F.Wang, X. Liu, *Chemical Society Review*, 38 (2009) 976-989.
- [64]. D.Dominik, *Acta Physica Polonica-Series A General Physics* 118.6 (2010) 1108.
- [65]. S.Hraiech, *Journal of Rare Earths* 31.7 (2013) 685-693.
- [66]. T.Belkhir, Doctoral thesis, Université Mohamed Khider Biskra, 2019.
- [67]. E.Boulbar, Doctoral thesis, University of Orleans, 2010.
- [68]. N. G. Boetti, D. Pugliese, E. C.Ginistrelli, J. Lousteau , D. Janner and D. Milanese, *Applied sciences*, 7.12 (2017).
- [69]. S. Mihi, doctoral thesis, University mohamed khider biskra, 2019.
- [70]. M.Kochanowicz, D.Dorosz, J.Żmojda, J.Dorosz, *Acta Physica Polonica, A*, 122 .5 (2012).
- [71]. A.S.Gouveia-Neto, E. B.Da Costa, L. A.Bueno, S. J. Ribeiro, *Optical Materials*, 26.3, (2004) 271-274.
- [72]. J.Legendziewicz, , M.Guzik, , J.Cybińska, A.Stefan, V. Lupei, *Journal of alloys and compounds*, 451.1-2 (2008)158-164.
- [73]. Y.Gao, Q. H.Nie, T. F.Xu, X. Shen, *Spectrochimica Acta Part A: Molecular and Biomolecular Spectroscopy*, 61.13-14, (2005) 2822-2826.
- [74]. V. P.Tuyen, , V. X.Quang, P.Van Do, L. D., Thanh, N. X. Ca, V. X. Hoa, M. Nogami, *Journal of Luminescence*, 210 (2019) 435-443.
- [75]. Y. Cheroura, Z.Smara, A.Potdevin, D. Boyer, A. Chafa, O.Ziane, R. Mahiou, *Materials Research Bulletin*, 125 (2020) 110809.
- [76]. L. Smentek, *Molecular Physics*, 101.7 (2003) 893-897.

Chapter I: Glass, generalities and theoretical considerations

- [77]. R.Belhoucif, M.Velázquez, Y.Petit, O. Pérez, B.Glorieux, O.Viraphong, A.Kellou, *CrystEngComm*, 15.19 (2013) 3785-3792.
- [78]. M. P.Hehlen, M. G. Brik, K.W.Krämer, *Journal of Luminescence*, 136 (2013) 221-239.
- [79]. S. V. J. Lakshma and S. Buddhudu, *J. Quant. Spectrosc. Radiat. Transferr Pergamon Press Ltd.* 24 (1980) 251-257
- [80]. M.Dejneka, E.Snitzer, R. E.Riman, *Journal of Luminescence*, 65.5 (1995) 227-245.
- [81]. R. T.Génova, I. R.Martin, U. R. U. R.Rodríguez-Mendoza, F.Lahoz, A. D. Lozano-Gorrin, P.Nunez, V. Lavín, *Journal of alloys and compounds*, 380.1-2 (2004) 167-172.
- [82]. Ł. Sójka, Z. Tang, H. Zhu, E. Bereś-Pawlik, D. Furniss, A. B. Seddon, T. M.Benson and S. Sujecki, *Optical Society of America*, 2 (2012) 11
- [83]. C. W Nielson, G. F Koster, *The M. I. T. Press, Cambridge, Massachusetts*, 1963.
- [84]. W. Carnall, H. Crosswhite, H.M Crosswhite, dans *Spectral energy level structure and transition probabilities in the spectra of the trivalent lanthanide LaF₃*, argonne national laboratory, Argonne, 1977.
- [85]. A.A. Kaminskii, *Crystalline lasers: Physical processes and operating schemes*, CRC Press, 1996.
- [86]. M. J. Weber, *The Journal of Chemical Physics* 48 (1968) 4774.
- [87]. P. Kabro, *Doctoral thesis, Concordia University*, 1997.
- [88]. P.P. Proulx, *doctoral thesis, Université Montreal Québec Canada*, 1992.
- [89]. A. K.Parchur, R. S. Ningthoujam, *RSC Advances*, 2.29 (2012) 10859-10868.
- [90]. J. Raja, M. R.Amjad, M. R. Dousti, Sahar, *Current Applied Physics* 15 (2015) 1-7.
- [91]. I. Vasilief, *Doctoral thesis, University Claude Bernard - Lyon I*, 2003.
- [92]. M. J. Weber, *The Journal of Chemical Physics* 48 (1968) 4774.
- [93]. S. Chaussement, *Authorization to Conduct Research, University of Angers*, 2011.
- [94]. C. W Nielson, G. F Koster, *the M. I. T. Press, Cambridge, Massachusetts*, 1963.

Chapter I: Glass, generalities and theoretical considerations

- [95]. G. Wang, J. Zhang, S.Dai, J. Yang, Z.Jiang, *Physics Letters A* 341 (2005) 285-290.
- [96]. M.Ennouri, I.Jlassi, H.Elhouichet, B. Gelloz, *Journal of Luminescence*, 216 (2019)116753.
- [97]. M. P. Hehlen, M. G. Brik, K. W. Kramer, *Journal of Luminescence* 136 (2013) 221–239.
- [98]. W.J. Miniscalco, Doctoral thesis, Marcel Dekker New York, 2001.
- [99]. W. T. Carnall, P. R. Fields, and K. Rajnak, *J. Chem. Phys.* 49 (1968) 4424.
- [100]. M. Mancier, *Courrier du Savoir* ,26 (2018) 449-456.
- [101]. V.R. Kumar, N. Veeraiah, B.A. Rao, S. Buddhudu, *J. Mater. Sci*, 33 (1998) 2659-2662.
- [102]. J.W.Aubatin, doctoral thesis, University of Lorraine, 2014.
- [103]. Lu.Chunfeng, H. Guo, Y. Xu, H.Chaoqi, Min Lu, Xin He, Pengfei Wang, L.Weinan, B. Peng, *Materials Research Bulletin* 60 (2014) 391-396.
- [104]. D. E. McCumber, *Phys. Rev*, 136 (1964) A954-A957.
- [105]. S. A. Payne, L. L. Chase, L. K. Smith, W. L. Kway, and W. F. Krupke, *IEEE J. Quant.Elec*, 28 (1992) 2619-2629.
- [106]. L. M.Marcondes, C. R.da Cunha, B. P.de Sousa, S.Maestri, R. R.Gonçalves, F. C.Cassanjes, G. Y.Poirier, *Journal of Luminescence*, 205 (2019) 487-494.
- [107]. S.Hau, C.Gheorghe, L.Gheorghe, F.Voicu, M.Greculeasa, G.Stanciu, M.Enculescu, *Journal of Alloys and Compounds*, 799 (2019) 288-301.
- [108]. R.Moncorgé, *Cristaux laser à ions de terres rares*. In *Collection de la Société Française d'Optique* EDP Sciences. 8 (2003) 69-98.
- [109]. A.Langar, C.Bouzidi, H.Elhouichet, M. Férid,. *Journal of luminescence*, 148 (2014) 249-255.
- [110]. I.Jlassi, H.Elhouichet, M.Ferid, C. Barthou, *Journal of Luminescence*, 130(12) (2010) 2394-2401.
- [111]. Y.Pepe, M.Erdem, A.Sennaroglu, G.Eryurek, *Journal of Non-Crystalline Solids*, 522 (2019) 119501.
- [112]. K.Ouannes, M. T.Soltani, M.Poulain, G.Boulon, G. Alombert-Goget, Y.Guyot, K.Lebbou, *Journal of alloys and compounds*, 603 (2014) 132-135.
- [113]. M. Chavoutier, doctoral thesis, Université Bordeaux 1, 2010.

Chapter I: Glass, generalities and theoretical considerations

- [114]. I.Jlassi, S. Mnasri, H. Elhouichet, Journal of Luminescence, 199 (2018) 516-527.
- [115]. K.Ouannes, doctoral thesis, University Mohamed Khieder Biskra, 2014.

Chapter II: Glass preparation and experimental techniques

Introduction:

This chapter defines the experimental procedure followed during this thesis; it is mainly devoted to the description of different techniques used to characterize glasses studied. In this chapter, we present all the experimental details of the thermal characterization technique (measured by DSC), the mechanical properties, density measurement, the refractive index measurement, and Raman spectroscopy, FTIR infrared spectroscopy, UV-V spectroscopy and luminescence spectrofluorometer.

II.2 Experimental strategies:

II.2.1 Choice of the matrix:

In order to find a new glassy matrix capable of incorporating the amount of antimony and phosphate, glasses containing Sb have a high refractive index and non-linear properties. These characteristics can be used for non-linear optical devices [1] and as photosensitive materials [2,3]. Recently, some interesting properties of $\text{Sb}_2\text{O}_3\text{-NaPO}_3$ glasses have been demonstrated. These glasses have been shown to have good thermal properties, a glass transition temperature and a higher refractive index [4,5]. Among the properties of these glasses is a large transmission window, a high gain density and low phonon energy [6,7]. These studies have shown that there is a considerable improvement in the infrared transmission of these glasses [8,9] and that large bulk samples can be obtained. Tungsten oxide was chosen as the 3rd oxide of the ternary system. The incorporation of WO_3 into the phosphate matrix also shows great transparency in the visible and near infrared [10,11]. Tungsten ions are supposed to have an influence on the properties of antimony phosphate glasses, for the simple reason that tungsten ions exist in different valence states W^{+6} , W^{+5} and also in state W^{+4} , independently of the oxidation state of the tungsten ion also tungsten oxide participates in the glass network with different- structural units like the ions WO_4 (Td) and WO_6 (Oh) of W^{+6} and W^{+5}O_3 (Oh) of the ions W^{+5} [12].

Sodium metaphosphate (NaPO_3) is chosen here as a network former in our system. The glasses are then synthesized with a constant content of Sb_2O_3 . By setting this parameter, namely the variation in the concentration of tungsten oxide, we can better understand the influence of WO_3 on the thermal, physical, optical and structural properties of these glasses. After choosing the composition which has good properties and we studied the spectroscopic properties of doped glasses with rare earth.

II.2.2 Synthesis method:

The starting materials used for the synthesis of the glasses are: Sb_2O_3 , NaPO_3 , WO_3 , Pr_2O_3 and Yb_2O_3 high-purity raw materials (99.6%). Glasses are made using the melt quenching technic were the raw powders are put in a silica crucible and heated to 300 °C for 1 hour to remove residual moisture and the adsorbed gases. The reagents are weighed according to the chosen compositions and mixed in stoichiometric proportion. After choosing the composition, we calculated masses of Sb_2O_3 , NaPO_3 , WO_3 , Er_2O_3 , Pr_2O_3 and Yb_2O_3 by the following relation:

$$m_x = Xx \times \frac{m_{\text{glass}}}{M_{\text{glass}}} \times M_x \quad (\text{II.1})$$

X_x : stoichiometric coefficient, M_x : The molar mass of raw material, m_{glass} : the mass of glass, M_{glass} : The molecular weight of glass and the molecular weight of raw materials.

Finally placed in silica crucibles. The mixture of approximately 3 g is brought into fusion over a Bunsen burner flame, for 10 to 15 minutes in the air close to a temperature of approximately 1000 ° C. time necessary for the total melting of the powder, the homogenization they have been quickly soaked by pouring it onto a stainless steel plate to be heated below the glass transition temperature $(T_g-10)^\circ\text{C}$ to avoid excessive thermal shock; the glasses were annealed for 6 h at a temperature $(T_g-10)^\circ\text{C}$ to relieve the mechanical stresses than the glasses polish using Minitech 233 Megapol Pressi, using abrasive papers in gradation from coarser to thinner "240", "400", "800", and "1200 to obtain samples with 1 to 2 mm parallel faces, and appropriate thickness for optical analysis and elastic measure.

II.2.3 Glass synthesis steps:

Step 1: heating the raw material at 300 ° C for 1 h (fig II.4).

Step 2: Powder weighing of batch compositions mixed in stoichiometric proportion (figII.1).

Stage 3: Fusion on a Bunsen burner for 10 to 15 minutes at 1000 ° C (fig II.2).

Step 4: Pouring onto a heated plate at $T = (T_g-10)^\circ\text{C}$ (figII.3).

Step 5: Annealing at a temperature $(T_g-10)^\circ\text{C}$ for 6 hours (figII.4).

Step 6: Polishing the glasses (figII.5).

Step7: Final requiring cylindrical glasses (figII.6).

Chapter II: Glass preparation and experimental techniques



Figure II.1: Balance.



Figure II.2: Benzene spout



Figure II.3: heated plate



Figure II.4: Nabertherm oven



Figure II.5: type polisher Minitex 233 Megapol Pressi

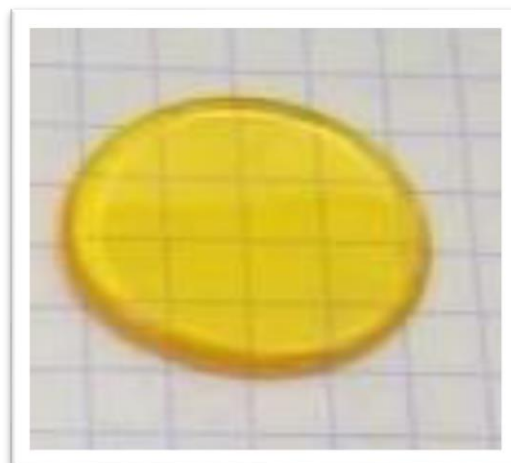


Figure II.6: Glass

Chapter II: Glass preparation and experimental techniques

II.2.4 Starting materials:

The starting oxides used in the synthesis of the glasses have a minimum purity of 99% and they come from Sigma Aldrich. The physicochemical characteristics of the oxides used are collated in Table II.1 and the compositions of the synthesized glasses are in Table II.2.

Table II.1: Physicochemical characteristics of the starting materials.

Starting materials	Molar mass	Density (g/cm ³)	T _f (°C)
Sb ₂ O ₃	291,5	5,2 (séna) 5,67 (val)	656
NaPO ₃	119,98	2,48	628
WO ₃	231,84	7,16	1473
Pr ₂ O ₃	329,8	7,07	2183
Yb ₂ O ₃	394,08	9,17	2355

Table II.2: Nomenclature of processed glasses.

Samples	Sb ₂ O ₃	NaPO ₃	WO ₃	Pr ₂ O ₃	Yb ₂ O ₃
SNW	60	40	0	-	-
SNW	60	35	5	-	-
SNW	60	30	10	-	-
SNW	60	25	15	-	-
SNW	60	20	20	-	-
SNW	60	15	25	-	-
SNWPr	60	40	0	0,05	-
SNWPr	60	35	5	0,05	-
SNWPr	60	30	10	0,05	-
SNWPr	60	25	15	0,05	-
SNWPr	60	20	20	0,05	-
SNWPr	60	15	25	0,05	-
SNWPr	47,5	47,5	5	0	-
SNWPr	47,5	47,5	5	0,05	-
SNWPr	47,5	47,5	5	0,1	-
SNWPr	47,5	47,5	5	0,25	-
SNWPr	47,5	47,5	5	0,3	-
SNWPrYb	47,5	47,5	5	0,1	0,25
SNWPrYb	47,5	47,5	5	0,1	0,5
SNWPrYb	47,5	47,5	5	0,1	0,75
SNWPrYb	47,5	47,5	5	0,1	1

II.3 Characterization techniques:

II.3.1 Thermal properties (Differential scanning calorimetric (DSC)):

The thermal characterization was carried out by differential scanning calorimetry (LABSYS Evo (fig II.7)), the samples from 10 to 40 mg are placed in aluminum crucibles, which can withstand a temperature of 600 ° C. The capsule is sealed with covers to avoid any risk of contamination of the oven cell; another empty capsule of the same kind is taken as a reference [13]. The two capsules are placed in the oven enclosure on highly sensitive contacts (thermocouples) the temperature rise speed is 10 ° C / min and the maximum temperature used is 500 ° C. The estimated error is ± 2 ° C. The DSC curve of glass allows us to determine the characteristic temperatures of the material Tg, Tx, Tp and Tf Glass transition temperature, the start of crystallization, maximum crystallization peak, and melting respectively for different heating rates and, for isothermal holdings, to determine the kinetics of crystallization at a given temperature. The absolute uncertainty on the measurement is estimated to be less than ± 2 ° C for Tg and Tx, and ± 1 ° C for Tp.



Figure II.7: Differential scanning calorimetric (DSC).

II.3.2 Mechanical properties:

II.3.2.1 Density measurement:

The density of the glasses is measured according to Archimedes' principle using an Ohaus Adventurer AX type microbalance (figII.8) with a sensitivity of 10^{-4} (g) and pure water as the immersion liquid, where accuracy of approximately $\pm 0.05\%$ is achieved.



Figure (II.8): Balance equipped with a hydrostatic weighing device (type OHAUS Adventurer AX).

Elastic Properties (Ultrasonic Method):

The elastic properties are measured by the Pulse-Echo technique. The ultrasonic measurements were carried out using a high power ultrasonic Pulse Receiver (Olympus NDT, 5900 PR, USA) using respectively X-cut and Y-cut quartz transducers each with a frequency of 10 MHz and a digital storage oscilloscope (Lecroy, Wave Runner 104 MXi 1GHz, USA), for recording ultrasonic signals. As can be seen in Figure II.9, the set-up allows measuring the sound velocity in a glass sample with a known thickness L where the longitudinal velocity V_L and the transverse velocity V_T are calculated using the same procedures used in reference [14].



Figure (II.9): Pulse-Echo set up: Immersion transducer with Olympus Panametrics-NDT Model 5800 generator, coupled with an oscilloscope 20GHz (type HAMEG).

II.3.8 Vickers hardness (Duramin struers):

The principle consists in applying a force to the polished and flat surface of a sample. To characterize the hardness and the deformation mode of the glass surface, the indentation technique was used. The deformation of the surface depends on the retention time of the Vickers indenter on the glass surface, on the temperature and on the applied load, and the hardness of the material can then be calculated from the projected surface of the impression [15].

Vickers hardness (HV) was measured using a Duramin20 (Struers equipment) micro hardness tester, where an indentation load of 200 g (HV0.2) is applied for a time of 20 seconds. At each load, at least five indents were spaced at about 38.97 μm intervals averaging the HV values were obtained using the formula II.2 [16, 17].

$$HV = 1,8544 * F/d^2 \quad (II.2)$$

Where HV is Vickers hardness, F is the applied force and d is the value of the measured mean diagonals of the indentation mark.



Figure II.10: Duramin struers of Vickers hardness.

II.3.3 Optical properties:

II.3.3.1 UV-Visible spectroscopy:

The transmittance spectra of the glasses were recorded between 200 and 1100 nm at a spectral resolution of 0.1 nm using a Perkin Elmer Lambda 35 UV / Vis spectrophotometer (FigII.9).

The spectroscopic techniques which are based on the interaction of radiation with glass in the area extending from the near ultraviolet-visible, we can measure the optical properties (transmittance, absorbance, absorption coefficient, index of refraction, thickness, gap energy and Urbach energy).

Chapter II: Glass preparation and experimental techniques

Spectroscopy The absorption in the UV-visible spectral range directly influences the perceived color of the chemicals involved, it's associated with the transition element present, A spectrum, therefore presents bands due to the absorption of glass, it measures the intensity of light passing through a sample (I), and compared it with the intensity of light before it passed through the sample (I₀). The ratio (I / I_0) is called the transmittance, and is generally expressed as a percentage (T%). The absorbance, A is based on the transmittance, and is generally expressed in transmission Eq II.3:

$$A = -\log (T/100\%) \quad (\text{II.3})$$

The optical absorption corresponds to the transitions it is conditioned by its interaction with the glass ions. The absorption limit, therefore corresponds to the threshold from which all radiation is absorbed [18,19].



Figure II.11: Perkin Elmer Lambda 35 UV-Vis spectrophotometer.

II.3.3.2 Determination of absorption coefficients:

To determine the absorption coefficient (α), we used the Bouguer-Lambert-Béer relation II.4, II.5 [20]:

$$I/I_0 = T = e^{-\alpha d} \quad (\text{II.4})$$

$$\alpha = (1/d) * (\ln 100/T(\%)) \quad (\text{II.5})$$

d: the thickness of the sample.

T(%): measured transmission.

II.3.3.3 Optical gap and disorder:

From the transmittance spectra, we deduced the optical gap E_g and the parameter E_{00} (Urbach energy), We evaluated the optical band gap energy (E_g) by extrapolating the linear region of $(ah\nu)^2$ with respect to $(h\nu)$ to the values where $(ah\nu)^2 = 0$ for the direct transition, obtained from Eq II.6 [21] and indicate in Figure II.10 (a).

$$(ah\nu)^2 = C (h\nu - E_g) \quad (\text{II.6})$$

The optical absorption coefficient $\alpha(\lambda)$ was obtained from EqII.7 [22]

$$\alpha(\lambda) = 1/d \ln (I_0/I_t) \quad (\text{II.7})$$

d: is the thickness of the sample.

I₀: is the incident light intensity.

I_t: is the transmitted light intensity.

The Urbach energy values E_{00} were calculated from the extrapolation of the linear portion of the curves $\ln(\alpha)$ with respect to $h\nu$, they were obtained from Eq II.8 [22] and shown in figure II.10 (b).

$$\ln \alpha = (h\nu/E_{00}) - C \quad (\text{II.8})$$

C is a constant.

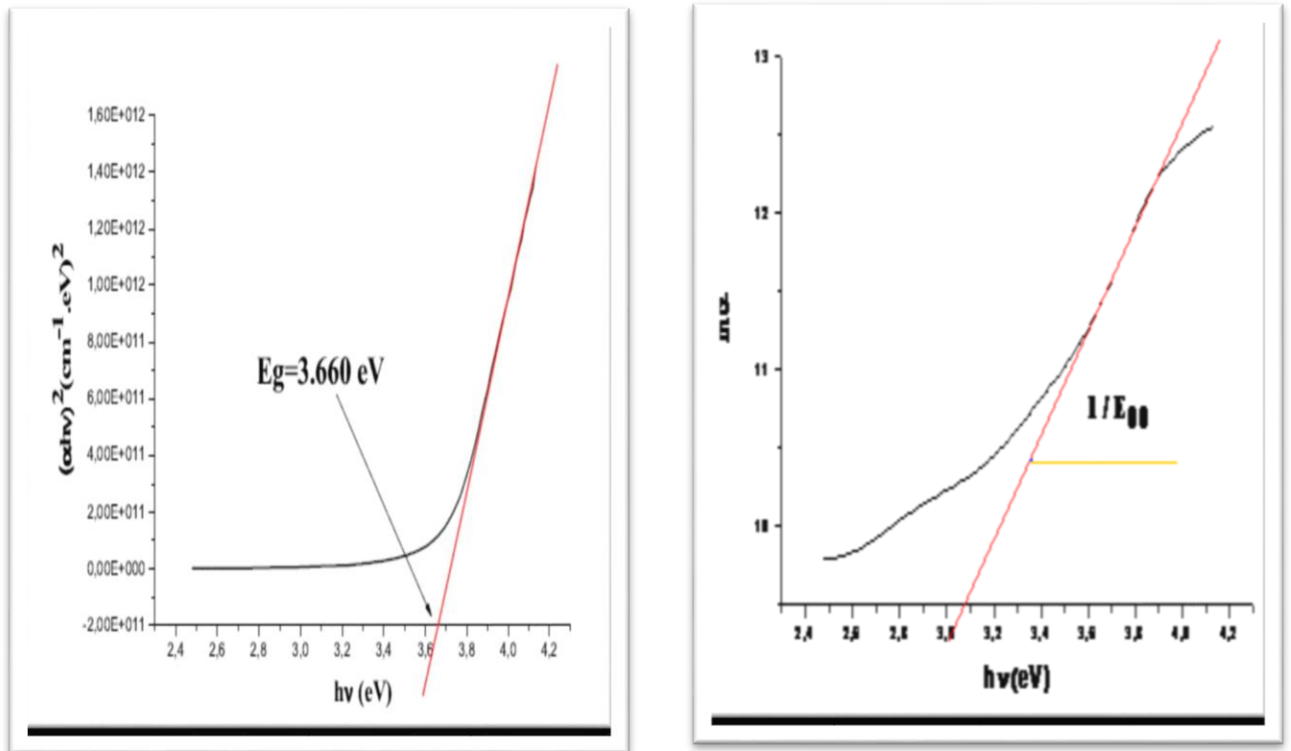


Figure II.12: a) determination of the energy gap by extrapolation from $(\alpha h\nu)^2$ as a function of $h\nu$ and b) Variation of $\ln \alpha$ as a function of $h\nu$.

II.3.7 Refractive index measurements:

The refractive index was measured by a UVISEL ellipsometer from HORIBA Jobin Yvon in wavelengths selected between 400 and 700 nm and with a fixed 70° incidence angle.

When light passes through two media with different refractive index, it is refracted according to the law of Snell Descartes defined by:

$$n_1 \cdot \sin \varphi_1 = n_2 \cdot \sin \varphi_2 \quad (II.9)$$

The refractive index increases with the molar mass of the glass elements (the electronic density). The index thus depends on the polarizability of the elements. It decreases when the wavelength increases [23].

Chapter II: Glass preparation and experimental techniques

The ellipsometer is showed in fig II.14. The UVISEL software allows to control the acquisition data, modulator frequencies, high Voltage, light source and associated devices, the monochromator, and the communication remote, It consist five Important parts:

1-Auto collimating system.

2-Detection head.

3-Manual sample (stage with height, tilt, theta adjustment).

4-Automatic goniometer.

5-Excitation head with manual microspot.

The Principe of determination of absorption coefficient is obtained by solving Maxwell's equation for a plane wave (Eq II.10)

$$E = \text{Re} [E_0 \exp i (wt - k \cdot r + \phi)] \quad (\text{II.10})$$

E_0 : Amplitude

$$W \text{ frequency: } 2\pi f = 2\pi Z / c \quad (\text{II.11})$$

$$K: \text{ propagation vector } (2\pi / \lambda) * z \quad (\text{II.12})$$

ϕ : phase

The attenuation of the wave is described by Beer's law:

$$I = I_0 \exp (-\alpha z) \quad (\text{II.13})$$

$$\text{With: } \alpha = 4\pi k / \lambda \text{ Absorption coefficient} \quad (\text{II.14})$$

z : direction of propagation

k : is the extinction coefficient the absorption of light in a material

$$\text{Refraction index is: } n = c/v \quad (\text{II.15})$$

It is the ratio between the light speed in vacuum and the light speed in matter where light speed in vacuum is larger than light speed in material.

Chapter II: Glass preparation and experimental techniques

The measurements were carried out on glasses having parallel faces with repeated scans by the changing the integration time up to 2s. , We have confirmed there is the backside reflection met on transparent substrates, to adjust the light line between 60 and 80° using 395 volt. [24,25,26].



Figure II.13: Uvisel ellipsometer from HORIBA Jobin Yvon.

II.3.4 Infrared spectroscopy:

The infrared transmission spectra of the glasses are measured at room temperature by a Fourier transform infrared spectroscopy (FTIR) using a Perkin Elmer spectrum Two spectrophotometer (fig II.11), it covers the spectral range from 8300 to 350 cm^{-1} .



Figure II.14: Perkin Elmer Spectrum Two FTIR spectrophotometer.

IR transmission characterizes the transparency of glass in the infrared and makes it possible to obtain molecular information which some infrared radiation can absorb at wavelengths that correspond to the vibration frequencies of the bonds in a compound, given and corresponds to some low energy electronic transitions in the infrared region because the absorption bands are directly related to the bond strength constant between atomic nuclei.

In an infrared spectrometer, the infrared beam coming from the IR source is directed towards the interferometer. The generation of this last during the recombination of the beams coming from the fixed mirror and the rest passes through the separator and is directed on the mobile mirror which moves at a fixed frequency. The beam then arrives at the detector to be transformed into an electrical signal. The detector signal appears as an interferogram, ie a signature of the intensity as a function of the position of the mirror and

it is possible to convert the interferogram by a Fourier transform [27, 28].

Three intrinsic phenomena that condition is:

Chapter II: Glass preparation and experimental techniques

- ✓ **Electronic absorption:** electronic absorption limits the transmission window towards high frequencies, it calculated from the relation II.16:

$$\nu = \frac{Eg}{h.c} \quad (\text{II.16})$$

- ✓ **Phonon absorption:** Many phonons absorption limits transmission in the low frequency range, the vibration frequency is given by Eq II.17:

$$\nu = \frac{1}{2\pi} \sqrt{\frac{K}{u}} \quad (\text{II.17})$$

K: is the force constant of the bond and u: the reduced mass of the two atoms.

Diffusion phenomena: depending on the wavelength and the size of the scattering centres ($CD < \lambda$): Rayleigh scattering

(CD order of λ): broadcast of Mie.

($CD > \lambda$): important distribution.

The presence of transition elements or rare earth, traces of water, hydroxyl, sulfate or other groups of impurities causes the appearance of absorption bands that alter the transmission window [29].

II.3.4.1 Fourier Transform Spectrometers (FT-IR):

There are two main types of devices. Their differences lie mainly in the system of wavelength selectors: the Dispersive spectrometers and Fourier transform spectrometers (FT-IR) (non-dispersive) the latter is This device is the interferometer for measuring all the frequencies simultaneously, it comprises of a light source, the device, the sample compartment, the detector and the analog-to-digital converter (fig II.12 (b)).

II.3.4.2 UATR technique:

The UATR is made up of an optical base on which is fixed the crystal stage the latter is a solid diamond is set in a stainless steel stage to ensure the best mechanical and chemical resistance, we put the glasses on the stainless steel stage and we start the analysis (fig II.12 (a)), The detector measures the amount of energy for each frequency that passes through the sample, the diamond stage is fully recognized by the software, which identifies the number of reflections, the serial number and nature of the crystal. This information is

Chapter II: Glass preparation and experimental techniques

recorded with each intensity spectrum as a function of the wave number. Finally, the stainless steel plate can be cleaned with a dry cloth or soaked in water or solvent after analysis [30].



Figure II.15: a) UATR techniques of the Perkin Elmer spectrophotometer. Spectrum Two. b) Spectrum Two spectrometer (FT-IR).

II.3.5 Raman spectroscopy:

Raman scattering spectroscopy is a method of structural analysis the frequency difference between the incident rays and the scattered rays called Raman displacement. This technique allows obtaining a lot of information's on the molecular composition such as the modes of molecular vibrations (phonons) as well as the chemical bonds.

Raman spectroscopy uses the principle of inelastic scattering of an induced dipole that radiates using a laser beam. This induced dipole is linked to the polarizability of the molecule and corresponds to a deformation of its electronic cloud. For there to be Raman scattering, there must be a variation in the polarizability of the molecule during vibration. In Raman, the excitation is monochromatic, and therefore has fixed energy, greater in order of magnitude than that of molecular vibrations. During the interaction, the molecule is brought into a high energy state and of short lifespan: it is called "virtual state"

* The de-excitation is done at the same frequency as the excitation: it is the diffusion Rayleigh elastic.

Chapter II: Glass preparation and experimental techniques

* The de-excitation is done at a frequency lower than that of the excitation: it is the inelastic Raman Stokes diffusion.

* the scattered photon can have a higher energy (anti-Stokes line) or lower (Stokes line) than the incident photon)): this is the Raman Stokes or anti-Stokes scattering.

For the last two cases, the energy difference corresponds to a vibrational energy gap.

The scattered light is collected using another lens and is sent to a monochromator, then its intensity is measured using a photomultiplier and the Raman scattering spectrum of the material is obtained [31, 32, 33].

The Raman measurements were performed by Thermo Scientific Nicolet™ Almega Raman spectrometer with Olympus visible microscope (50×, 100×) and two different gratings (2400 and 1200 lines/mm) and laser beam of 532 and 785 nm was used for excitation respectively, Provided an optimum spatial of ~1 μm and frequency resolution of the order 1 cm⁻¹ at the highest resolution.

II.3.6 Luminescence:

The emission, excitation and lifetime spectra were recorded by a FluoroMax®-4 type spectrofluorimeter using a Xenon lamp as laser excitation source (figure (II.13)). The lamp is mounted vertically to increase the stability and reduce the lifetime of the lamp. The lamp source is focused on employing an elliptical mirror. The reflective surface efficiently collects all wavelengths and focuses them on the input slit of the excitation monochromator. Before the excitation light reaches the sample, a photodiode reference detector measures the intensity as a function of time and wavelength. It gives information on the electronic properties of the material, it explores the long-term average fluorescence of a glass subjected to UV, visible or near IR radiation, When we have three levels 0, 1 and 2 the energy of light intense must be equal to a level of absorption of the rare earth granted with the transition 0 → 2, excites the system. Electrons are then promoted on level 2. These electrons relax up to level 1 Finally, these electrons return to level 0 by emitting a photon of energy equal to the energy difference between levels 1 and 0 or directly from level 2 to level 0, We then observe an emission of light, called photoluminescence, whose energy corresponds to the optical transition relative to the electronic levels involved [34, 35, 36].



Figure II.16: Horiba Yvon FluoroMax®-4 spectrofluorimeter.

The emission spectra are recorded from the optical converter at wavelengths greater than 300-850 nm or CCD camera with a sensitivity of 1000 nm, the excitation spectra between 200 nm and 750 nm were performed using the Xe lamp (450W), With a continuous emission spectrum.

References:

- [1] E.L. Falcao, C.B. de Araujo, C.A.C. Bosco, G.S. Maciel, H. Acioli, M. Nalin, Y. Messaddeq, *J. Appl. Phys.* 97 (2005) 0135035.
- [2] M. Nalin, Y. Messaddeq, S.J.L. Ribeiro, M. Poulain, V. Briois, *J. Optoelectron. Adv. Mater.*, 3 (2001) 553.
- [3] F.S. De Vicente, M.S. Li, M. Nalin, Y. Messaddeq, *J. Non-Cryst.Solids*, 330 (2003) 168.
- [4] M. Nalin, G. Poirier, S.J.L. Ribeiro, Y. Messaddeq, L. Cescato, *Journal of Non-Crystalline Solids*, 353 (2007) 1592–1597.
- [5] S. H. SANTAGNELI, *Journal of Non-Crystalline Solids*, 357 (2011) 2126 – 2131.
- [6] G.Poirier, S. Ottoboni, F. Castro Cassanjes, A.Remonte, Y. Messaddeq, S.L. Ribeiro, *J. Phys Chem. B*, 112 (2008) 4481-4487.
- [7] N.I. Fernandes, *Solid State Ionics*, 181 (2010) 1125–1130.
- [8] M.Nalin, M.Poulain, M.poulain, S.Ribeiro, Y.Messaddeq, *journal of non-crystalline solids* 284 (2001) 110-116.
- [9] P. Subbalakshmi, N. Veeraiah, *Journal of Physics and Chemistry of Solids*, 64(2003) 1027–1035.
- [10] S. H. SANTAGNELI, *Journal of Non-Crystalline Solids*, 357 (2011) 2126 – 2131.
- [11] Y. Gandhi, K.S.V. Sudhakar, M. Nagarjuna, N. Veeraiah, *Journal of Alloys and Compounds*, 485 (2009) 876–886.
- [12] E.L. Falcao, C.A.C. Bosco, G.S. Maciel, C.B. de Araujo, H. Acioli, M. Nalin, Y. Messaddeq, *Appl. Phys.*, 83 (2003) 1292.
- [13] Andrée-Anne Trudel, these de doctorat, université Laval canada,2015.
- [14] H. Toratani, H.E. Meissner, T. Izumitani and S.E. Stokowski, *J. Non-Cryst Solids*, 95-96 (1987) 701-708.
- [15] [32] J. L. Le Quéré, E. Sémon, *Analisis Magazine*, 26 (1998) 3.
- [16] M. Rioux, doctoral thesis, Laval University Canada, 2017.
- [17] M.Tiegel, R. Hosseinabadi, S.Kuhn, A.Herrmann, C.Rüssel, *Ceram. Int.*, 41-6 (2015) 7267-7275.

Chapter II: Glass preparation and experimental techniques

- [18] M Hamzaoui, S Azri, MT Soltani, R Lebullenger, M Poulain, Phys. Scr, 157 (2013).
- [19] P.M. Devshette, N.G. Deshpande, G.K. Bichile, Journal of Alloys and Compounds, 2007.
- [20] J. L. Van Heerden, R.Swanepoel, Thin Solid Films 299 (1997) 72-77.
- [21] V. A.Mukhanov, O. O. Kurakevych, and V. L. Solozhenko, Journal of Superhard Materials, 30-1 (2008) 71-72N. Elkhoshkhany Hager, M. Mohamed, E. Yousef, Results in Physics, 13 (2019) 102222.
- [22] M.Tiegel, R. Hosseinabadi, S.Kuhn, A.Herrmann, C.Rüssel, Ceramics International, 41-6 (2015) 7267-7275.
- [23] M. Matecki, M. Poulain, Mat. Res. Bull, 22 (1987) 345-350.
- [24] E. Harfmann, Doctoral thesis, Bordeaux University, 1995.
- [25] D. A. Skoog, F. J. Holler, T. A. Nieman, Principles of Instrumental Analysis, Thomson Learning, 1998.
- [26] C. N.Banwell, E. M. McCash, Fundamentals of molecular spectroscopy, 1972. M.Tiegel, R. Hosseinabadi, S.Kuhn, A.Herrmann, C.Rüssel, Ceramics International, 41-6 (2015) 7267-7275.
- [27] Z. Ben Achour, T. Ktari, B. Ouertani, O. Touayar, B. Bessais, J. Ben Brahim, Sensors and Actuators A, 134 (2007) 447–451.
- [28] J. L. Le Quéré, E. Sémon, Analisis Magazine, 26 (1998) 3.
- [29] J. G. Solé, L. E. Bausa, D. Jaque, Introduction to the Optical Spectroscopy, 2005.
- [30] P.M. Devshette, N.G. Deshpande, G.K. Bichile, Journal of Alloys and Compounds, 2007.
- [31] C. N.Banwell, E. M. McCash, Fundamentals of molecular spectroscopy, 1972.
- [32] N. Elkhoshkhany Hager, M. Mohamed, E. Yousef, Results in Physics, 13 (2019) 102222.
- [33] Desserouer, Frédéric, U.S. Patent No, 8 (2015) 934,171.
- [34] C.Primoz, Spectroscopy Techniques and Projects at 1.2-m UK Schmidt Telescope. (2012).
- [35] Laude, Jean-Pierre, U.S. Patent No, 5 (1999) 991-482.
- [36] X.Ziang, L. Shifeng, Q.Laixiang, P.Shuping, W.Wei, Y.Yu, G. G. Qin, Optical Materials Express, 5-1 (2015) 29-43.

Chapter III: Structural and physical properties of glasses

Introduction:

This chapter is devoted to the investigation of the different properties carried out on the different glasses synthesized in this study. The purpose is to study the evolution of the different properties of glasses as a function of the replacement of NaPO_3 by WO_3 .

Thermal properties include the characteristic temperature of glasses measured differential scanning calorimetry (DSC). Mechanical properties consist of the micro-hardness carried out by Vickers apparatus and the elastic properties encompasses the elastic moduli measured by the pulse-echo method. The optical properties of glasses gather the optical gap, the disorder, and the absorbance and transmittance spectra. They are measured using UV-Vis spectrophotometer. Further, the refraction indices of the glasses studied have been measured by ellipsometry. The structural investigation has been studied using FTIR and Raman spectra.

III.1 Structural study

III.1.1 FTIR spectroscopy

Figure III.1 illustrates the vibration spectra of glasses obtained by FTIR spectroscopy (a) in the spectral range $[1600-400 \text{ cm}^{-1}]$, (b) in the spectral range $[4500-400 \text{ cm}^{-1}]$ for the undoped glasses. And (c) in the spectral range $[4500-400 \text{ cm}^{-1}]$ for Pr^{+3} doped glasses and (d) for $\text{Pr}^{+3}/\text{Yb}^{+3}$ co-doped glasses.

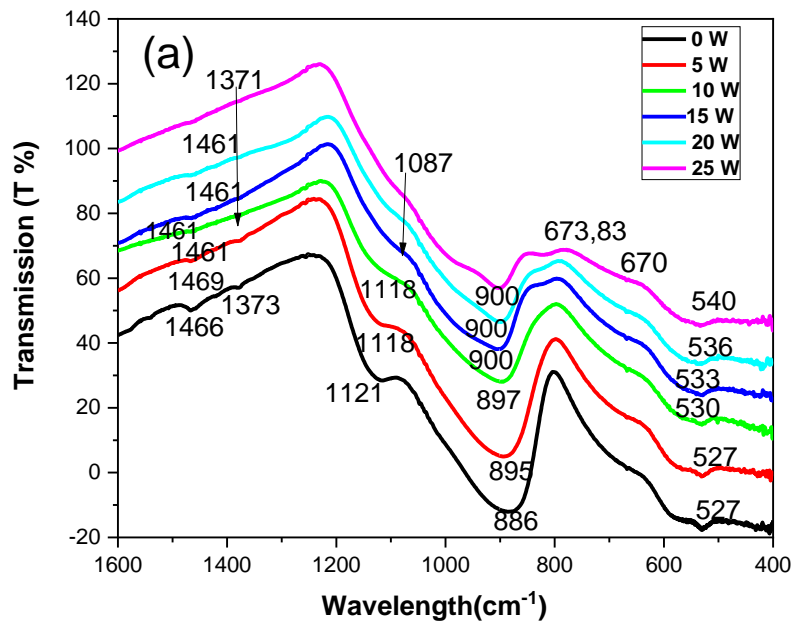


Figure III.1 (a): Infrared spectrum of glasses (SNW).

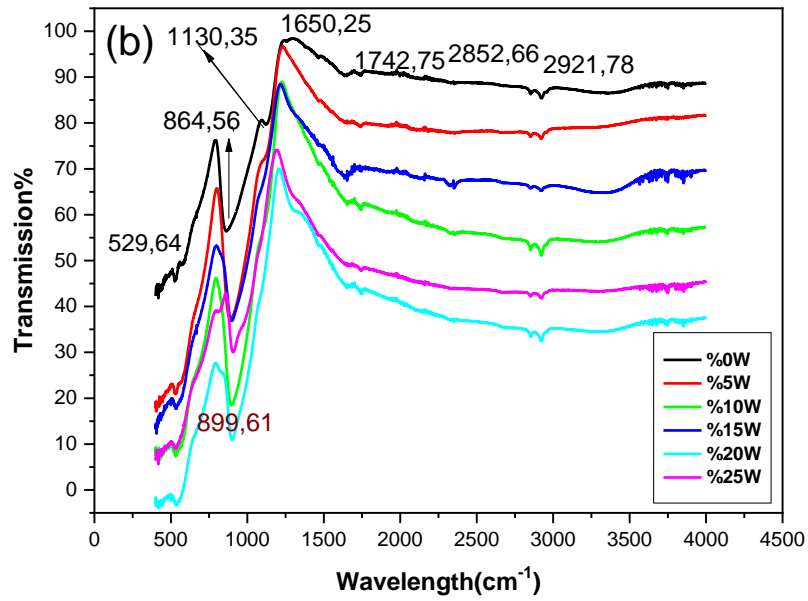


Figure III.1 (b): Infrared spectrum of glasses (SN0.1Pr W).

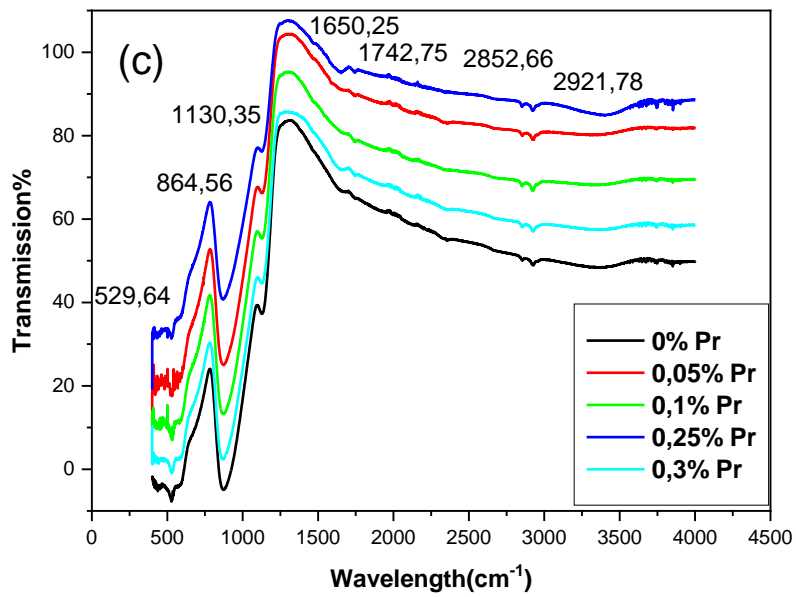


Figure III.1 (c): Infrared spectrum of glasses (SNWxPr).

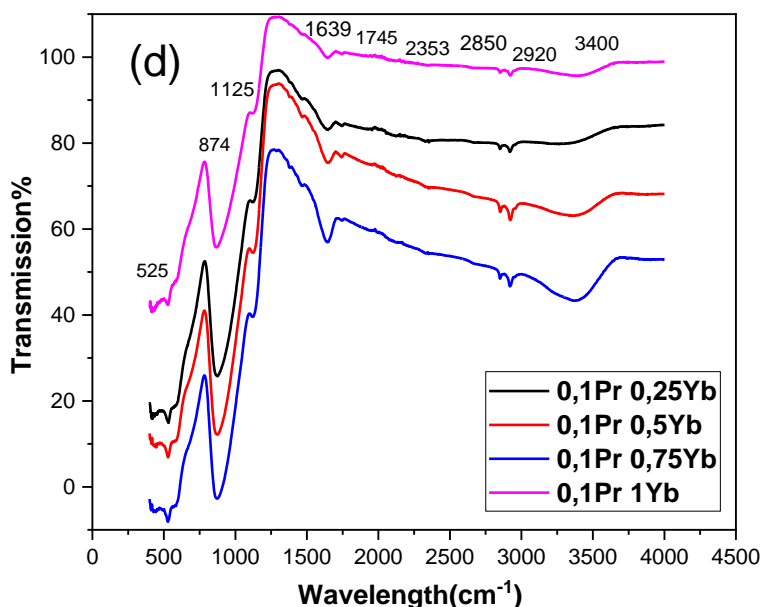


Figure III.1 (d): Infrared spectrum of glasses (SNW0.1Pr xYb).

In all spectra, the results showed seven characteristic absorption bands. Figure III.1 (a) of the host glass, (non-doped) summarizes the structure of the glasses studied. The first band at 525-540 cm^{-1} is due to the doubly degenerate bending vibrations of $[\text{SbO}_3]$ unit of Sb_2O_3 valentinite. This band is generally observed at 540 cm^{-1} . Its shift probably related to the formation of P-O-W linkages of the random phosphate chains Q_0 formed together with octahedra WO_6 , the band observed at 670 cm^{-1} is due to the mode of elongation vibration ν_4 of Sb-O and 673 cm^{-1} due to vibration Sb-O-W. The band from 864 to 900 cm^{-1} is attributed to W-O-W vibration modes. On the other, the formation of structural units containing Stretching vibrations of W-O- and W=O are confirmed by the presence of the band at 990 assigned of units WO_4 or WO_6 . The Q_2 (P-O) structural units of metaphosphate transformed into Q_1 and Q_0 structural units with the addition of Sb_2O_3 and the depolymerization of the phosphate chain occurred with the increase of WO_3 , the band manifested by the shoulder at about 1090-1130 cm^{-1} is attributed to the P-O-P of phosphate unite Q_1 symmetric elongation vibration mode of PO_3^{-2} , the bands located in the interval (1371-1466 cm^{-1}) (1639-1740 cm^{-1}) which have very low intensities due to the presence of water molecules.[1, 2].

(2350-2925 cm^{-1}) have attributed to the presence of hydrogen liaisons, the characteristic hydroxyl groups of water from the air. (3400 cm^{-1}) just in the compositions 47.5 Sb_2O_3 47.5 NaPO_3 5 WO_3 0.1 Pr_6O_{11} x Yb_2O_3 , (x= 0.25, 0.5, 0.75, 1) this liaisons related to bending

Chapter III: Structural and physical properties of glasses

symmetric stretching vibrations of O–H, the intensity of this band is more for lower concentrations 0,25 mol% and in the value 1mol% Yb^{+3} and it decreases when there is an increment in the Yb^{+3} ions concentration, but less of 1 mol% which indicates that the glass is more stable is because O–H content in the glass decreases as the Yb^{+3} concentration increases. [3].

III.1.2 Raman spectra:

Raman spectra of glasses system is shown in Figure III.2

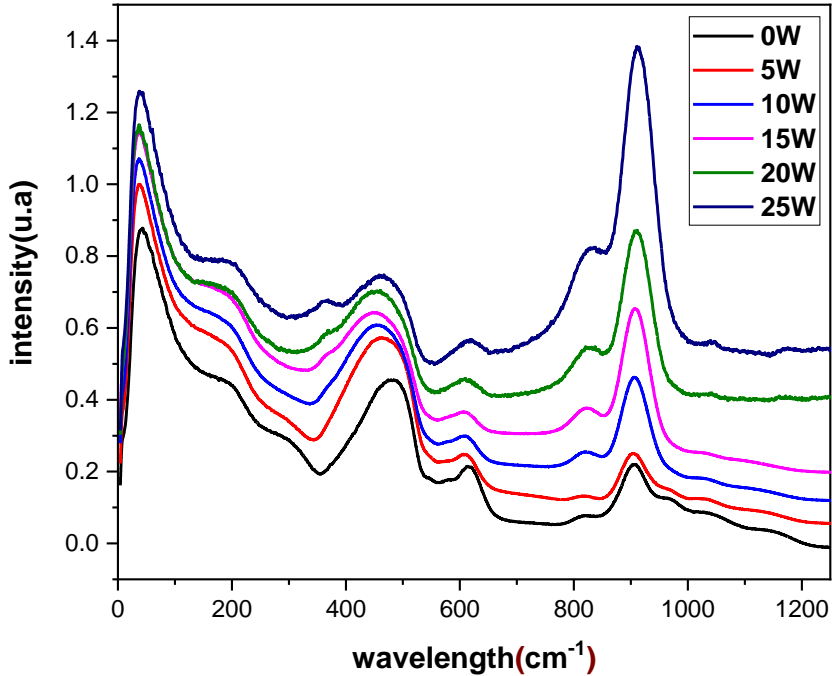


Figure III.2: Raman spectra of 60Sb₂O₃- (40-x) NaPO₃ -xWO₃ glass system.

From Raman analysis, it is concluded that The Boson peak (BP) between (35, 40 cm⁻¹), this peak represents the signature of the homogeneity of the glass as a result of the excess density of vibration states [4], The band positioned around 821 cm⁻¹ with structural units WO₄ and 831 cm⁻¹ with WO₆ are ascribed to Asymmetric stretching vibrations W-O and W=O associated with terminal oxygen atoms associated of unites. In the composition range from 5 to 10 mol% of WO₃ is an indication of WO₄ units and 15,20, 25% is an indication of WO₆ units, shift in peak toward the higher wave-numbers due to the higher number of oxygen and the transformation of [WO₄] units to [WO₆] units that assigned to the bending vibrations of W-O-W, the observed rise in intensity indicates that wo4 units (5,10% of WO₃) more than WO₆ units(20, 25% of WO₃) [5,6,7]. Whereas the band around 602-610 cm⁻¹ can be related to P-O-W vibration due to the bridging oxygen and tungsten atom of WO₃ with the Q₂ (P-O) structural units of metaphosphate. The apparition of a weak band around 1031-1115 cm⁻¹ is due to the formation of symmetric stretching vibration PO₃⁻² species of (Q₁) and asymmetric

stretching of $(\text{PO}_4)^{3-}(\text{Q}_0)$ that ascribed to the P-O-P to the breaking of the phosphate chains by tungsten thus a diminution of the Q_2 units [8].

On the other hand, the distinct vibration of the trigonal pyramids (tp) SbO_3 of the structural unit and which are located at $453\text{-}470\text{ cm}^{-1}$, the band of 200 cm^{-1} is attributed to Sb-O-W vibration modes and 1150 cm^{-1} related to water molecules [9].

III.2 Thermal properties:

III.2.1 Differential scanning calorimetric results

An illustration (fig III.3) of the DSC curves of $60\text{ Sb}_2\text{O}_3 (40\text{-}x)\text{ NaPO}_3 x\text{ WO}_3$, $60\text{ Sb}_2\text{O}_3 (40\text{-}x)\text{ NaPO}_3 x\text{ WO}_3 0.1\text{ Pr}_2\text{O}_3$ ($x=0,5,10,15,20,25$), $47.5\text{ Sb}_2\text{O}_3 47.5\text{ NaPO}_3 5\text{ WO}_3\text{-} x\text{ Pr}_6\text{O}_{11}$ ($x=0.05, 0.1, 0.25, 0.3$), $47.5\text{ Sb}_2\text{O}_3 47.5\text{ NaPO}_3 5\text{ WO}_3 0.1\text{ Pr}_6\text{O}_{11} x\text{ Yb}_2\text{O}_3$, ($x=0.25, 0.5, 0.75, 1$) mol %. All the DSC measures were performed in the range $[30\text{-}500^\circ\text{C}]$ to measure T_g , T_x and T_p of SNW glasses.

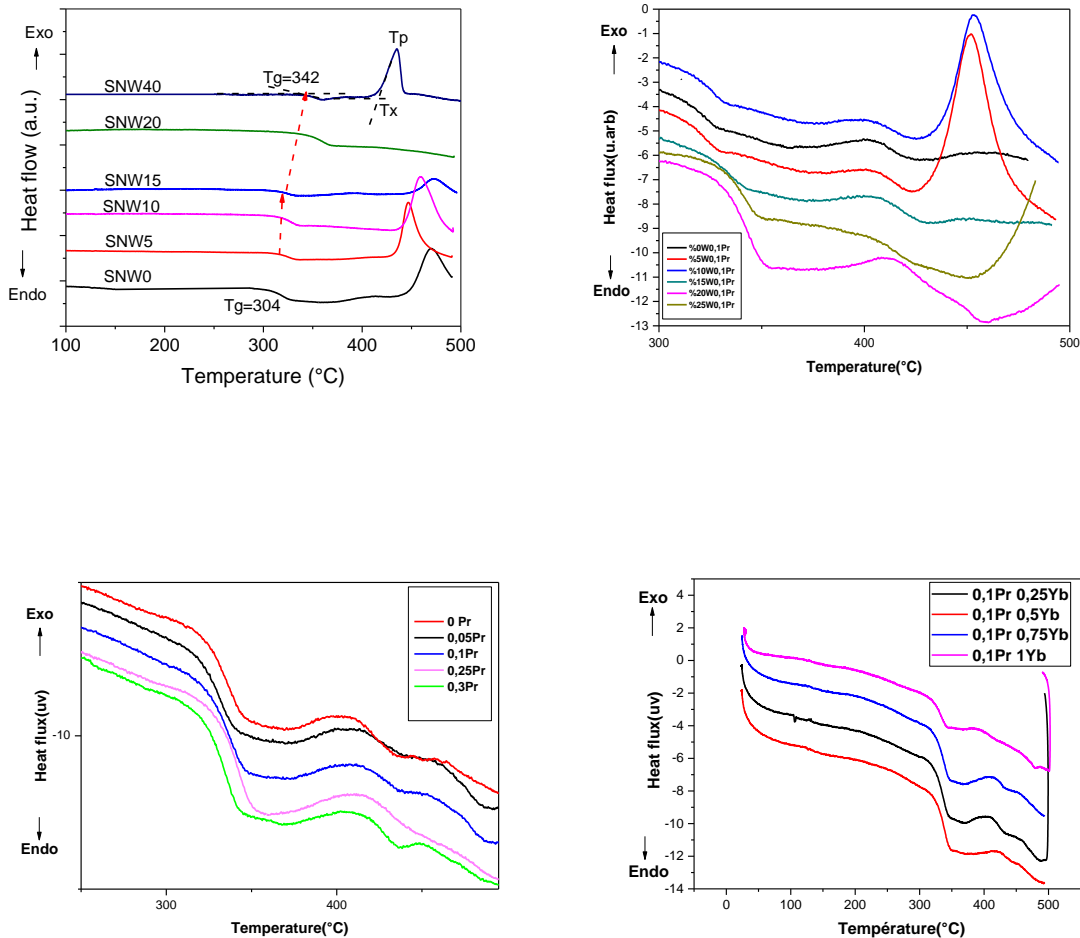


Figure III.3: System DSC Curves of glasses.

III.2.2 Characteristic temperatures:

The characteristic temperatures, transition temperature Vitreous (T_g), the onset of crystallization (T_c), the crystallization peak (T_p), are given in Table III. 1.

Table III.1: Summary of DSC data of glasses.

Composition (mol %)	$T_g(^{\circ}\text{C})$	$T_c(^{\circ}\text{C})$	$T_p(^{\circ}\text{C})$	$DT=T_c-T_g (^{\circ}\text{C})$
60S 40N 0W	305	442	470	137
60S 35N 5W	309	434	446	125
60S 30N 10W	310	447	460	137
60S 25N 15W	311	450	473	146
60S 20N 20W	326	/	/	/
60S 20N 30W	334	450	483	116
60S 20N 40W	342	435	435	93
60S 40N 0W 0,1Pr	327,82	431,63	239,36	103,81
60S 35N 5W 0,1Pr	311,14	428,36	457,96	117,22
60S 30N 10W 0,1Pr	315,43	427,33	453,68	111,9
60S 25N 15W 0,1Pr	314,25	432,52	451,60	118,26
60S 20N 20W 0,1Pr	320,62	460,04	411,49	139,42
60S 15N 25W 0,1Pr	320,62	453,68	/	138,06
47,5S 47,5N 5W 0Pr	317,50	376,57	404,09	59,07
47,5S 47,5N 5W 0,05Pr	316,46	372,41	407,20	55,95
47,5S 47,5N 5W 0,1Pr	318,54	373,45	408,24	54,91
47,5S 47,5N 5W 0,25Pr	320,61	360,73	411,48	40,12
47,5S 47,5N 5W 0,3Pr	314,26	371,3	408,24	57,12
// 0,1Pr0,25Yb	314,84	369,43	404,31	58,14
// 0,1Pr0,5Yb	314,84	371,75	420,59	56,91
// 0,1Pr0,75Yb	314,84	370,94	410,05	56,1
// 0,1Pr1Yb	314,84	369,43	388,03	54,59

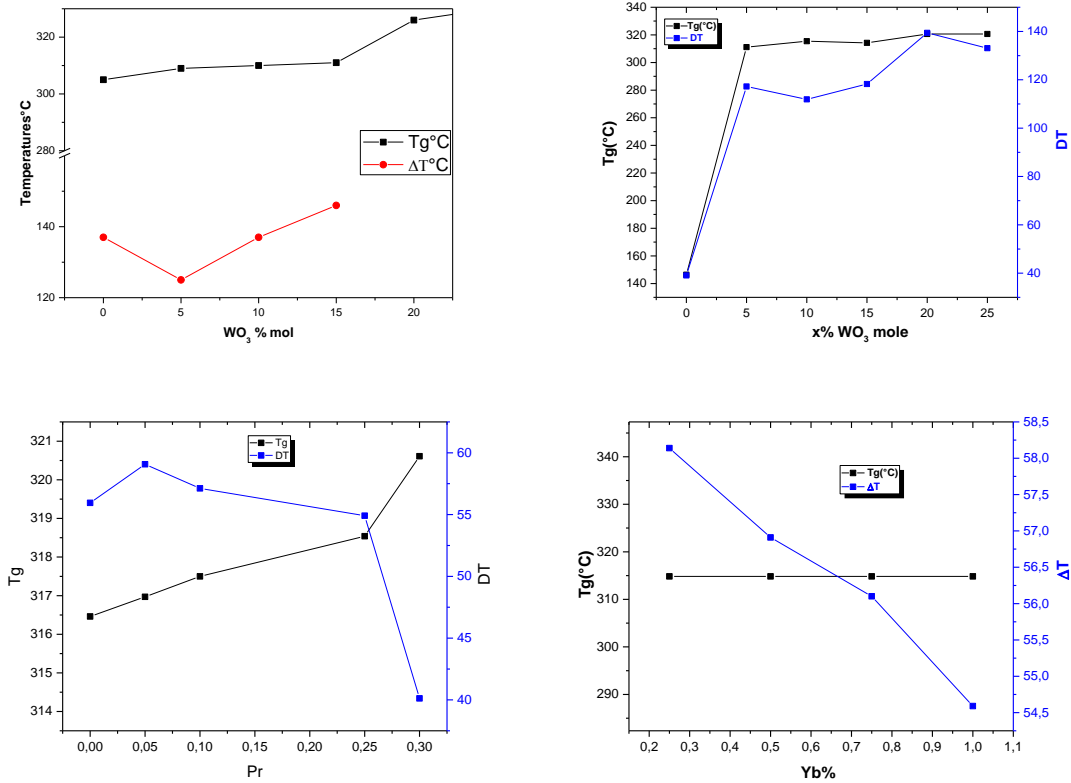


Figure III.4: variation of glass temperature T_g and thermal stability DT

When the concentration of WO_3 increases from 5 to 30 (mol%), all the characteristic temperatures T_g , T_c and T_p increase. Consequently, ΔT takes high values up to 146 °C for SNW15 glass and probably more for SNW20 glass (T_p and T_c not seen in the DSC patterns of fig1 due to the limited range [0- 500°C] in the DSC set up). For SNW25, SNW30 and SNW40, the stability of the glasses decreases gradually down to 93 °C.

The increase in T_g values with the rise in WO_3 content can generally be linked to three factors: either to the increase in the bonding force or to the crosslink density or the tightness of the packing in the network provided by the tungsten groups [10].

According to the compositional dependence of the T_g drawn in fig. 2, when the level of WO_3 is increased from 5 to 15 (mol %), the variation of T_g is practically constant, within the error range (± 2 °C). However, it increases in the range of 15 to 40 (mol.%) with a dramatic increase from 8 to 15 %. This behaviour is related to the change in the structural role of tungsten incorporation in these glasses. From 5 to 15 (mol. %), WO_3 is probably in the form of discrete ions of WO_4^{2-} and Na^+ groups due to the presence of a high amount of sodium provided by $NaPO_3$ and therefore, discrete tetrahedral units of Na_2WO_4 are probably formed as reported in alkali- tungsten oxide glasses [11, 12].

Recently, C. de Araujo et al reported that the gradual replacement of NaPO₃ by WO₃ in NaPO₃-WO₃ glasses first produces P-O-W bonds. The progressive insertion of WO₃ induces the creation of W-O-W bands, which serve for the crosslinking of the PO₄ chains and WO₆ units. Accordingly, the structure of the glass changes from a uni-or two-dimensional to a three-dimensional structural network based on tetrahedral SbO₃, PO₄ and interconnected polyhedral WO₆. It is also possible that the gradual substitution of WO₃ instead of NaPO₃ causes the P-O-P and Sb-O-P linkages to disappear, which was replaced by the W-O-P or W-O-Sb. Therefore, As a result of the three factors mentioned above, and the structural roles of tungsten, sodium and phosphorus ions in these glasses are under investigation.

The increase of the glass transition temperature T_g from 304 to 340 °C (Figure III.4) with the addition of WO₃ in the compositions that contain a high concentration of antimony not doped and doped by Pr⁺³ would be due to the fact that the tungsten oxide groups (WO₄ and WO₆) form a single network with the phosphate tetrahedral; these groups would enter the phosphate network. This means that the strengthening of the glass network would be linked to the presence of Sb-O-W bonds. The addition of WO₃ is due to the melting temperature of tungsten oxide of about 1473°C and that of Sb₂O₃ which is 656°C and NaPO₃ (628°C) This incorporation has the effect of increasing the viscosity of the glasses and the combination of the three oxides, lead to a vitreous matrix of intermediate T_g according to the old rule of thumb, where T_g follows T_f as per the ratio T_g/T_f = 2/3 (in Kelvin) [13]. These results suggest that the incorporation of WO₃ in the matrix makes the glass network much stiffer [14, 15].

In the composition of the same concentration of antimony and phosphate the DT < 100 also DT decrease with the increase of Pr⁺³ or the co doped Pr⁺³/Yb⁺³ in the glasses, the glass transition temperature T_g in this composition from 314°C to 320 °C but in the case of co doped Pr⁺³/Yb⁺³ T_g is constant (T_g=314,84). We observe also the existence of a second peak exothermic which indicates the crystallization of two crystalline phases.

III.3 Mechanical Properties:

III.3.1 The molar volume (V_m), oxygen molar volume (V_o) and density (d):

The density of the glasses is measured by Ohaus Adventurer AX Explorer balance according to Archimedes' standard principle. The measurements have been measured with an error equal to ±0.0001 g/cm³ and the result is an average calculated over 5 consecutive measurements carried out on the same. The Vickers hardness was measured using a Duramin20 (Struers).

Chapter III: Structural and physical properties of glasses

The molar volume (V_m) and oxygen molar volume (V_o) was calculated by using the following equations [16]:

$$V_m = \sum X_i M_i / \rho_g \quad \text{III.1}$$

$$V_o = \sum \frac{X_i M_i}{\rho_g} \left(\frac{1}{\sum X_i n_i} \right) \quad \text{III.2}$$

Where x_i : the molar fraction, M_i : molecular weight, ρ_g : the glass density, n_i : the number of oxygen atoms in each oxide constituent.

For calculating the thickness of the samples is used, digital caliper type Berent (BT4171).

The values of density, the molar volume (V_m) and oxygen molar volume (V_o) and thickness of glasses are given in Table III.2.

Table III.2: results of density, hardness, molar volume, oxygen molar volume and thickness

Composition (mole%)	d(g/cm ³)	Hv	V _m (cm ³ .mol ⁻¹)	V _o (cm ³ mol ⁻¹)	th (mm)
60S 40N 0W	4,394	328	40.16	16,9051	1,68
60S 35N 5W	4,613	345	38.71	16,5067	1,49
60S 30N 10W	4,729	373	38.20	16,4961	1,57
60S 25N 15W	4,87	388	37.52	16,4013	1,47
60S 20N 20W	4,99	403	37.52	16,3805	2,48
60S 40N 0W 0,1Pr	4,2535	258	52,4682	17,4719	2,33
60S 35N 5W 0,1Pr	4,459	270	51,3045	17,0844	1,75
60S 30N 10W 0,1Pr	4,6343	301	50,5707	16,8400	1,59
60S 25N15W0,1Pr	4,7971	311	50,0203	16,6567	2,37
60S 20N 20W0,1Pr	5,0338	333	48,7794	16,2435	2,36
60S 15N 25W0,1Pr	5,3474	342	46,9646	15,6392	1,88

Chapter III: Structural and physical properties of glasses

47,5S 47,5N 5W 0Pr	4,2735	254	48,4673	16,1557	2,24
47,5S 47,5N 5W 0,05Pr	4,263	267	48,6788	16,1965	1,80
47,5S 47,5N 5W 0,1Pr	4,2553	270	48,8869	16,2361	1,76
47,5S 47,5N 5W 0,25Pr	4,2333	278	49,5029	16,3510	1,40
47,5S 47,5N 5W 0,3Pr	4,222	289	49,7563	16,4049	1,65
// 0,1Pr0,25Yb	4,4664	248	46,7969	16,314	1,61
// 0,1Pr0,5Yb	4,4063	254	47,8824	16,6489	1,39
// 0,1Pr0,75Yb	4,3924	259	47,8096	16,5804	2,02
// 0,1Pr1Yb	4,3807	265	48,3871	16,7371	1,88

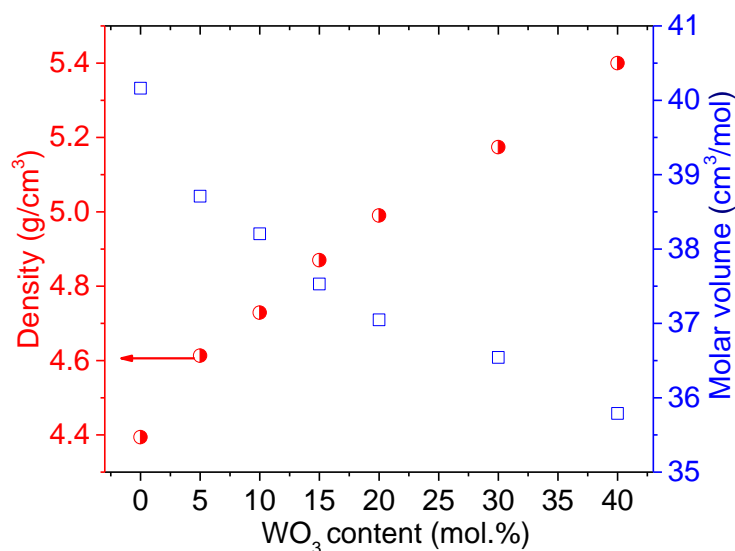


Figure III.5: Compositional dependence of density and molar volume of SNW_x glasses.

The density and their correspondent molar volume have been collected in Table III.2, and their compositional dependence has drawn in Fig. III.5. the linear increase in density with the gradual increase in the content of WO₃ is consistent with the additive density rule since the density of WO₃ (7.16 g/cm³) is greater than that of NaPO₃ (2.48 g/cm³). Therefore the addition of WO₃ makes the glass denser.

On the contrary, the molar volume values decreased with the rise in the WO₃ content from 40.16 to 35.78 (cm³/mol). The diminution in molar volume shows that the structural arrangement of the network changes significantly with the composition and can be explained quite simply by a decrease in ionic radii, where R(W⁺) = 0.80 and 0.56 (nm) for 4 and 6

Chapter III: Structural and physical properties of glasses

coordination, respectively, and $R(\text{Na}^+) = 0.95$ (nm). Thus, the gradual decrease in NaPO_3 has led to a decrease in the sodium atoms, resulting in a decrease in the molar volume of the glass.

The increase in density correlates directly with the increase of WO_3 content of (231.84 g/mol) in the compositions $60\text{Sb}_2\text{O}_3 - (40-x) \text{NaPO}_3 - x\text{WO}_3$ and $60\text{Sb}_2\text{O}_3 - (40-x) \text{NaPO}_3 - x\text{WO}_3 - 0.1 \text{Pr}_2\text{O}_3$, the density dependence on composition is in accordance with the weight and size of oxides and the density of each element [17].

the increasing of density and number of oxygen atoms relate to the decrease of the molar mass M of glass, molar volume (V_m) and oxygen molar volume (V_o) were according to equations III.1, III.2, WO_3 induces the formation of voluminous tungsten structural units such as WO_6 octahedron and WO_4 in the glass network more than the formation additional no bridging oxygen thus to the loss of oxygen of the substitution of NaPO_3

The influence of concentration of Pr^{+3} and $\text{Pr}^{+3}/\text{Yb}^{+3}$ on the glasses 47,5S 47,5N 5W x Pr ($x=0, 0.05, 0.1, 0.25, 0.3$) and 47,5S 47,5N 5W 0,05Pr x Yb ($x=0.25, 0.5, 0.75, 1$) is a decrease in the density and increase in molar volume and oxygen molar volume. Since the ionic radius of Pr^{+3} ions is large there will be an expansion in the glass structure and hence the molar volume and oxygen molar volume increases (V_m), also rises by the existence of excess oxygen NBO (non-bridging oxygen) in the glass network of the addition of Pr_6O_{11} and Yb_2O_3 . [18].

The results of hardness have been collected in table III.2 accurately to 1%. The values of $\text{HV}_{0.2}$ lie between 328 and 425 N/mm^2 with increasing WO_3 content. These values are slightly higher than other NaPO_3 containing glasses [19] and in the same range of $\text{SnO-NaPO}_3\text{-WO}_3$ glasses [20] but also higher than alkali-antimony glasses [21].

For many glasses, the increase in the hardness with the increase in elastic moduli like that indicated in the relation (III.3) [22]:

$$H_v = C. (\alpha. G. K)^{1/2} \quad \text{(III.3)}$$

Where C: a constant.

α : resistance factor of the link.

K: the volume modulus.

G: the shear modulus.

Therefore, hardness evolution is closely related to elastic properties. It's also worth noting that HV is closely related to the dilatometric softening point [23]. This last point is closely related to the glass transition temperature; therefore, the increase in the hardness is a behavior similar to that of the glass transition temperature.

Hardness is the merit of surface to endure indentations, Surface hardness is related to concentrations of glasses components also it depends on polishing procedures that can result in increased surface hardness affect compressive strength and flexural strength in this system the Hardness increases with the addition of tungsten, Pr^{+3} , $\text{Pr}^{+3}/\text{Yb}^{+3}$ concentration, it's noticed that The hardness values of not doped glass are higher than doped and co doped glasses. Pr_6O_{11} acts as a network modifier and increase the number of bridging oxygen (BO) ions that strengthen the rigidity of the glass [24].

III.3.2 Elastic Properties (Ultrasonic Method):

Elastic properties are suitable to give information on structural stability on the forces between the atoms or ions to understand the nature of bonds [25]

The elastic properties of the SNW glass series are studied by ultrasound technique using the pulse-echo method. allows to determine elastic material properties such as bulk modulus (K), longitudinal (L), shear modulus (G), and Poisson's ratio (σ) and Young's modulus E, the results have been measured by sound velocity (V_L), shear ultrasonic velocity (V_s) and density measurements, we report the results in table III.3

Elastic modulus and Poisson's ratio of glass were calculated by the following equations [26]:

$$L = \rho V_L \quad \text{III. 4}$$

$$G = \rho V_t \quad \text{III. 5}$$

$$k = \frac{\rho}{3}(3V_L^2 - 4V_t^2) \quad \text{III. 6}$$

$$E = \rho V_t^2 \frac{3V_L^2 - 4V_t^2}{V_L^2 - V_t^2} \quad \text{III. 7}$$

$$\sigma = \frac{V_L^2 - 2V_t^2}{2(V_L^2 - V_t^2)} \quad \text{III. 8}$$

Young's modulus expresses the ability of a material to deform under the effect of applied stress. It is higher as the sudden strain is minimal. As a result, the propagation velocity of the

Chapter III: Structural and physical properties of glasses

acoustic wave is faster and higher when the material is more compact. A rigid and undeformable glassy structure has a high Young's modulus.

Table III.3: sound velocities, elastic modules

Composition(mole%)	e(mm)	$\tau_L(us)$	$\tau_T(us)$	$V_L(m/s)$	$V_T(m/s)$	L(Gpa)	G(Gpa)	K(Gpa)	σ	E(Gpa)
60S 40N 0W	1,68	1,09	1,89	3082,57	1777,77	41,75	13,89	23,24	0,251	34,74
60S 40N 5W	1,49	0,961	1,67	3100,94	1784,43	44,36	14,69	24,77	0,252	36,79
60S 40N10W	1,57	0,995	1,73	3155,78	1815,03	47,09	15,58	26,32	0,252	39,04
60S 40N15W	1,47	0,893	1,55	3292,27	1896,77	52,79	17,52	29,44	0,252	43,86
60S 40N20W	2,48	1,43	2,5	3468,53	1984,00	60,03	19,64	33,84	0,255	49,37
60S 40N25W	2,44	1,35	2,36	3614,81	2067,80	65,47	21,42	36,90	0,257	53,85
60S40N0W0,1Pr	2,33	1,56	2,68	29 87,18	1738,81	37,95	12,86	20,81	0,244	31,99
60S40N5W0,1Pr	1,75	1,17	2,07	2991,45	1690,82	39,90	12,75	22,91	0,265	32,26
60S40N10W0,1Pr	1,59	1,11	1,74	2864,86	1827,59	38,03	15,48	17,40	0,157	35,81
60S40N15W0,1Pr	2,37	1,52	2,73	3118,42	1736,26	46,65	14,46	27,37	0,275	36,89
60S40N20W0,1Pr	2,36	1,44	2,5	3277,78	1888	54,08	17,94	30,16	0,251	44,92
60S40N25W0,1Pr	1,88	1,15	2, 1	3269,57	1790,48	57,16	17,14	34,31	0,285	44,09
47,5S47,5N5W0Pr	2,24	1,28	2,16	3500	2074,07	52,35	18,38	27,84	0,229	45,20
47,5S47,5N5W0,05Pr	1,80	1,08	1,88	3333,33	1914,89	47,37	15,63	26,52	0,253	39,20
47,5S47,5N5W0,1Pr	1,76	1,04	1,9	3384,62	1852,63	48,75	14,60	29,27	0,286	37,57
47,5S47,5N5W0,25Pr	1,40	0,91	1,41	3076,92	1985,82	40,07	16,69	17,82	0,143	38,16
47,5S47,5N5W0, 3Pr	1,65	1,07	1,64	3084,11	2012,19	40,16	17,09	17,37	0,129	38,61
// 0,1Pr0,25Yb	1,61	1,16	1,91	2775,86	1685,86	34,42	12,69	17,49	0,208	30,66
// 0,1Pr0, 5Yb	1,39	1	1,66	2780	1674,70	34,05	12,36	17,58	0,215	30,03
// 0,1Pr0,75Yb	2,02	1,36	2,48	2970,59	1629,03	38,76	11,66	23,22	0,285	29,96
// 0,1Pr1	1,88	1,22	2,29	3066,88	1641,92	41,20	11,81	25,46	0,299	30,68

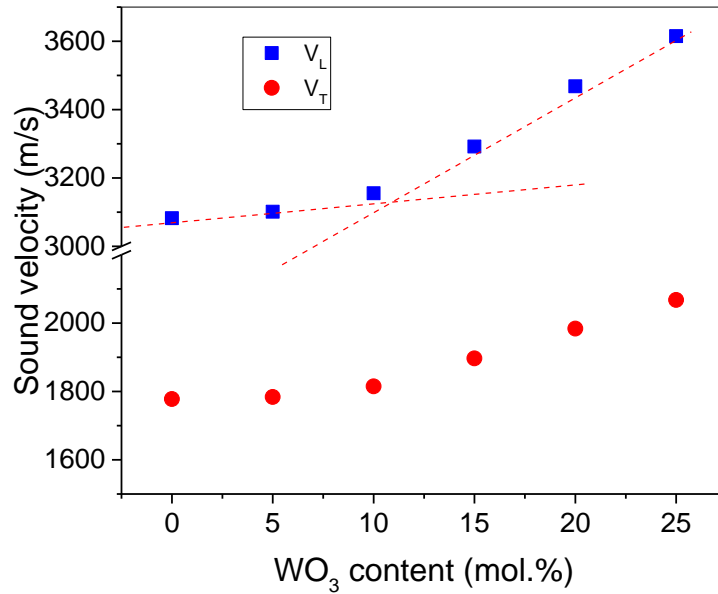


Figure III. 6. Longitudinal and transverse sound velocity of SNW_x glasses, lines are drawn as guides for the eyes.

The results show that the sound velocities V_L and V_S increase with increasing WO_3 . Subsequently, L , G , K and E increase when the content of tungsten oxide rise from 0 to 10 mol% and take more pronounced values for a higher content of WO_3 , as seen in Fig. III. 6. Thus, the longitudinal modulus L ranged from 41,75 to 66,64 GPa, the shear modulus from 13,89 to 21,80 GPa, the bulk modulus from 23,24 to 37,56 GPa and Young's modulus from 34,74 to 54,81 GPa. These values are higher than in the zinc-antimony glasses [21]. On the other hand, similar studies performed on the propagation of ultrasonic waves in tellurium glasses [27, 28] have shown that increasing the level of WO_3 in glasses increases elastic moduli.

It is easy for the ultrasonic wave to move inside the network of the glass due to the increasing density with tungsten oxide, Young's modulus related to the bonding strength of atoms (the stiffness of materials), hence, increase the connectivity of the glass network become more stiff, the values of Poisson's ratio (σ) remains constant in the range of 0.25 Elastic properties provide information for the structure.

Tungsten oxide enters the Antimony phosphate network, Therefore, part of tungsten ions will exist as WO_4 or WO_6 groups while the remaining exists as bridges between Sb_2O_3 and $NaPO_3$ groups such as $Sb-O-W$, $P-O-W$ producing of polarized oxygen ions. An increase in WO_3 content breaks the $P-O-P$ bonds as discussed in the FTIR analysis, WO_3 is acting as a very

Chapter III: Structural and physical properties of glasses

good intermediate in the glass network by consuming the NBOs (created in the process of depolymerization) which effectively increases the rigidity of the glass network, produce a lesser number of non-bridging oxygen and improves the elastic properties like increasing network rigidity and stability[29, 30], In the case of glasses doped Pr_6O_{11} , Poisson ratio is observed increase from 0.229 at $x = 0$ mol% to 0.253 at $x = 0.05$ mol% respectively. The values then decrease until $x = 0.25$ mol% at 0.164 and gradually increase until $x = 0.3$ mol% at 0.175.while the glasses co doped $\text{Pr}^{+3}/\text{Yb}^{+3}$ Poisson ratio increased from 0.208 to 0.299.

Young's modulus is related to hardness and density. Moreover, in 0 and 0.3 mole% Pr^{+3} low values for Young's modulus while Pr^{+3} from 0.1 to 0.25 mole% E increased from 45.62 to 46.82 Gpa, due to Pr^{+3} ions covalent bonds formed resulting in an increase in bridging oxygen. in the case of $\text{Pr}^{+3}/\text{Yb}^{+3}$ when Yb^{+3} from 0.25 mole% to 1 mole% E remains constant in the range of 30 Gpa. When the values of Elastic modulus decreases as a result of the conversion of BO to NBO [31, 32].

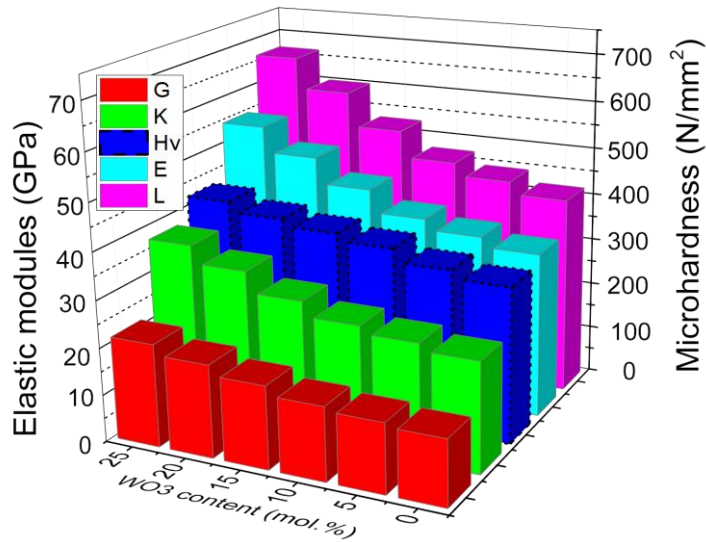


Figure III. 7. Elastic moduli and hardness of SNW glasses.

The replacement of NaPO_3 by WO_3 seems to significantly affect the structural organization of these glasses due to the large variation in Young's modulus and another elastic modulus. The elastic moduli tend to increase as the network evolves from a two-dimensional structure composed of PO_4 chains distributed randomly within the SbO_3 bi-chains in the SNW0 glass to a more strongly cross-linked compact structure in SNW glasses. From the curves drawn in

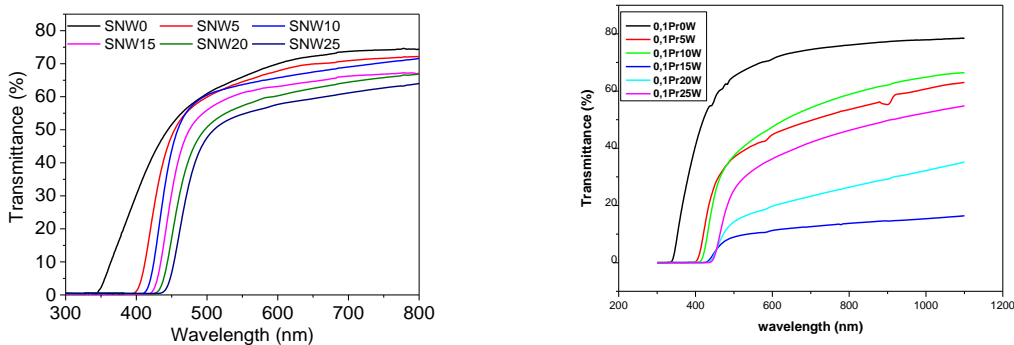
Figure.III.7. It was observed that the increase in elastic moduli is more noticeable when the level of WO_3 is higher than 10%, which suggests that the network connectivity and the crosslink density are improved by the insertion of more WO_6 units. This behaviour is closely correlated with the increase in T_g , as seen in the previous section.

Apart from the elastic modulus, Poisson's ratio remains practically invariant and close to 0.252. According to T. Rouxel [33], Poisson's ratio could reside indicative of the structural organization of the vitreous network. Thus, ν is equal to 0.4, 0.25 or 0.15 for a glassy network with the connectivity of one, two or three, respectively. We can conclude that the insertion of WO_3 preserves the two-dimensional structure of these glasses.

III.4 Optical properties

III.4.1 UV-Visible transmission (Transmittance spectra):

The transmittance spectra are shown in figure (III.5). They were recorded using a Perkin Elmer Precisely spectrophotometer covering the UV-Visible range between 200 and 3000 nm of glasses $60 \text{ Sb}_2\text{O}_3 (40-x) \text{ NaPO}_3 x \text{ WO}_3$, $60 \text{ Sb}_2\text{O}_3 (40-x) \text{ NaPO}_3 x \text{ WO}_3 0.1 \text{ Pr}_2\text{O}_3$ ($x=0,5,10,15,20,25$), $47.5 \text{ Sb}_2\text{O}_3 47.5 \text{ NaPO}_3 5 \text{ WO}_3-x \text{ Pr}_6\text{O}_{11}$ ($x= 0.05, 0.1, 0.25, 0.3$), $47.5 \text{ Sb}_2\text{O}_3 47.5 \text{ NaPO}_3 5 \text{ WO}_3 0.1 \text{ Pr}_6\text{O}_{11} x \text{ Yb}_2\text{O}_3$.



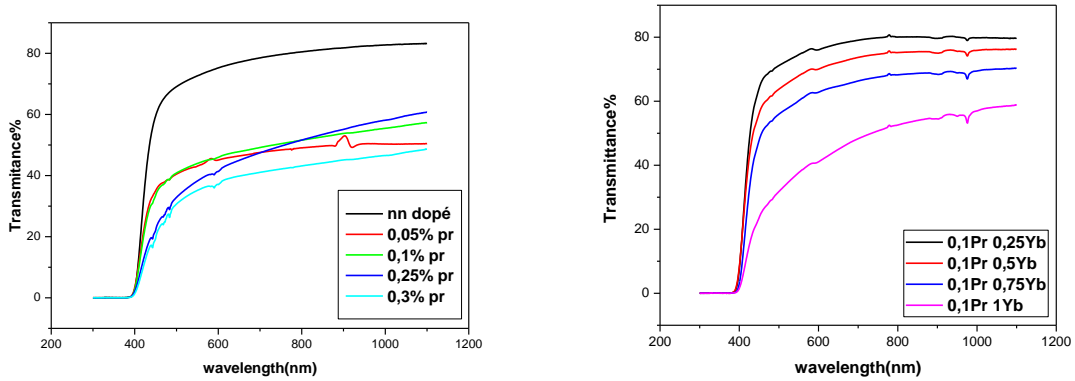


Figure III.8: Transmittance spectra in the UV, visible ranges

The transmittance spectra in the UV-Visible range of SNW glasses are shown in Fig. 6. Except for the $60\text{Sb}_2\text{O}_3\text{-}40\text{NaPO}_3$ composition, these glasses are opaque to ultraviolet and blue radiation, explaining the yellowish colour of the otherwise transparent samples. Furthermore, the limit of the absorption frontier in the UV-V range depends on the content of tungsten oxide and shifts to a higher wavelength within the 400-450 nm range of glasses with more WO_3 content. Apart from the intrinsic absorption and the defects introduced into the glass, the transparency of the glass depends, also on the refractive index ($n > 1.6$ in our glasses) wherever part of the incident radiation undergoes high reflections, that depends on the following relation $R=(n-1)^2/(n+1)^2$ where R is the reflectivity and n is the refraction index [34].

III.4.2 Optical Gap and Urbach energy:

From the transmission spectra and the thickness of the sample (th) we have deduced two important parameters, namely the optical gap E_g and the parameter E_{00} (Urbach energy) which gives an evaluation of the width of the band tails of the states located in the gap.

Values of E_g were obtained by extrapolation of the straight lines from the curves representing $(\alpha h\nu)^2$ to intersect the photon energy axis at zero absorption, as seen in (figure III.9) .

At low absorption level $\alpha(h\nu) < 10^4 \text{ cm}^{-1}$ [35], The Urbach energy values were calculated from the inverse of the slope of the extrapolation of the linear part of the $\ln(\alpha)$ vs $h\nu$ curves.[36] (figure III. 10). The values of E_g and ΔE are listed in Table 3, and their compositional dependence has shown in figure III. 11 An accuracy of 0.01 eV estimates for the values of E_g and 0.005 eV for ΔE .

Chapter III: Structural and physical properties of glasses

Previous works report that the optical band gap of vitreous Sb_2O_3 , WO_3 and NaPO_3 was equal to 3.8 eV [37], 2.75 eV [38], and 5.098 eV [39], respectively, thus, replacing NaPO_3 by WO_3 shifts the absorption edge to longer wavelengths and smaller E_g values.

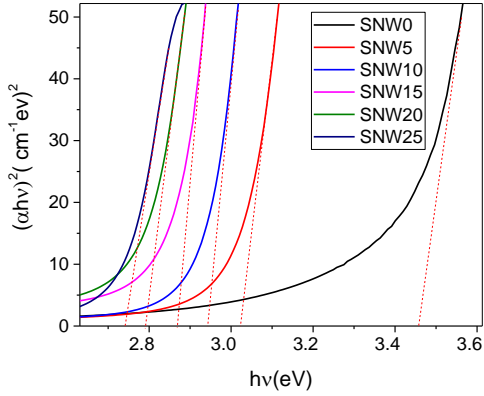


Figure III.9: $(\alpha h\nu)^2$ vs. $(h\nu)$ plot of glass.

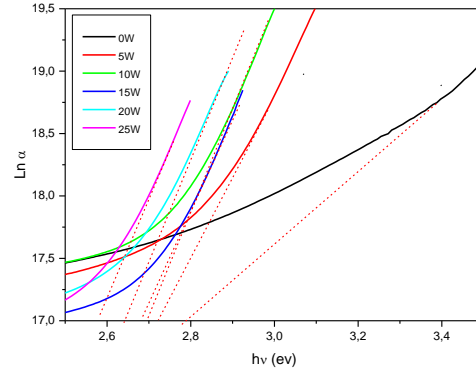


Figure III.10: $(\text{Ln } \alpha)$ vs. $(h\nu)$ plot of glass.

Table III.4 illustrates the values of the optical gap and disorder of the different samples.

Samples	$E_{00}(\text{eV})$	$E_g(\text{eV})$
60S 40N 0W	0.042	3.46
60S 40N 5W	0.038	3.02
60S 40N 10W	0.031	2.94
60S 40N 15W	0.030	2.87
60S 40N 20W	0.037	2.79
60S 40N 25W	0.038	2.74
60S 40N 0W 0,1Pr	0,3571	3,6
60S 35N 5W 0,1Pr	0,3597	2,97
60S 30N 10W 0,1Pr	0,3649	2,9
60S 25N 15W 0,1Pr	0,3703	2,8
60S 20N 20W 0,1Pr	0,3802	2,77
60S 15N 25W 0,1Pr	0,3921	2,7
47,5S 47,5N 5W 0Pr	0,35	3
47,5S 47,5N 5W 0,05Pr	0,355	3
47,5S 47,5N 5W 0,1Pr	0,357	3
47,5S 47,5N 5W 0,25Pr	0,36	3
47,5S 47,5N 5W 0,3Pr	0,366	3
47,5S 47,5N 5W 0,1Pr0,25Yb	0,354	3
47,5S 47,5N 5W 0,1Pr0, 5Yb	0,357	3
47,5S 47,5N 5W 0,1Pr0,75Yb	0,358	3
47,5S 47,5N 5W 0,1Pr1Yb	0,384	3

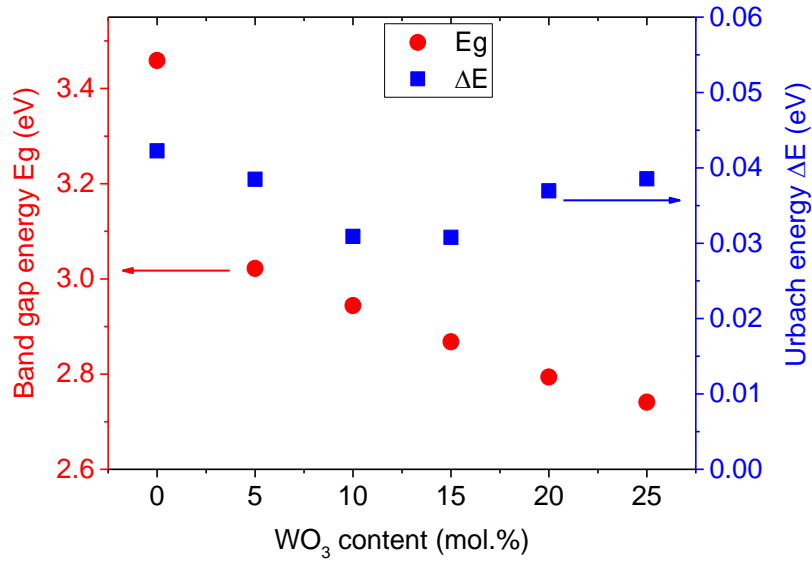


Figure III. 11: The optical band gap (E_g) and Urbach energy (ΔE) of SNW glasses.

The optical gap energy E_g is decreasing slightly with the introduction of tungsten oxide in SNW and SNWPr glasses and the UV-Vis absorption edge red-shifts with increasing WO_3 content in the glass.

The SNW0 composition presents the higher value of E_g , and the insertion of WO_3 reduces the band gap energy linearly from 3.02 to 2.74 eV, and enhances the creation of non-bridging oxygen's, which modifies the structure of the glass and consequently decreases E_g .

Unlike the optical band gap energy, WO_3 induces the formation of tetrahedron $[WO_4]$. This means that we have the creation of oxygen not pontoon and therefore. Also, the addition of RE (Pr^{+3}) makes the same creation, for more WO_3 additions, octahedron $[WO_6]$ occurred inside the glass and the number of the tetrahedron environment increases in the expenses of the tetrahedron $[WO_4]$ that's decreases the optical gap. Also the optical gap energy E_g influence on structural changes may increase the degree of electron localization, which increases the number of centers donors in the glass matrix due to decreases from the donor centre [40]. The Urbach energy ΔE in these glasses was found practically constant concerning the content of WO_3 . Since Urbach energy generally expresses the scale of the disorder in the system, smaller values of ΔE indicate that the defect centres are smaller [41], as observed in

10 to 15 mol% of WO₃. A slight increase is observed for more than 15 mol%, corresponding to the structural change observed in T_g and sound velocity results.

In the case of the variation of Pr₆O₁₁ and Yb₂O₃ the optical gap is constant attributed to no change in the average bond energy of the system because the variation of rare earth concentration was very small

Also Transmittance is related to the electronic transitions d-d the excited states of the electrons begin to overlap on the W⁺⁶ sites with the increase of WO₃. As a result, the strip of impurities becomes more extensive in the main gap band. The degree of disorder in the gap band (E₀₀) increases with the amount of increase of WO₃, Pr₂O₃, Yb₂O₃ which causes more defects or localized states (unsaturated bonds) reducing This evolution could have moved the absorption edge of the lowest energy, at high content of oxides the saturation of defects Increase because of the formation of dangling bonds[42].

Refractive index (HORIBA Jobin Yvon):

The refractive indexes were measured by a HORIBA Jobin Yvon in wavelengths between 600 and 689 nm, illustration of 60 Sb₂O₃ (40-x) NaPO₃ x WO₃, 47.5 Sb₂O₃ 47.5 NaPO₃ 5 WO₃- x Pr₆O₁₁ (x= 0.05, 0.1, 0.25, 0.3) glasses.

In this study, the refractive index, n, has been measured by spectroscopic ellipsometry. For greater precision, Sellmeier's formula [43] has been utilized to adjust the measured values of n.

$$n^2 = (A+B/(1-C/\lambda^2))+D/(1-E/\lambda^2) \quad \text{(III.9)}$$

Where A, B, C, D and E are fitting constants.

As an example, the refraction index of SNW25 glass shows in Figure III. 12 the refractive index depends essentially on the polarizability of the atom. Highly polarizable atoms, like heavy metal oxides (antimony, lead, tungsten, etc.), increase n. Therefore, with increasing concentration of WO₃ from 0 to 25 (mol. %) in the glass, the refractive index increased in the range [1.58-1.8] at λ=486.1 nm. The increase in the refractive index of SNW glasses is due to the strong polarizability of the tungsten atoms that gradually replaces the less polarizable phosphate atoms. Figure III. 13 show the compositional dependence of n value for selective wavelengths.

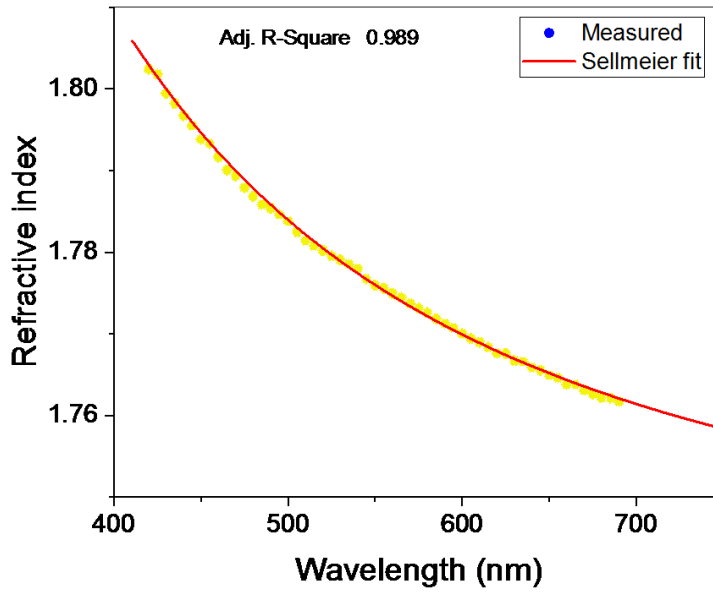


Figure III. 12: Dispersion curve of SNW25 glass in the visible region.

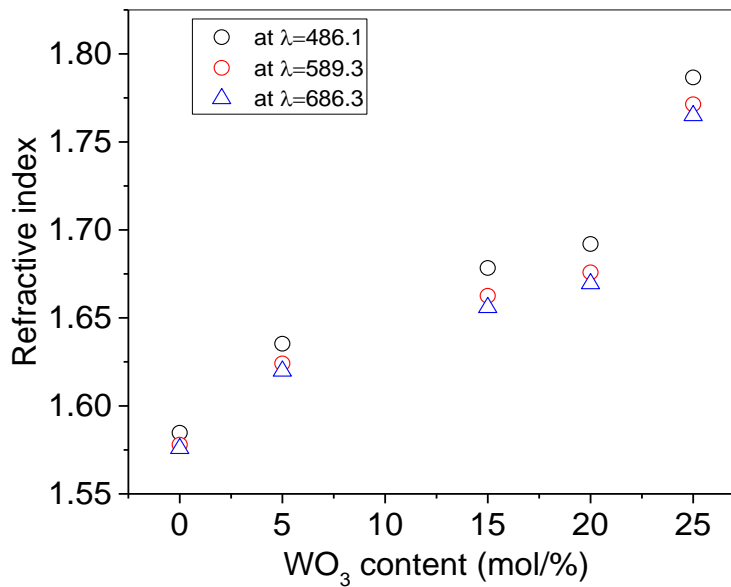


Figure III. 13: Refractive index of SNWx glasses at selective wavelengths.

As shown in Figure III. 12 For SNW25 glass, refractive index measurements indicate that n decreases with an increasing wavelength from 400 to 700 nm, mainly due to the dispersion of the refractive index vs wavelength $dn/d\lambda$. Experimentally, the Abbe number has commonly

Chapter III: Structural and physical properties of glasses

used to express the refractive index, dispersion $dn/d\lambda$ of the refractive index is given by the following formula:

$$v_d = n_D - 1/n_F - n_c \quad (\text{III. 10})$$

Where n_C , n_D and n_F are the refractive indices of the material at the wavelengths of the Fraunhofer C, D₁, and F spectral lines (656.3, 589.3, and 486.1 nm, respectively) [43]. The compositional dependence of the Abbe number of these glasses is indicated in Figure III. 14. We can see the linearity between the Abbe number and the composition of the glass according to WO₃ content. The Abbe number of SNW_x glasses is from 40 to 30 with increasing WO₃ content from 5 to 25 (mol. %). Traditionally, optical glasses with an Abbe number > 50 have been called crown glasses, while for < 50, they have been considered flint glasses [44]. Therefore, SNW5, SNW15, SNW20 and SNW25 glasses, which have an Abbe number less than 50, can be considered flint glasses, i.e. glasses with high refractive index and a high degree of light dispersing power compared to other types of glass, thus potential candidates for optical devices.

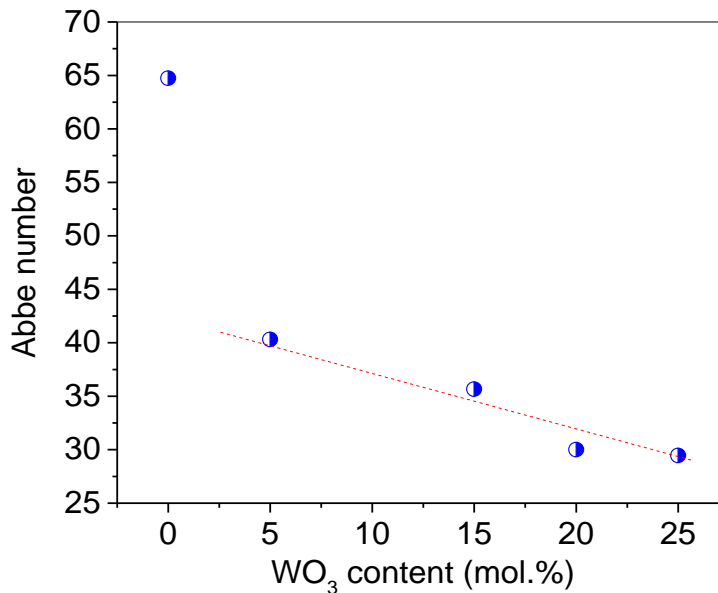


Figure III. 14: Compositional dependence of the Abbe number in the SNW_x glasses, line is drawn as guide for the eyes.

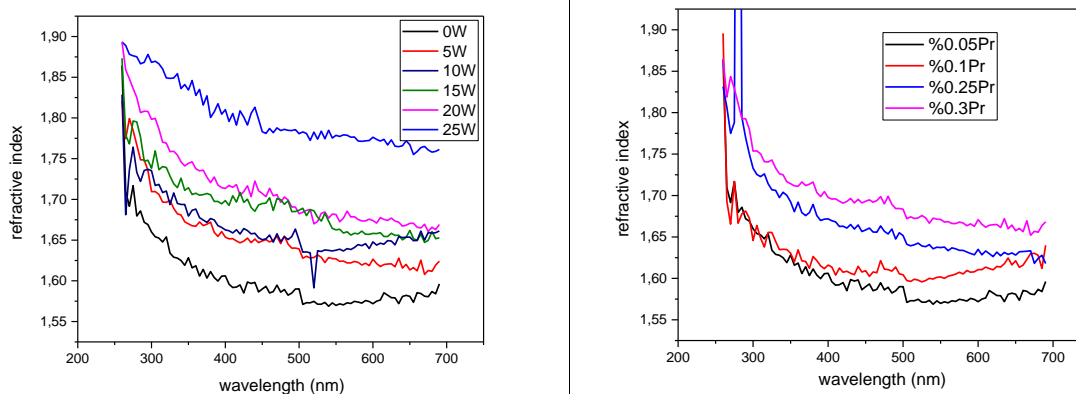


Figure III.15: The results of refractive index of the glasses.

Figure III.15 shows the refractive index increases with WO_3 , Pr_2O_3 , concentration, in the respect of WO_3 concentration, at 600 nm (1.62, 1.67, 1.72, 1.78, 1.82, 1.83) at 655 nm (1.61, 1.68, 1.72, 1.80, 1.83, 1.84), it related to the increase of non-bridging oxygen's (NBOs) and the molar mass of the glass elements (the electronic density). The density of WO_3 is 7, 16 g/cm^3 higher than that of NaPO_3 : 2, 48 g/cm^3 , the tungsten increase from 0 to 25 with the decrease of phosphate from 40 to 20 thus to make increasing in refractive index, also the tungsten atom is highly polarizable. It therefore, interacts strongly with light transmitted and thus modifies some of its properties such as its speed. Moreover, the introduction of transition metals WO_3 in glass generally increases their refractive index [45], which also can be explained by the fact that WO_6 units are more polarizing than SbO_3 units. In addition, the rise in WO_3 content results in W–O–W linkages, As a result, WO_3 Indicated large clusters of WO_6 . These clusters are considerably more polarizing than WO_6 units, the refractive index decreases with the increasing wavelength of the incident photon as seen in Figure III.15 [46, 47].

On the other hand, the density of Pr_2O_3 is 7,07 g/cm^3 higher than other elements in SNW_xPr glasses [48].

III. Conclusion:

In this chapter, we have studied the different structural, thermal, mechanical, physical, and optical properties of the three systems SN_xWr glasses with different concentrations of WO_3 (0-25 mol.%), SNW_xPr ($x = 0.05, 0.1, 0.25, 0.3$) and $\text{SNWPr}_{0.1x}\text{Yb}$ ($x = 0.25, 0.5, 0.75, 1$) mol% glasses are very thermally stable and have good transparency were prepared using a melt quenching process, The Fourier transform infrared (FTIR) and Raman spectra show that glasses include SbO_3 , PO_3^{-2} , WO_4 , and WO_6 groups with P-O-W, Sb-O-P, P-O-P, and W-O-W vibrations, such increase is also observed for the measurement of density, micro hardness, and the elastic moduli (longitudinal modulus (L), shear modulus (G), bulk modulus (K), and Young's modulus (E)). However, Poisson's ratio constant is practically invariant; the insertion of WO_3 reduces the optical band gap while the insertion of Pr_6O_{11} then Yb_2O_3 remains constant and increase the refractive index, the glasses studied prove to be potential candidates for optical devices.

References:

- [1]. Y. M. Moustafa, K. EL-EGILI, *Journal of Non-Crystalline Solids*, Amsterdam, 240, 1-3, (1998)144-153.
- [2]. D.F.Franco, H. Fares, A.E.Souza, S.H.Santagneli, M. Nalin, *eclética química journal*, 42, (2017) 51-52.
- [3]. Y. C. Ratnakaram, S. Babu, L. KrishnaBharat, C. Nayak, *Journal of Luminescence*175 (2016)57-66.
- [4]. B. Montanari, A. J. Barbosa, S. J.L. Ribeiro, Y. Messaddeq, G.Poirier, Maximo S. Li, *Applied Surface Science* 254 (2008) 5552-5556.
- [5]. N. ElkhoshkhanyHager M. Mohamed, El.S. Yousef, *UV–Vis-NIR, Results in Physics* 13 (2019) 102-222.
- [6]. I.W. Donald, *Preparation, J. Mater. Sci.* 28 (1993) 2841–2886.
- [7]. M.F. Daniel, B. Desbat, J.C. Lassegues, B. Gerand, M. Figlarz, *J. Solid State Chem.* 67 (1987) 235–247.
- [8]. H. Fares, I.Jlassi, H. Elhouichet, M. Férid, *Journal of Non-Crystalline Solids* 396-397 (2014) 1-7.
- [9]. D. Manzani, T. Gualberto, J. M.P. Almeida , M. Montesso , C. R.Mendonça ,V. A.G. Rivera , L. D. Boni , M.Nalin , S. J.L. Ribeiro, *Journal of Non-Crystalline Solids* 443 (2016) 82–90.
- [10]. N.H. RAY, *J. Non-Cryst. Solids*, 15 (1974) 423-434.
[https://doi.org/10.1016/0022-3093\(74\)90148-3](https://doi.org/10.1016/0022-3093(74)90148-3).
- [11]. M. Tatsumisago, I. Sakono, T. Minami, M. Tanaka, *J. Mater. Sci.*, 17 (1982) 3593-3597. <https://doi.org/10.1007/BF00752202>.
- [12]. R. G. Gossink, *Technische Hogeschool Eindhoven.* (1971). <https://doi.org/10.6100/IR125012>
- [13]. W. Kauzmann, *Chem. Rev.*, 43 (1948) 219.
<https://doi.org/10.1021/cr60135a002>.
- [14]. M. Nalin, Y. Messaddeq, S. J. L. Ribeiro, M. Poulain, V. Briois, G. Brunklaus, C. Rosenhahn, B. D. Mosel and H. Eckert, *J. Mater. Chem.*, 14(2004) 3398-3405.
<https://doi.org/10.1039/B406075J>.
- [15]. C. C. de Araujo, W. Strojek, L. Zhang, H. Eckert, G. Poirier, S. J. L. Ribeiro and Y. Messaddeq, *J. Mater. Chem.*, 32(2006). <https://doi.org/10.1039/B605971F>.

- [16]. A. E. Ersundu, M. Çelikbilek, M. Baazouzi, M. T. Soltani, J. Troles, & S. Aydin, *Journal of alloys and compounds*, 615(2014) 712-718.
- [17]. R. D. Shannon, *Acta Crystallogr. A*, 32 (1976) 751-67. <https://doi.org/10.1107/S0567739476001551>.
- [18]. N. W. Sangwaranatee, N. Kiwsakunkran, & J. Kaewkhao, *Journal of Physics* 1428-1 (2020) 012031.
- [19]. K. V. Shah, V. Sudarsan, M. Goswami, A. Sarkar, S. Manikandan, R. Kumar, B. I. Sharma, V. K. Shrikande and G. P. Kothial, *Bull. Mater. Sci.*, 2655(2003) 715–720.
- [20]. S. Chenu, R. Lebullenger and J. Rocherulle, *J. Mater. Sci.*, 45 (2010) 6505–6510 <https://doi.org/10.1007/s10853-010-4739-2>.
- [21]. M. Hamzaoui, S. Azri, M. T. Soltani, R. Lebullenger, M. Poulain, *Phys. Scr*, 157 (2013). <https://doi.org/10.1088/0031-8949/2013/T157/014029>.
- [22]. M. Yamane, J. D. Mackenzie, *J. Non-Cryst. Solids*, 15 (1974) 153. [https://doi.org/10.1016/0022-3093\(74\)90044-1](https://doi.org/10.1016/0022-3093(74)90044-1).
- [23]. A. R. Hilton, C. E. Jones and M. Baru, *Phys. Chem.* 105. (1966).
- [24]. D. Venturini, M. S. Cenci, F. Demarco, G. B. Camacho, *Powers JM.* 31 (2006) 11–17.
- [25]. S. Azianty, A. K. Yahya, *Journal of Non-Crystalline Solids*, 378 (2013) 234–240.
- [26]. C. Eevon, M. K. Halimah, Z. Azmi, & C. Azurahaman, *Chalcogenide Letters*, 13(6) (2016) 281-289.
- [27]. S. Azianty, A. K. Yahya, *J. Non-Cryst. Solids*, 378 (2013) 234–240. <https://doi.org/10.1016/j.jnoncrysol.2013.07.016>.
- [28]. S. Yousefa, A. Adawyb, N. El Koshkanyb, E. R. Shaaban, *J. Phys. Chem. Solids*. 67 (2006) 1649–1655. <https://doi.org/10.1016/j.jpcs.2006.02.014>.
- [29]. M. Çelikbilek, A. Erçin Ersundu, S. Aydin, *J. Am. Ceram. Soc.* 96 (2013) 1470–1476.
- [30]. S. Azianty, A. K. Yahya, *J. Non-Cryst. Solids* 378 (2013) 234–240.
- [31]. S. N. Nazrin, M. K. Halimah, F. D. Muhammad, J. S. Yip, L. Hasnimulyati, M. F. Fazny, I. Zaitizila, *Journal of Non-Crystalline Solids*, 490 (2018) 35–43.
- [32]. Y. B. Saddeek, K. Aly, T. Alharbi, A. Dahshan, S. A. Issa, M. Ahmad, *Applied Physics A*, 125-11 (2019) 1-6.

- [33]. T. Rouxel, *J. Am. Ceram. Soc.*, 90 (2007) 3019–3039. <https://doi.org/10.1111/j.1551-2916.2007.01945.x>.
- [34]. B. Zhang, Q. Chen, L. Song, L. Huiping, H. Fengzhen, J. Zhang, *Journal of non-crystalline Solids* 354 (2008) 1948–1954.
- [35]. S.Y. Moustafa, M.R. Sahar, S.K. Ghoshal, *Results phys.* 7 (2017) 1396-1411.
- [36]. R. Barczynski, *Journal of non-crystalline solids*, Amsterdam, 354, 35-39, (2008) 4275-4277.
- [37]. P. P. González-Borrero, F. Sato, A. N. Medina, M. L. Baesso, A. C. Bento, G. Baldissera, C. Persson, G. A. Niklasson⁴, C. G. Granqvist, and A. Ferreira da Silva, *Appl. Phys. Lett.*, 96 (2010)061-909. <https://doi.org/10.1063/1.3313945>.
- [38]. D. Holland, M. R. Sahar, M.M. Ahmed, *Mater. Sci. Forum*, 67–68 (1991) 257–262. doi:10.4028/www.scientific.net/MSF.67- 68.257.
- [39]. P. Hee, R. Christensen, Y. Ledemi, J. E. C. Wren, M. Dussauze, T. Cardinal, E. Fargin, S.Kroeker and Y. Messaddeq, *J. Mater. Chem. C*. 2(2014) 7906-7917. <https://doi.org/10.1039/C4TC01024H>.
- [40]. M. Nalin, G. Poirier, S.J.L. Ribeiro, Y. Messaddeq, L. Cescato, *Journal of Non-Crystalline Solids* 353 (2007)1592–1597.
- [41]. T. Som, B. Karmakar, *J. Non-Cryst. Solids*, 356 (2010) 987–999. <https://doi.org/10.1016/j.jnoncrysol.2010.01.026>.
- [42]. P. Petkova , M.T. Soltani , S. Petkova and V. Nedkova, *ACTA PHYSICA POLONICA A*, 121-1 (2012) 759.
- [43]. G. Ghosh, *Appl. Opt.*, 36 (1997) 1540. <https://doi.org/10.1364/AO.36.001540>.
- [44]. J.E. Shelby, *Optical Materials-Color Filter and Absorption Glasses*, Editor(s): Robert D. Guenther, *Encyclopedia of Modern Optics*, Elsevier, 2005, Pages 440-446, ISBN 9780123693952, <https://doi.org/10.1016/B0-12-369395-0/00871-X>.
- [45]. S. H. Kim, T. Yoko, *J. Am. Cer. Society*, 78 (4) (1995)1061-1065.
- [46]. S.k. Ahmmad, M. A. Samee, A. Edukondalu, and S. Rahman, *Results in physics*, 2 (2012) 175-181.
- [47]. K. Yoshimoto, A. Masuno, H. Inoue, and Y. Watanabe, *Journal of the American Ceramic Society*, 95-11 (2012) 3501–3504.
- [48]. C. Primož, *Spectroscopy Techniques and Projects at 1.2-m UK Schmidt Telescope*. (2012).

**Chapter IV- Spectroscopic study of the
Pr³⁺doped and Pr³⁺ /Yb³⁺ co-doped Sb₂O₃-
WO₃-NaPO₃ glasses.**

Introduction:

Antimony oxide glasses are favorable for optical amplifiers because of their properties [1]. The addition of WO₃ to various amorphous materials makes them photochromic. In addition, the luminescence characteristics can be influenced [2, 3]. The attention paid to broadband optical amplifiers has constantly stimulated research on NIR transmitters. Among the RE, the praseodymium Pr³⁺ ion is particularly interesting because of its broadband NIR luminescence in the low-loss wavelength region which corresponds to the ¹D₂ → ¹G₄ transition of Pr³⁺. Praseodymium doped glasses have many applications in devices such as semiconductor lasers where laser action in the visible spectral region has been observed for the transition ¹D₂ → ³H₄, because its energy level contains many metastable multiples ³P_{0,1,2}, ¹D₂, ¹G₄ which offer emission in the blue, green, orange and red wavelengths [4,5]. Another important rare earth element consist of Ytterbium Indeed, Yb³⁺ is important for its use as an infrared sensitizer due to its large effective absorption cross section, and as an effective excitation donor to other rare earth ions, the combination of Pr³⁺ and Yb³⁺ ions have a greater potential for further development in optical applications[6]. In this chapter, we study the visible and nearby emission infrared of the Pr³⁺ ion and Pr³⁺/Yb³⁺ of glasses in the compositions 47.5 Sb₂O₃ 47.5 NaPO₃ 5 WO₃- x Pr₂O₃ (x= 0.05, 0.1, 0.25, 0.3), 47.5 Sb₂O₃ 47.5 NaPO₃ 5 WO₃ 0.1 Pr₂O₃ xYb₂O₃, (x= 0.25, 0.5, 0.75, 1), using the theory of Judd-Ofelt (J-O) to determine the spectroscopic properties (absorption and emission cross sections, radiative lifetime, etc.).

IV. Spectroscopic properties

IV. 1. Absorption spectroscopy:

From the absorption spectra, it is possible to calculate the absorption coefficients as well as the absorption cross sections at different wavelengths. In addition, various spectroscopic information's can be determined, such as the probabilities of radiative transitions, branching ratios, integrated emission cross sections and the radiative lifetime of different energy levels of rare earth ions, using Judd-Ofelt analysis.

Chapter IV- Spectroscopic study of the Pr³⁺doped and Pr³⁺/Yb³⁺ co-doped Sb₂O₃-WO₃-NaPO₃ glasses.

Absorption spectra for the glasses studied are recorded between 200 and 1100 nm at a spectral resolution of 0.1 nm using a Perkin Elmer Lambda 35 UV / Vis spectrophotometer. The optical density is defined by:

$$DO = A = -\log \frac{I}{I_0} \quad (\text{IV. 1})$$

With

A: is the absorbance or optical density at a wavelength λ .

I: transmitted intensity.

I₀: is the intensity of the incident beam.

On the other hand, Beer-Lambert's law describes the variation in the intensity of radiation electromagnetic radiation through a transparent medium (a glass), given by the following relation:

$$I(\lambda) = I_0(\lambda) \cdot e^{-\alpha(\lambda)d} \quad (\text{IV. 2})$$

Where:

$\alpha(\lambda)$: the absorption coefficient in cm⁻¹

d: the thickness of the sample.

By combining the two equations (IV.1) and (IV.2), we obtain:

$$\alpha(\lambda) = \frac{DO \cdot \ln 10}{d} = \frac{2.303 \cdot DO}{d} \quad (\text{IV. 3})$$

The effective absorption section σ_{abs} at the wavelength λ of a transition between the level of rare earth is the coefficient of proportionality between the absorption coefficient $\alpha(\lambda)$ and the number of doping ions per unit of volume N (cm⁻¹), given by the following relation:

$$\sigma a(\lambda) = \frac{\alpha(\lambda)}{N} \quad (\text{IV. 4})$$

The number of N-doping ions per cm³ can be expressed by the relationship (IV.5):

$$N(\text{ions/cm}^3) = \frac{(b \cdot N_A \cdot \rho \cdot x)}{M_{\text{glass}}} \quad (\text{IV. 5})$$

With

x: The concentration of the rare earth ion in molar percentage.

N_A: The number of Avogadro (6.022045 * 10²³ mol⁻¹).

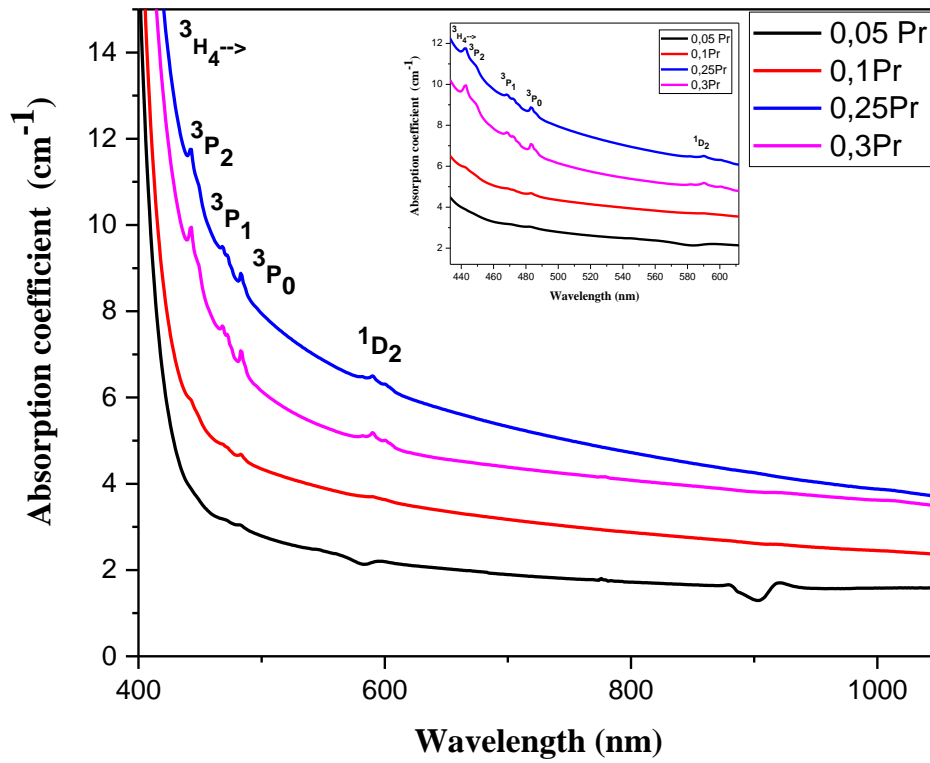
ρ: The density of the glass

b: Factor represents the number of rare earth atoms in the molecule.

M_{glass}: The molar mass of the glass.

➤ **Case of 47.5 Sb₂O₃ 47.5 NaPO₃ 5 WO₃- x Pr₆O₁₁ glasses:**

The absorption spectra of glasses doped with praseodymium are shown in Figure (IV.1) From these spectra, there are eight absorption bands. Four absorption bands in the visible region and four bands in the infrared attributed to internal transitions of the ⁴f₂ configuration of the Pr³⁺ ion at 2269, 1974, 1549, 1449, 590, 483, 472 and 443 nm, and corresponding to the absorptions of the ground state ³H₄ to the excited states ³H₆, ³F₂, ³F₃, ³F₄, ¹D₂, ³P₀, ³P₁ and ³P₂, respectively. These absorption bands are used for the calculation of Judd-Oflet parameters.



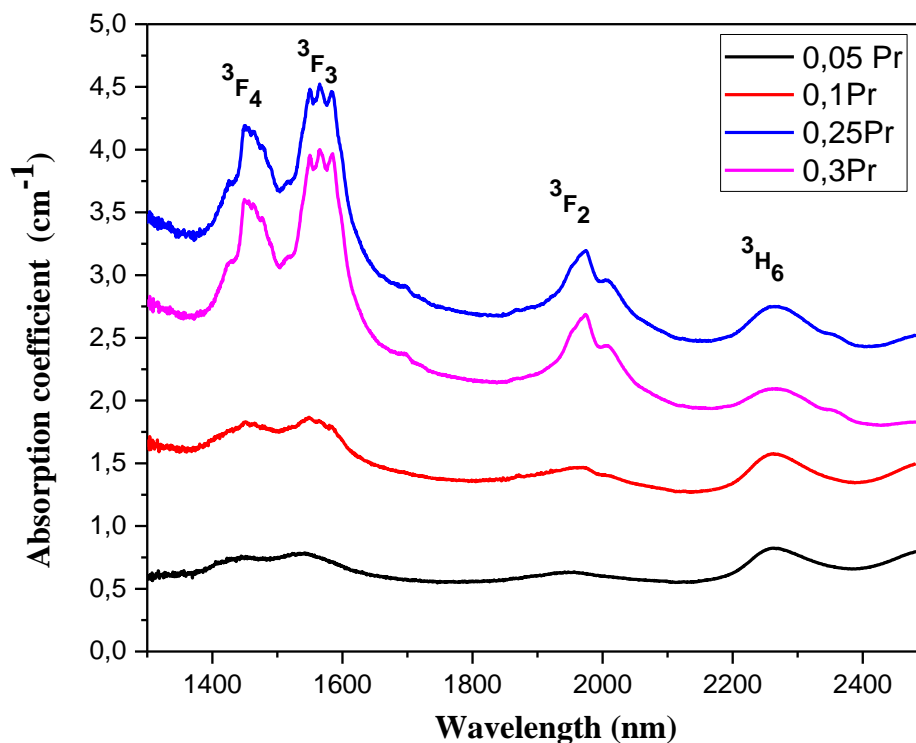


Figure IV.1: Absorption spectrum in visible, NIR of SNW glasses doped xPr³⁺ (x = 0.05, 0.1, 0.25, 0.3 mol.%)

The ³F₂, ³F₃ and ³F₄ bands show that there is a double peak structure, due to electric dipolar and low magnetic dipole contribution [7] which is neglected in our calculation. It can be noted that there is no peak absorption of level ¹G₄, transmitter level for transition to 1.3. The optical density of the different bands was found to increase with the dopant Pr³⁺ in the glasses.

Chapter IV- Spectroscopic study of the Pr⁺³doped and Pr³⁺/Yb³⁺ co-doped Sb₂O₃-WO₃-NaPO₃ glasses.

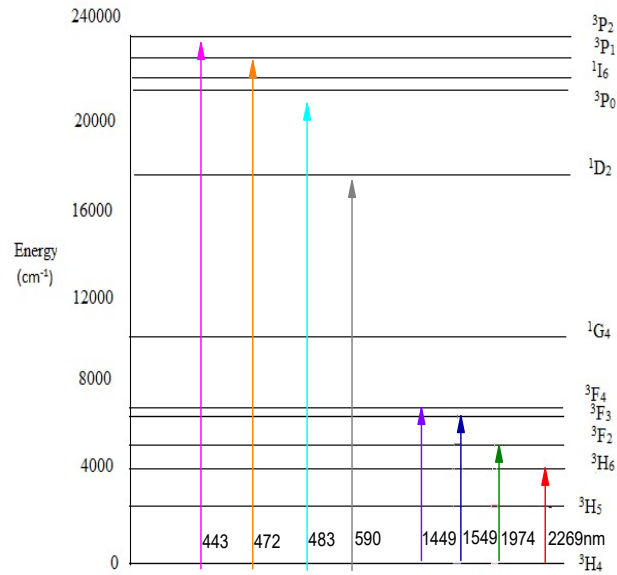


Figure (IV.2): Energy diagram of praseodymium ion in the SNW glasses.

IV. 1. 1. Determination of Judd-Ofelt parameters:

IV. 1. 1. 1 Oscillator strengths and Judd-Ofelt intensity parameters

Judd-Ofelt theory allows us to determine the radiative properties of rare earth ions from the forces of oscillators F or the forces of transitions S via the determination of the phenomenological parameters Ω_2 , Ω_4 , Ω_6 . The measured oscillator force S_{meas} for an electrical dipole transition of each multiple was determined using the following expression [8]:

Chapter IV- Spectroscopic study of the Pr⁺³ doped and Pr⁺³/Yb³ co-doped Sb₂O₃-WO₃-NaPO₃ glasses.

$$S_{\text{meas}}(\mathbf{J} \rightarrow \mathbf{J}') = \frac{3ch(2J+1)}{8\pi^3\lambda e^2} \left[\frac{9n}{(n^2+2)^2} \right] \int \sigma(\lambda) d\lambda \quad (\text{IV. 6})$$

Judd-Ofelt theory provides a theoretical expression of oscillator strength [9], given by:

$$S_{\text{calc}}(\mathbf{J} \rightarrow \mathbf{J}') = \sum_{t=2,4,6} \Omega_t |\langle \psi | U^{(t)} | \psi' \rangle|^2 \quad (\text{IV. 7})$$

h: Planck constant

c: Speed of light in vacuum,

e: Charge of the electron

n: Refractive index

$\int \sigma(\lambda) d\lambda$: The integrated area of the absorption bands.

Judd-Ofelt analysis minimizes the square of the difference between S_{meas} (equ. IV. 6) and S_{calc} (equ. IV. 6) by the least squares method [10]. The reduced matrix elements of the tensor operator $U(t)$ of rank t , do not depend on the host matrix either and were calculated by Carnall [11]. The results obtained from the forces of the transitions, the RMS deviation and the Ω_t parameters of the SNWxPr⁺³ glasses are collated in Tables 1 and 2 respectively.

The calculations of the parameters of (J-O) S_{cd} , S_{cal} , r.m.s, of the 47.5 Sb₂O₃ 47.5 NaPO₃ 5 WO₃- x Pr₆O₁₁ (x= 0.05, 0.1, 0.25, 0.3) glasses are presented in table (IV.1).

Chapter IV- Spectroscopic study of the Pr³⁺ doped and Pr³⁺/Yb³⁺ co-doped Sb₂O₃-WO₃-NaPO₃ glasses.

Table IV.1: Transition, oscillator strength and RMS of 47.5 Sb₂O₃ 47.5 NaPO₃ 5 WO₃- x Pr₆O₁₁ (x= 0.05, 0.1, 0.25, 0.3) glasses.

Variations of Pr ₆ O ₁₁	X=0.05			X=0.1			X=0.25			X=0.3		
	λ_{max} (nm)	$S_{ed} \times 10^{-20}$	$S_{cal} \times 10^{-20}$	λ_{max} (nm)	$S_{ed} \times 10^{-20}$	$S_{cal} \times 10^{-20}$	λ_{max} (nm)	$S_{ed} \times 10^{-20}$	$S_{cal} \times 10^{-20}$	λ_{max} (nm)	$S_{ed} \times 10^{-20}$	$S_{cal} \times 10^{-20}$
Transition from ³H₄ to												
³ P ₂	443	3.47	2.65	443	1.94	1.740	443	0.163	0.682	443	0.071	0.628
³ P ₁	472	9.82	9.94	472	6.48	6.566	472	2.604	2.652	472	2.406	2.451
³ P ₀	483	16.3	14.9	483	10.75	9.787	483	4.322	3.863	483	3.992	3.558
¹ D ₂	590	7.74	9.12	590	5.11	5.983	590	2.054	2.340	590	1.897	2.153
³ F ₄	1449	0	1.04	1449	0	0.683	1449	0	0.269	1449	0	0.247
³ F ₃	1565	0	0.82	1565	0	0.551	1565	0	0.235	1565	0	0.219
³ F ₂	1974	0	0.81	1974	0	0.544	1974	0	0.232	1974	0	0.216
³ H ₆	2267	0	2.60	2267	0	1.703	2267	0	0.668	2267	0	0.615
RMS $\times 10^{-20}$	1.65			1.06			0.48			0.46		

Large r.m.s will be observed, which is mainly caused by inclusion of hypersensitive transition (³H₄ → ³P₂) only [12]. Therefore, in the present work, the Judd-Ofelt parameters were recalculated excluding the ³H₄ → ³P₂ transition, in order to reduce the r.m.s which gave a significant improvement.

The calculations of the parameters of χ and $\Sigma\Omega_t$ of the 47.5 Sb₂O₃ 47.5 NaPO₃ 5 WO₃- x Pr₆O₁₁ (x= 0.05, 0.1, 0.25, 0.3) glasses are presented in table (IV.2).

Chapter IV- Spectroscopic study of the Pr⁺³ doped and Pr⁺³/Yb³ co-doped Sb₂O₃-WO₃-NaPO₃ glasses.

Table IV.2: Judd-Ofelt parameters and spectroscopic quality factor of 47.5 Sb₂O₃ 47.5 NaPO₃ 5 WO₃- x Pr₆O₁₁ (x= 0.05, 0.1, 0.25, 0.3) glasses compared with other glass systems reported in the literature.

Glass code	References	Paramètres (J-O) ($\times 10^{-20}$ cm ²)				Trend
		Ω_2	Ω_4	Ω_6	$\chi = \Omega_4/\Omega_6$	
47,5S 47,5N 5W 0,05Pr	[Present]	11.63	4.77	17.88	0.26	$\Omega_4 < \Omega_2 < \Omega_6$
47,5S 47,5N 5W 0,1Pr	[Present]	7.67	3.19	11.71	0.27	$\Omega_4 < \Omega_2 < \Omega_6$
47,5S 47,5N 5W 0,25Pr	[Present]	3.075	1.316	4.567	0.28	$\Omega_4 < \Omega_2 < \Omega_6$
47,5S 47,5N 5W 0,3Pr	[Present]	2.839	1.268	4.200	0.30	$\Omega_4 < \Omega_2 < \Omega_6$
SL1W1Pr0.25	[13]	4.762	2.207	6.549	0.33	$\Omega_4 < \Omega_2 < \Omega_6$
TeO ₂ -WO ₃ -PbO- La ₂ O ₃	[14]	3.09	1.32	4.13	0.31	$\Omega_4 < \Omega_2 < \Omega_6$
PbO-Al ₂ O ₃ -SiO ₂	[15]	0.707	1.333	5.135	0.25	$\Omega_2 < \Omega_4 < \Omega_6$
PbO-Sb ₂ O ₃ -B ₂ O ₃	[16]	5.917	4.770	21.35	0.22	$\Omega_4 < \Omega_2 < \Omega_6$

When the JO model was applied with the (³H₄ → ³P₂) hypersensitive transition included in the procedure, it was observed that the omega, parameters assumed a negative value. But, with the exclusion of this transition, the omega (Ω_4) become positive and in this case, these parameters could be used to improve the calculated radiative properties of the glasses doped with Pr⁺³, this can be seen from the comparison between the calculated and experimental results of the radiative.

The parameters of (J-O) follow the trend $\Omega_2 < \Omega_4 < \Omega_6$ for SNWPr_x glasses (x = 0.05, 0.1, 0.25, 0.3 mol.%). Similar results have been reported in the literature [13, 14, 15, 16] The comparison of the values of the parameter Ω_2 for the four glass samples of Table (IV.2) shows a tendency to decrease with the increase in the Pr₆O₁₁ content (from 0.05 to 0.3 mol%). Generally, Ω_2 determines the covalence of the metal ligand bond while Ω_4 and Ω_6 represent the viscosity and rigidity of the host materials in which the ions are found [17]. The Ω_2 values show a strong asymmetric and covalent environment around the Pr⁺³ ions, caused mainly by the high contents of WO₃ with

the possible existence of the jump mechanism between the two tungsten sites (W⁺⁵, W⁺⁶) [18].

The value of Ω_6 is inversely proportional to the covalency of the Pr-O bond. The large Ω_6 value is probably due to the low optical basicity of glass without non-bridging oxygen ions, which was formed by the incorporation of alkali ions.

The similar behavior of Ω_2 and Ω_6 suggests that the environmental effect is dominant, The spectroscopy quality factor, $\chi = \Omega_4 / \Omega_6$ in our glasses vary from 0.26 to 0.30 giving low values. The low of this this factor predict high stimulated emission for the active laser medium [19, 20].

IV. 1. 1. 2. Calculation of the radiative parameters:

To study the fluorescence properties of Pr⁺³ in SNW glasses, the radiative properties such as radiative transition probability (A_{rad}), fluorescence branching ratio (B) and radiative lifetime (τ_{rad}) for the emission transitions have been calculated using the emission measurements and intensity parameters, The obtaining parameters Ω_2 , Ω_4 and Ω_6 makes it possible to calculate the radioactive emission probability $A_{rad}(J, J')$ according to the equation (IV. 8)[21].

$$A_{rad}(J, J') = \frac{64 \pi^4 e^2}{3h(2J+1)\lambda^3} \left[\frac{n(n^2+2)^2}{9} S_{ed} + n^3 S_{md} \right] \quad (IV. 8)$$

The radiative lifetime τ_{rad} of an excited level and the branching rate $\beta_{(JJ')}$ for each transition are defined by the relations (IV. 9) and (IV. 10) respectively [22], the data obtained are summarized in the table 3.

$$\tau_{rad}(J, J') = \frac{1}{\sum_{J'} A_{rad}(JJ')} \quad (IV. 9)$$

$$\beta_{(JJ')} = \frac{A_{rad}(JJ')}{\sum_{J'} A_{rad}(JJ')} \quad (IV. 10)$$

We present in tables (IV.3) the radiative properties such as the probability of radiative transition (A_{rad}), radiative lifetimes (τ_{rad}), and branching ratios (β) for the excited states $^3P_2, ^3P_1, ^3P_0, ^1D_2, ^3F_3$ for the SNW glasses doped with Pr⁺³.

Chapter IV- Spectroscopic study of the Pr⁺³ doped and Pr⁺³/Yb³ co-doped Sb₂O₃-WO₃-NaPO₃ glasses.

Table IV.3: The radiative parameters of 47.5 Sb₂O₃ 47.5 NaPO₃ 5 WO₃- x Pr₆O₁₁ (x= 0.05, 0.1, 0.25, 0.3) glasses.

Transition	Pr ₆ O ₁₁		X=0.05		X=0.1		X=0.25		X=0.3				
	λ_{max} (nm)	A_{rad} (s ⁻¹)	β	τ_{rad} (ms)	A_{rad} (s ⁻¹)	B	τ_{rad} (ms)	A_{rad} (s ⁻¹)	β	τ_{rad} (ms)	A_{rad} (s ⁻¹)	β	τ_{rad} (ms)
³ P ₂ → ³ H ₅	491	4188	1.0000	0.2388	2353.9	1.0000	0.4248	1089.8	1.0000	0.9176	1024.8	1.0000	0.9758
³ P ₁ → ³ H ₅	525	1357.1	0.6988	0.5149	907.6	0.6988	0.7699	387.5	0.6988	1.8033	360.8	0.6988	1.9370
→ ³ F ₃	695	585	0.3012		391.2	0.3012		167	0.3012		155.5	0.3012	
³ P ₀ → ³ H ₆	600	2761	0.4196	0.1520	1846.5	0.4196	0.2273	788.4	0.4196	0.5323	734	0.4196	0.5717
→ ³ F ₂	642	2253.8	0.3425		1507.3	0.3425		643.5	0.3425		599.1	0.3425	
→ ³ F ₄	725	1565	0.2378		1046.6	0.2378		446.9	0.2378		416	0.2378	
¹ D ₂ → ³ H ₆	822	331.9	0.5978	1.8008	178	0.5978	3.3587	70	0.5978	8.5406	64.4	0.5978	9.2759
→ ³ F ₃	103	165.8	0.2986		88.9	0.2986		35	0.2986		32.2	0.2986	
→ ¹ G ₄	147	57.6	0.1037		30.9	0.1037		12.1	0.1037		11.2	0.1037	
³ F ₃ → ³ H ₄	163	430.3	1.0000	2.3239	233.5	1.0000	4.2818	92.2	1.0000	10.8469	84.9	1.0000	11.7746

We observe from the table (IV.3) that the higher β was observed for the ³P₂→³H₅ and ³F₃→³H₄ transitions, compared to β is weaker, than the ¹D₂ → ¹G₄, ¹D₂ → ³F₃ and ³P₀→³F₄ transitions. Usually, the higher A_{rad} values indicate the intensity of the stronger luminescence (³P₂→³H₅, ³P₀ → ³H₆, ³P₀ → ³F₂ and ³P₀ → ³F₄) suggests them to be probable laser transitions. It was also noted that the high radiative transition probability (4188 s⁻¹) is the ³P₂ → ³H₅ transition of 0.05 Pr⁺³ doped SNW glass. The probability of total radiative transition was in the order of ³P₂> ³P₀>³P₁> ³F₃>¹D₂ in all SNW glasses doped Pr⁺³. A greater probability of spontaneous emission high offers a better opportunity to get laser stocks. The radiative life time for a transition, τ_{rad} is reciprocal of A_{rad} . The minimum τ_{rad} values have been obtained for (³P₂→³H₅, ³P₀ → ³H₆, ³P₀ → ³F₂ and ³P₀ → ³F₄) transitions. This fact coupled with radiative lifetime for ³P₀ level further support the ³P₀ → ³H₆ and ³P₀ → ³F₂ transitions to be the most probable laser transitions and the ³P₀ level to be an efficient fluorescence level, respectively [23, 24].

Chapter IV- Spectroscopic study of the Pr³⁺ doped and Pr³⁺/Yb³⁺ co-doped Sb₂O₃-WO₃-NaPO₃ glasses.

The integrated emission, effective section (Σ) is related to the radioactive transition probability (A_{rad}) according to the following relation [25]

$$\Sigma \left[\frac{\lambda_p^2}{8\pi c n^2} \right] A_{rad}(J, J') \quad (IV. 11)$$

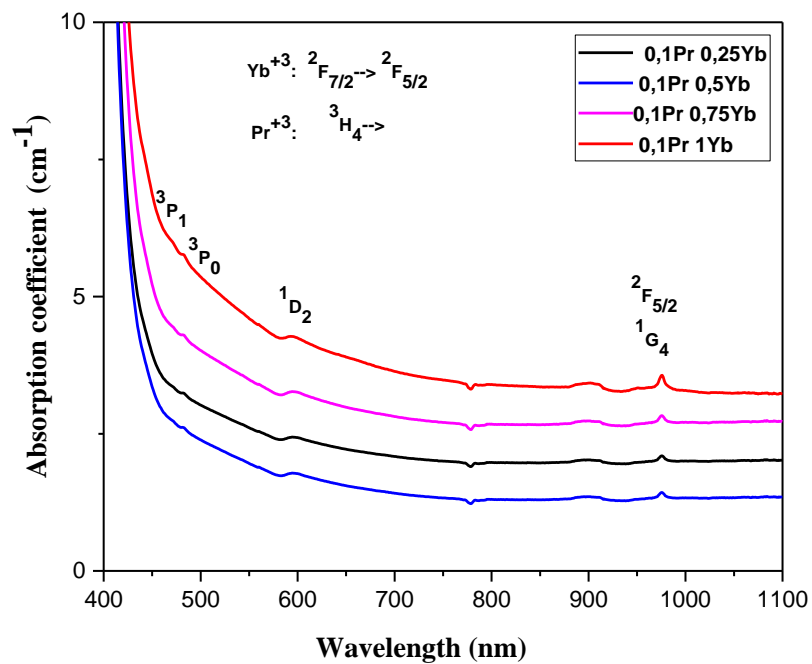
The values of the integrated emission of effective emission section (Table IV.4) are greater in 0.05 Pr and from $0.3 \cdot 10^{-18}$ cm to $15.17 \cdot 10^{-18}$ cm which indicates the possibility of the laser effect with these glasses.

Table IV.4: the integrated emission efficiency section (Σ) values.

Transition	Σ (10^{-18} cm)				
	λ_{max} (nm)	X=0.05	X=0.1	X=0.25	X=0.3
³ P ₂ → ³ H ₅	491	13.4	7.532	3.487	3.279
³ P ₁ → ³ H ₅	525	4.96	3.320	1.418	1.320
→ ³ F ₃	695	3.75	2.508	1.071	0.997
³ P ₀ → ³ H ₆	600	13.19	8.822	3.767	3.507
→ ³ F ₂	642	12.33	8.245	3.520	3.277
→ ³ F ₄	725	10.92	7.301	3.117	2.902
¹ D ₂ → ³ H ₆	822	2.98	1.596	0.628	0.578
→ ³ F ₃	1036	2.36	1.266	0.498	0.459
→ ¹ G ₄	1474	1.66	0.890	0.350	0.322
³ F ₃ → ³ H ₄	1630	15.17	8.236	3.251	2.995

➤ Case of Sb₂O₃ 47.5 NaPO₃ 5 WO₃ 0.1 Pr₆O₁₁ xYb₂O₃ co-doping praseodymium / ytterbium glasses:

In Figure (IV.3) are presented the absorption spectra of 7.5 Sb₂O₃ 47.5 NaPO₃ 5 WO₃ 0.1 Pr₆O₁₁ xYb₂O₃, (x= 0.25, 0.5, 0.75, 1) glasses.



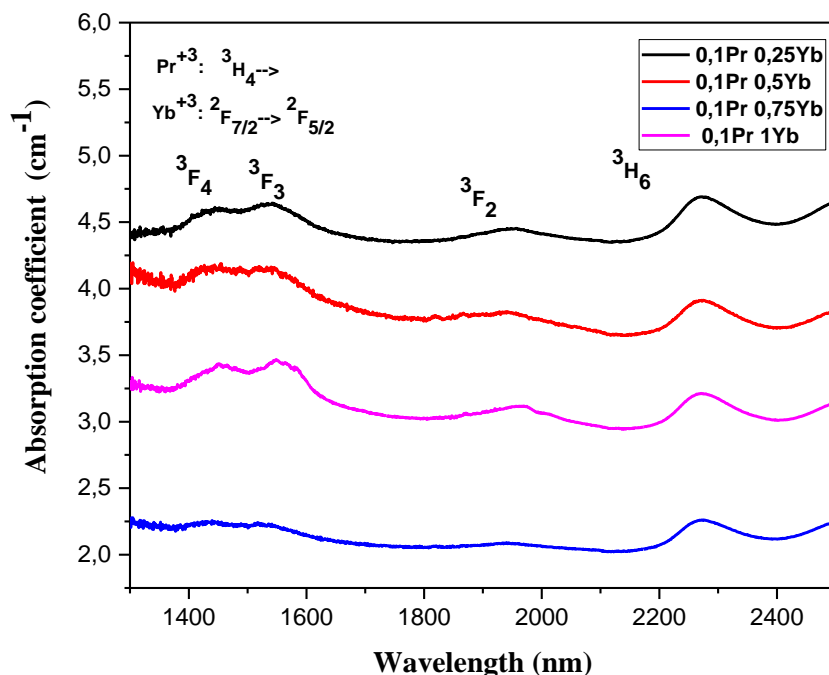


Figure IV.3: Absorption spectrum visible and NIR of 47.5 Sb₂O₃ 47.5 NaPO₃ 5 WO₃ 0.1 Pr₂O₃ xYb₂O₃, (x= 0.25, 0.5, 0.75, 1) glasses.

Fig IV.3 shows the bands assigned at 1974, 1565, 1449, 975, 590, 483, 470 are related to the transitions of Pr³⁺: ³H₄→³F₂, ³H₄→³F₃, ³H₄→³F₄, ³H₄→¹G₄, ³H₄→¹D₂, ³H₄→³P₀ and ³H₄→³P₁. The characteristic absorption of Yb³⁺ around 975 nm to the transition from the fundamental level ²F_{7/2} to the exciting level ²F_{5/2}. This intense band will be used to excite the samples in order to obtain the luminescence of the Pr³⁺ ions in the visible by energy transfer. The general appearance of the spectra is substantially the same except for the band at 975, the absorbance of which increases with the concentration of Yb³⁺, $\sigma_{\text{abs}}(975 \text{ nm } 0.5\text{Yb}^{+3}) = 4.60326 \times 10^{21} \text{ cm}^2$.

IV. 1. 2. Judd-Ofelt Analysis:

The (³H₄→³P₂) hypersensitive transition in the least squares fit method. The effect can be due to a small energy difference between 4f and 5d orbitals, which lead to strong 4f-5d mixing between these orbitals for Pr³⁺ ion. The JO intensity parameter was calculated by excluding hypersensitive transition (³H₄→³P₂), Significant improvement is found in the root mean square deviation (rms), Positive U₂ intensity values. The radiative transitions within the 4f configuration of Pr³⁺ ions can be analysed from the Judd-Ofelt theory, using absorption

Chapter IV- Spectroscopic study of the Pr³⁺doped and Pr³⁺/Yb³⁺ co-doped Sb₂O₃-WO₃-NaPO₃ glasses.

spectra of the Pr³⁺/Yb³⁺ glass. The oscillator strengths (f) for the observed transitions of Pr³⁺ ions with r.m.s deviation are given in Table IV.5. The low r.m.s deviation between experimental and calculated oscillator strengths indicates the validity of Judd-Ofelt theory.

Table IV.5: Transition, oscillator strengths and RMS of 47.5 Sb₂O₃ 47.5 NaPO₃ 5 WO₃- 0.1 Pr₆O₁₁ xYb₂O₃ (x= 0.25, 0.5, 0.75, 1) glasses.

Variations of Yb ₂ O ₃	X=0.25			X=0.5			X=0.75			X=1		
	λ_{max} (nm)	$S_{ed} \times 10^{-20}$	$S_{cal} \times 10^{-20}$	λ_{max} (nm)	$S_{ed} \times 10^{-20}$	$S_{cal} \times 10^{-20}$	λ_{max} (nm)	$S_{ed} \times 10^{-20}$	$S_{cal} \times 10^{-20}$	λ_{max} (nm)	$S_{ed} \times 10^{-20}$	$S_{cal} \times 10^{-20}$
³ P ₁	470	0.661	0.542	470	0.108	0.262	470	0.369	0.167	470	0.5	11.89
³ P ₀	483	2.950	3.034	483	1.495	1.546	483	1	1.040	483	0.752	78.63
¹ D ₂	590	4.779	3.662	590	2.422	1.802	590	1.62	1.169	590	1.218	85.21
¹ G ₄	975	0	1.616	975	0	0.771	975	0	0.483	975	0	33.92
³ F ₄	1449	0	0.110	1449	0	0.053	1449	0	0.034	1449	0	2.43
³ F ₃	1565	0	0.799	1565	0	0.415	1565	0	0.284	1565	0	21.85
³ F ₂	1974	0	0.799	1974	0	0.415	1974	0	0.284	1974	0	21.85
RMS $\times 10^{-20}$		1.13			0.60			0.47			0.42	

Table IV.6: Judd-Ofelt parameters and spectroscopic quality factor of 47.5 Sb₂O₃ 47.5 NaPO₃ 5 WO₃- 0.1 Pr₆O₁₁ xYb₂O₃ (x= 0.25, 0.5, 0.75, 1) glasses compared with other glass.

Glass code	References	Paramètres (J-O) ($\times 10^{-20}$ cm ²)				Trend
		Ω_2	Ω_4	Ω_6	$\chi = \Omega_4/\Omega_6$	
47,5S47,5N5W0,1Pr0.25Y	[Present]	1.654	4.621	2.793	1.654	$\Omega_2 < \Omega_6 < \Omega_4$
47,5S47,5N5W0,1Pr0.5Yb	[Present]	0.834	2.400	1.311	1.831	$\Omega_2 < \Omega_6 < \Omega_4$
47,5S47,5N5W0,1Pr0.75Y	[Present]	0.555	1.643	0.806	2.038	$\Omega_2 < \Omega_6 < \Omega_4$
47,5S 47,5N 5W 0,1Pr1Yb	[Present]	0.415	1.265	0.553	2.287	$\Omega_2 < \Omega_6 < \Omega_4$
80B ₂ O ₃ 10Na ₂ O 9BaF ₂ 1PrF ₃	[26]	0.17	8.41	4.23	1.98	$\Omega_2 < \Omega_6 < \Omega_4$
ZBLAN	[27]	2.90	6.40	5.50	1.41	$\Omega_2 < \Omega_6 < \Omega_4$
Zinc Sodium Sulphate	[28]	3.44	15.19	10.22	1.48	$\Omega_2 < \Omega_6 < \Omega_4$
Phosphat	[29]	3.89	1.01	0.55	1.83	$\Omega_2 > \Omega_4 > \Omega_6$

Chapter IV- Spectroscopic study of the Pr⁺³ doped and Pr⁺³/Yb⁺³ co-doped Sb₂O₃-WO₃-NaPO₃ glasses.

The order of magnitude of J-O parameters is $\Omega_2 < \Omega_6 < \Omega_4$. Results similar have been reported in the literature [26, 29], They exhibit a tendency to decrease with increasing Ytterbium content, which can be attributed to the high covalency and the high degree of homogeneity.

The Ω_2 parameter shows a strong asymmetric and covalent environment around the Pr⁺³ ions. The Ω_6 parameter is inversely proportional to the covalency of the Ln-O (lanthanide-oxygen) bonds and can be adjusted by the composition of the glass. The parameter Ω_4 decreases for more concentrations of Yb₂O₃ which suggests the formation of non-bridging oxygen, which can allow the coordination of rare earth ions, which indicates that our glasses have a higher degree of covalency between Pr⁺³ and O⁻². The spectroscopy quality factor, $\chi = \Omega_4 / \Omega_6$, from 2.29 to 1.65 is frequently used to estimate the laser emission efficiency of these glasses [30, 31].

**Chapter IV- Spectroscopic study of the Pr³⁺ doped and Pr³⁺/Yb³⁺ co-doped
Sb₂O₃-WO₃-NaPO₃ glasses.**

Table IV.7: The radiative parameters of 47.5 Sb₂O₃ 47.5 NaPO₃ 5 WO₃- 0.1 Pr₆O₁₁ xYb₂O₃ (x= 0.25, 0.5, 0.75, 1) glasses.

Yb ₂ O ₃	X=0.25				X=0.5				X=0.75				X=1			
Transitio n	λ_{max} (nm)	A_{rad} (s ⁻¹)	β	τ_{rad} (ms)	A_{rad} (s ⁻¹)	B	τ_{rad} (ms)	A_{rad} (s ⁻¹)	β	τ_{rad} (ms)	A_{rad} (s ⁻¹)	β	τ_{rad} (ms)			
³ P ₂ → ³ H ₅	499	899.9	1.0000	1.1113	572.4	1.0000	1.7471	460.8	1.0000	2.1703	404.9	1.0000	2.4698			
³ P ₁ → ³ H ₅	525	1314.7	0.6988	0.5315	682.8	0.6988	1.0234	467.4	0.6988	1.4949	359.9	0.6988	1.9416			
→ ³ F ₃	695	566.7	0.3012		294.3	0.3012		201.5	0.3012		155.1	0.3012	0.3012			
³ P ₀ → ³ H ₄	487	5002.1	0.4397		2597.9	0.4397		1778.5	0.4397		1369.3	0.4397	0.4397			
→ ³ H ₆	600	2674.8	0.2351	0.0879	1389.2	0.2351	0.1692	951.0	0.2351	0.2472	732.2	0.2351	0.3211			
→ ³ F ₂	642	2183.4	0.1919		1134.0	0.1919		776.3	0.1919		597.7	0.1919	0.1919			
→ ³ F ₄	725	1516.1	0.1333		787.4	0.1333		539.0	0.1333		415.0	0.1333	0.1333			
¹ D ₂ → ³ H ₆	822	0.0594	0.5978		29	0.5978		18.6	0.5978		13.4	0.5978	0.5978			
→ ³ F ₃	1036	29.7	0.2986	10.0585	14.5	0.2986	20.6431	9.3	0.2986	32.1841	6.7	0.2986	44.6879			
→ ¹ G ₄	1474	10.3	0.1037		5	0.1037		0.0032	0.1037		2.3	0.1037	0.1037			
³ F ₃ → ³ H ₄	1630	87.4	1.0000	11.4429	43	1.0000	23.2437	2.79	1.0000	35.8388	20.3	1.0000	49.1693			

Table IV.7 reports total radiative transition probabilities (A_{rad}), branching ratios (β) radiative and lifetimes (τ_{rad}) of excited states ³P₂, ³P₁, ³P₀, ¹D₂, ³F₃ for the SNW glasses codoped with Pr³⁺/Yb³⁺. It is observed that the trend of lifetimes decreases as ³F₃ > ¹D₂ > ³P₂ > ³P₁ > ³P₀. (The best results are the transitions of ³P₀). The fluorescence branching ratio (B), predicts the relative intensity of lines from given excited states and characterizes the lasing potential of that particular transition. There is a decreasing tendency of branching ratios for the emission transitions, ³F₃→³H₄ > ³P₂→³H₅ > ³P₁→³H₅ > ¹D₂→³H₆ > 0.5 > ³P₀→³H₄ > ³P₁→³F₃ > ¹D₂→³F₃ > ³P₀→³H₆ > ³P₀→³F₂ > ³P₀→³F₄ > ¹D₂→¹G₄, for a transition to be considered as favorable for

Chapter IV- Spectroscopic study of the Pr³⁺ doped and Pr³⁺/Yb³⁺ co-doped Sb₂O₃-WO₃-NaPO₃ glasses.

laser action, it should have a large (B) value Thus, the stronger fluorescence intensity may be found for ³P₀→³H₆ in visible region and ¹D₂→³F₃ in near infrared region.

The results collected in Table (IV.8), show that ΣΩt for the co-doped glasses Pr³⁺/Yb³⁺ decreases with the addition of Yb³⁺.

Table IV.8: The integrated emission efficiency section (Σ) values of 47.5 Sb₂O₃ 47.5 NaPO₃ 5 WO₃- 0.1 Pr₆O₁₁ xYb₂O₃ (x= 0.25, 0.5, 0.75, 1) glasses.

Transition	λ_{max} (nm)	Σ (10 ⁻¹⁸ cm)			
		X=0.25	X=0.5	X=0.75	X=1
³ P ₂ → ³ H ₅	499	2.97	1.892	1.523	1.338
³ P ₁ → ³ H ₅	525	4.81	2.498	1.710	1.317
→ ³ F ₃	695	3.63	1.887	1.292	0.995
³ P ₀ → ³ H ₄	487	15.75	8.178	5.598	4.310
→ ³ H ₆	600	12.78	6.638	4.544	3.499
→ ³ F ₂	642	11.94	6.203	4.247	3.270
→ ³ F ₄	725	10.58	5.493	3.761	2.895
¹ D ₂ → ³ H ₆	822	0.53	0.260	0.167	0.120
→ ³ F ₃	1036	0.42	0.206	0.132	0.095
→ ¹ G ₄	1474	0.30	0.145	0.093	0.067
³ F ₃ → ³ H ₄	1630	3.08	1.517	0.984	0.717

IV.2. Excitation spectrum and visible-NIR emission spectra and calculation of emission cross sections:

➤ Case of $47.5 \text{ Sb}_2\text{O}_3 \text{ } 47.5 \text{ NaPO}_3 \text{ } 5 \text{ WO}_3\text{- } x \text{ Pr}_6\text{O}_{11}$ glasses:

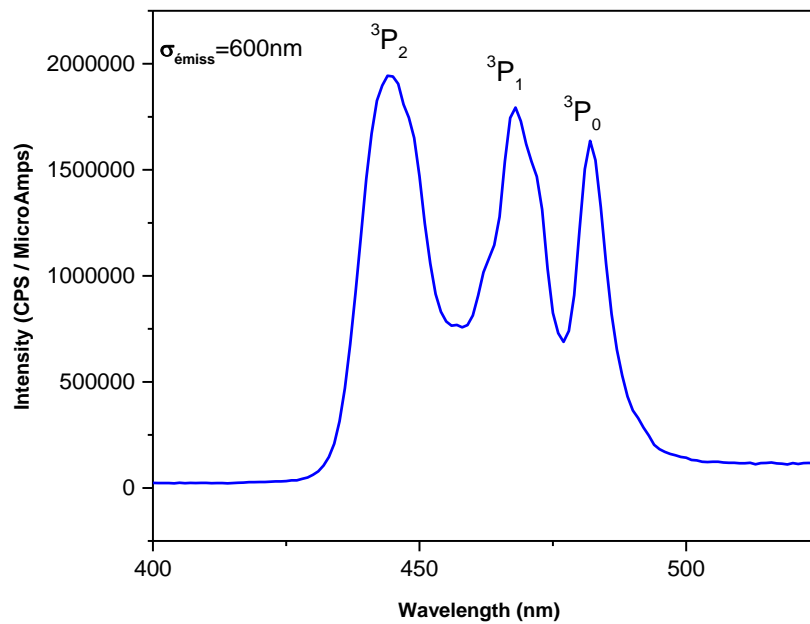


Figure IV.4: Excitation spectrum of SNW glasses doped 0.05 Pr^{3+} .

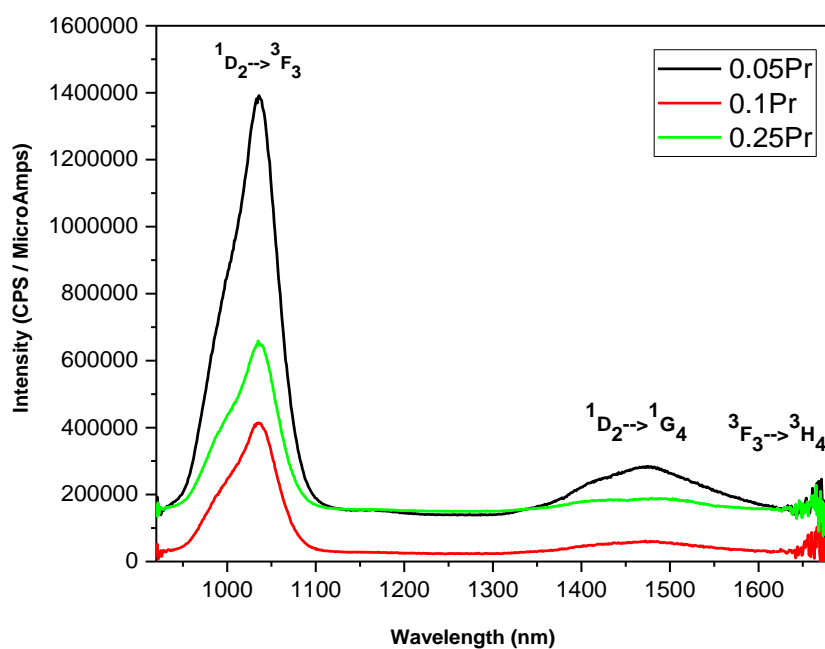
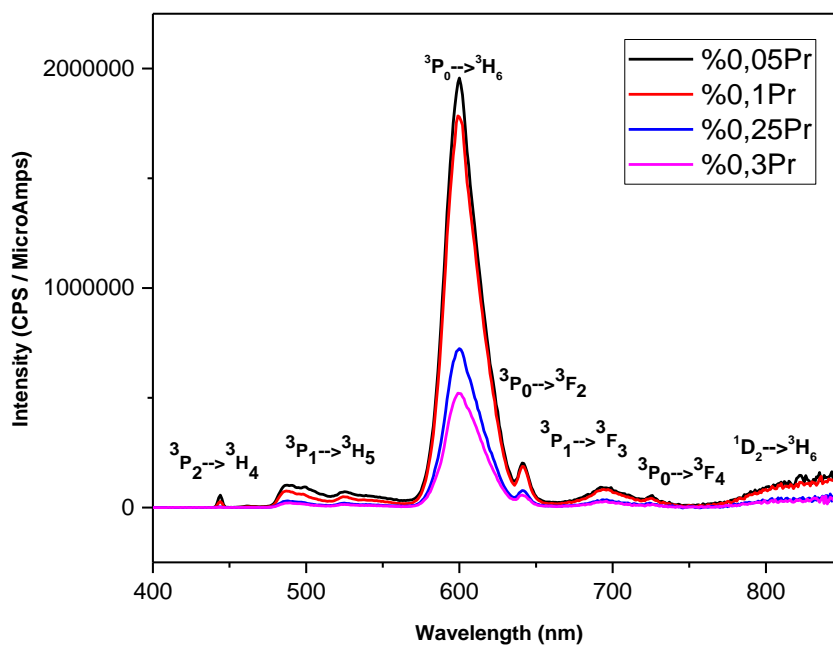


Figure IV.5: Emission spectrum in visible and in NIR of SNW glasses doped xPr³⁺ (x = 0.05, 0.1, 0.25, 0.3 mol. %).

Chapter IV- Spectroscopic study of the Pr³⁺doped and Pr³⁺/Yb³⁺ co-doped Sb₂O₃-WO₃-NaPO₃ glasses.

Among these excitation transitions, the peak at 444 nm is observed to be more intense and was thus used as the excitation wavelength to record the emission spectra of the prepared glass samples.

The emission spectra consist of seven emission bands in the visible region at 491 nm, 525 nm, 695 nm, 600 nm, 642 nm, 725 nm, 822 nm, which correspond to $^3P_2 \rightarrow ^3H_5$, $^3P_1 \rightarrow ^3H_5$, $^3P_1 \rightarrow ^3F_3$, $^3P_0 \rightarrow ^3H_6$, $^3P_0 \rightarrow ^3F_2$, $^3P_0 \rightarrow ^3F_4$, $^1D_2 \rightarrow ^3H_6$ transitions, respectively. And three emission bands in near-infrared are located at 1036 nm, 1474 nm and 1630 nm, corresponding to $^1D_2 \rightarrow ^3F_3$, $^1D_2 \rightarrow ^1G_4$, $^3F_3 \rightarrow ^3H_4$ transitions, respectively

In the present work we have concentrated on the emission of 3P_0 , 1D_2 states only as they possess the highest fluorescence intensity. A peculiar intensity variation is observed for $^3P_0 \rightarrow ^3H_6$, (giving orange color), $^3P_0 \rightarrow ^3F_2$ (red emission) and $^3P_2 \rightarrow ^3H_5$ (blue emission). The intensity of $^1D_2 \rightarrow ^3F_3$ transition decreases with the increase of Pr³⁺ concentration, reaching a maximum at 0.1 mol% and then increases for further increase of Pr³⁺ concentration. This phenomenon is well known as fluorescence quenching in RE ions owing to the enhancement of interaction among Pr³⁺ pairs at higher concentrations. The most intense peak is observed at 600 nm. Among these transitions, the maximum emission was obtained for the lowest concentration while further increasing in the concentration. This occurs because, when the Pr³⁺ concentration is more than 0.05 mol.%, the distance between the Pr³⁺ ions becomes short and the absorbed energy is exchanged nonradiatively between them. This in turn leads to a quenching effect that decreases the fluorescence intensity [32, 33].

**Chapter IV- Spectroscopic study of the Pr³⁺ doped and Pr³⁺/Yb³⁺ co-doped
Sb₂O₃-WO₃-NaPO₃ glasses.**

Table IV.9: Emission band position (λ_{\max} , nm), radiative transition probability (A_{rad} , s⁻¹), full width at half maximum (FWHM, nm), effective bandwidth ($\Delta\lambda_{\text{eff}}$, nm), peak stimulated emission cross-section ($\sigma_{\text{em}}^{\text{F-L}} \times 10^{-21}$, cm²), Optical gain ($\sigma_{\text{em}}^{\text{F-L}} \times \tau_{\text{rad}} 10^{-23}$ cm³) and the gain bandwidth ($\sigma_{\text{em}}^{\text{F-L}} \times \Delta\lambda_{\text{eff}} \times 10^{-28}$ cm³), of the Pr³⁺ doped SNW glasses.

Transition	Sample	wavelength	A_{rad}	FWHM	$\Delta\lambda_{\text{eff}}$	$\sigma_{\text{em}}^{\text{F-L}}$	$\times \tau_{\text{rad}} \sigma_{\text{em}}^{\text{F-L}}$	$\sigma_{\text{em}}^{\text{F-L}} \times \Delta\lambda_{\text{eff}}$
³ P ₂ → ³ H ₅	SNW0.05Pr	491	4188	21.7824	16,6042	0,30384	0,95405	5,045
	SNW0.1Pr	491	2353,9	18.9171	15,6999	0,17751	1,12362	2,78684
	SNW0.25Pr	491	1089,9	18.5718	15,9839	0,07921	1,257	1,26602
	SNW0.3Pr	491	1024,8	18.5212	16,1002	0,07079	1,38189	1,13979
³ P ₁ → ³ H ₅	SNW0.05Pr	525	1357,1	8.8305	2,3365	0,91456	17,5321	2,13687
	SNW0.1Pr	525	907,6	8.2831	3,1424	0,44696	16,02795	1,40452
	SNW0.25Pr	525	387,5	8.2551	3,6555	0,16095	11,91836	0,58835
	SNW0.3Pr	525	360,8	7.6057	3,9371	0,13323	11,36145	0,52452
→ ³ F ₃	SNW0.05Pr	695	585	21.7216	3,8153	0,74147	2,32822	2,82894
	SNW0.1Pr	695	391,2	20.7609	4,0961	0,4539	2,87322	1,85924
	SNW0.25Pr	695	167	19.0513	3,6555	0,21303	3,38077	0,77873
	SNW0.3Pr	695	155,5	19.7296	3,6486	0,19028	3,71435	0,69427
³ P ₀ → ³ H ₆	SNW0.05Pr	600	2761	24.3391	24,96472	0,29708	20,16578	7,41652
	SNW0.1Pr	600	1846,5	24.5306	25,3056	0,19263	26,42566	4,87474
	SNW0.25Pr	600	788,4	25.1904	25,768	0,07925	27,46731	2,04212
	SNW0.3Pr	600	734	25.8569	26,4141	0,06892	29,44466	1,82037
→ ³ F ₂	SNW0.05Pr	642	2253,8	6.7219	3,8153	2,07996	141,18779	7,93568
	SNW0.1Pr	642	1507,3	6.7813	4,0961	1,27341	174,68576	5,216
	SNW0.25Pr	642	643,5	6.77499	3,6555	0,59768	207,15103	2,18483
	SNW0.3Pr	642	599,1	7.35446	3,6486	0,53379	228,06285	1,9476
³ P ₀ → ³ F ₄	SNW0.05Pr	725	1565	5.1827	0,4209	21,29198	66,8568	8,96179
	SNW0.1Pr	725	1046,6	7.0808	0,4897	12,02818	76,13841	5,8902
	SNW0.25Pr	725	446,9	5.3157	0,3732	6,61226	104,93657	2,4677

**Chapter IV- Spectroscopic study of the Pr³⁺ doped and Pr³⁺/Yb³⁺ co-doped
Sb₂O₃-WO₃-NaPO₃ glasses.**

	r							
	SNW0.3Pr	725	416	5.6070	0,5287	4,16002	81,20358	2,1994
¹ D ₂ → ³ H ₆	SNW0.05Pr	822	331,9	4.4358	1,0917	2,87687	195,28171	3,14068
	r							
	SNW0.1Pr	822	178	2.4723	0,3681	4,49717	616,9212	1,65541
	SNW0.25Pr	822	70	3.0435	0,8858	0,72107	249,91646	0,63873
	r							
	SNW0.3Pr	822	64,4	1.2628	2,3081	0,24377	104,15015	0,56264
→ ³ F ₃	SNW0.05Pr	1036	165,8	67.2182	69,4905	0,05697	3,86695	3,9587
	r							
	SNW0.1Pr	1036	88,9	67.0011	71,5635	0,02915	3,99887	2,08611
	SNW0.25Pr	1036	35	65.1650	67,3669	0,01196	4,14577	0,80582
	r							
→ ¹ G ₄	SNW0.05Pr	1474	57,6	151.764	149,582	0,03768	2,55742	5,63561
	r			5	3			
	SNW0.1Pr	1474	30,9	145.375	125,566	0,02366	3,24611	2,9713
	SNW0.25Pr	1474	12,1	159.475	135,054	0,00845	2,92961	1,14158
	r			4	8			
³ F ₃ → ³ H ₄	SNW0.05Pr	1630	430,3	1.1205	0,3831	164,3380	46109,9709	62,9579
	r					5		1
	SNW0.1Pr	1630	233,5	0.6161	0,2585	129,8895	73631,7849	33,5764
	SNW0.25Pr	1630	92,2	1.3536	1,2689	10,2514	14669,3417	13,008
	r						4	

Emission band position (λ_{\max} , nm), radiative transition probability (A_{rad} , s⁻¹), full width at half maximum (FWHM, nm), effective bandwidth ($\Delta\lambda_{\text{eff}}$, nm), peak stimulated emission cross-section ($\sigma_{\text{em}}^{\text{F-L}} \times 10^{-21}$, cm²), Optical gain ($\sigma_{\text{em}}^{\text{F-L}} \times \tau_{\text{rad}} 10^{-23}$ cm³) and the gain bandwidth ($\sigma_{\text{em}}^{\text{F-L}} \times \Delta\lambda_{\text{eff}} \times 10^{-28}$ cm³), of the Pr³⁺ doped SNW glasses, have been collected in Table IV.9.

The observations suggest that the increase of doping concentration causes such interactions which modify the symmetry of the terminating level ³H₆ of the transition ³P₀, ³H₆, thus decreasing the decay probability from the ³P₀ level to the ³H₆ level.

It can be seen that the FWHM increases with the increase of Pr³⁺ and reaches a maximum FWHM bandwidth of 196 nm when Pr³⁺ concentrations is equal to 1.0 mol%. This broadband emission can be assigned to the Pr³⁺: ¹D₂→¹G₄ transition.

The value of the stimulated emission cross-section ($\sigma_{\text{em}}^{\text{F-L}}$) is of great interest. Using the stimulated emission cross-section values, the gain bandwidth and optical were also determined. The higher values of the gain bandwidth and optical gain parameter

Chapter IV- Spectroscopic study of the Pr⁺³ doped and Pr³⁺/Yb³⁺ co-doped Sb₂O₃-WO₃-NaPO₃ glasses.

indicate that the Pr⁺³ doped glasses may be suitable media for good optical amplification. For efficient luminescence applications

An intense emission at around 600 nm and 1036 nm [see Fig. IV.5]. The PL intensity decline at a higher Pr⁺³ doping level. the gain parameters such as optical gain ($\sigma_e \times \tau_{exp}$) and bandwidth gain ($\sigma_e \times \Delta\lambda_{eff}$) have been determined, where the higher values of bandwidth gain ($\sigma_e \times \Delta\lambda_{eff}$) are of ³P₀ and ³F₃ transitions.

Considerably large stimulated emission cross-section in the present glass is an attractive feature for low-threshold, high gain applications and can be utilized to obtain continuous wave laser action due to the ³P₀→³H₆, ¹D₂→³F₃ transitions [34, 35].

IV. 2. 1. Absorption, emission cross-section characteristics of 1474 nm band

The Mc-Cumber theory of reciprocity between the effective section of emission and that of absorption is given by the following equation [36]:

$$\sigma_{emis}^{M-C} = \sigma_{abs}(\lambda) \frac{Z_l}{Z_u} \exp\left[\frac{(E_{ZL} - \frac{hc}{\lambda})}{K_B T}\right] \quad (IV. 11)$$

Wherein Z_l and Z_u are lower and upper level partition functions, respectively. The constants used here are: $hc = 1 \times 10^7 \text{ nm cm}^{-1}$, and $K_B T = 208 \text{ cm}^{-1}$ at room temperature. E_{ZL} is the free energy required to excite a Pr⁺³ ion from its ground state to an excited state. The SNW0.25Pr sample has the highest value for the absorption and emission cross section of $6,918 \times 10^{-20} \text{ cm}^2$ et $2,438 \times 10^{-20} \text{ cm}^2$ respectively.

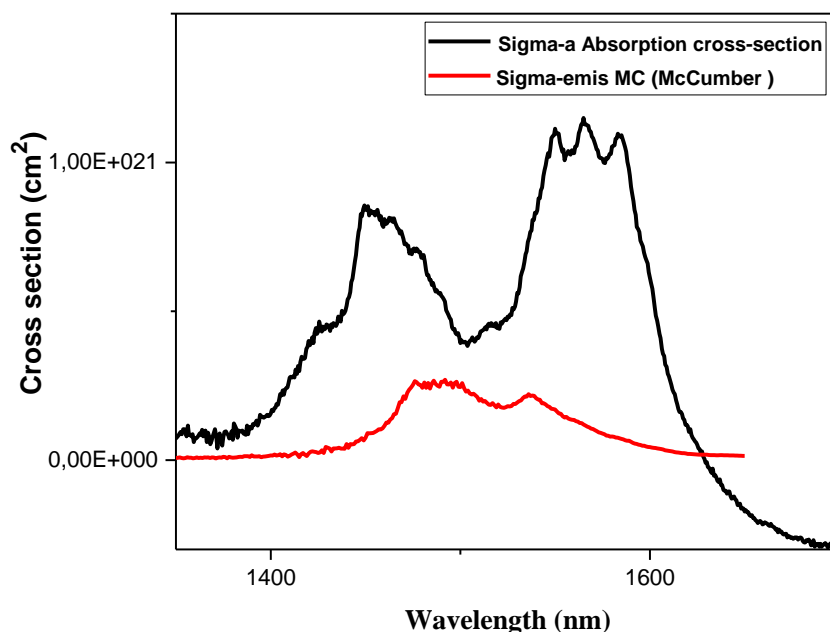


Figure IV.6: The absorption (σ_{abs}) and emission cross-sections (σ_{em}) of $^1D_4 \leftrightarrow ^1G_4$ transitions of SNW0.25Pr³⁺ glass.

Stimulated emission cross section, (σ_{em}) is the most important laser parameter. Its value signifies the rate of energy extraction from the laser material. The various laser transitions along with (σ_{em}) values are shown in (Fig IV.6). The high values of (σ_{em}) in (table IV.9.) for the transitions 3P_0 , 1D_2 and 3F_3 confirm them to be probable laser transitions. On comparing the results of our study with those of phosphate and chlorophosphate glasses, it is observed that there is a little different in the values of (σ_{em}) for the transitions 3P_0 , 1D_2 and 3F_3 . This may be partly due to the increase in covalency and partly due to the enhancement of the line strength. However, further higher concentrations of Pr₆O₁₁ could not be incorporated since the solubility limit for Pr₆O₁₁ has been found experimentally to be around 0.2 mol% with the increase in the doping concentration [37].

IV. 3. Fluorescence decay (Cas Pr³⁺ ions)

The decline curves for the ³P₀→³H₆ levels of Pr³⁺ ions were obtained under laser excitations at 444 nm for all SNWPr samples as a function of the increase in the percentage of praseodymium and are shown in Fig IV.7. The experimental lifetime can be judiciously calculated using the expression $\tau_{exp} = \int t I(t) dt / \int I(t) dt$, where I(t) is the fluorescence decline curve, another the quantum efficiency, defined by the relation following $\eta = \tau_{rad} / \tau_{exp}$. The values obtained are collected in Table IV.10.

Table IV.10: The radiative lifetimes (τ_{rad} , ms), experimental lifetime (τ_{exp} , ms) and quantum efficiency η (%) of Pr³⁺ doped antimony based glasses (SNW).

Composition	τ_{exp} (ms)	τ_{rad} (ms)	η (%)
SNW0.05Pr	0.15	0.16	94
SNW0.1Pr	0.20	0.22	91
SNW0.25Pr	0.25	0.53	47
SNW0.3Pr	0.26	0.57	45

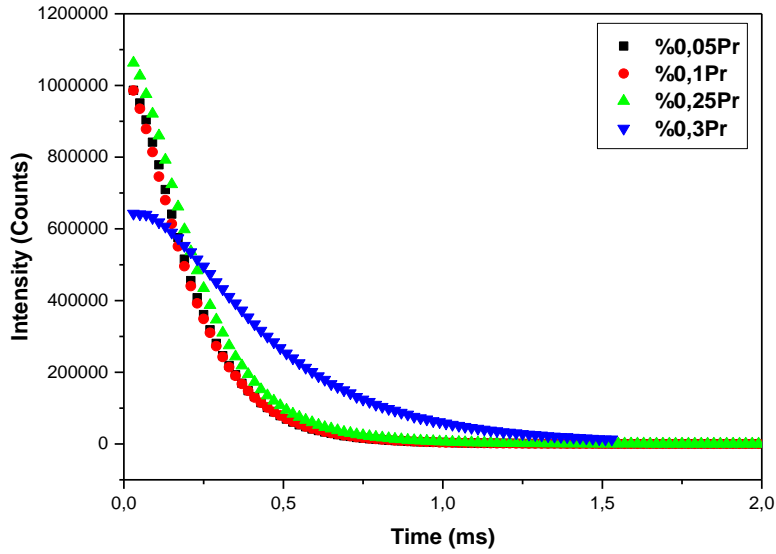
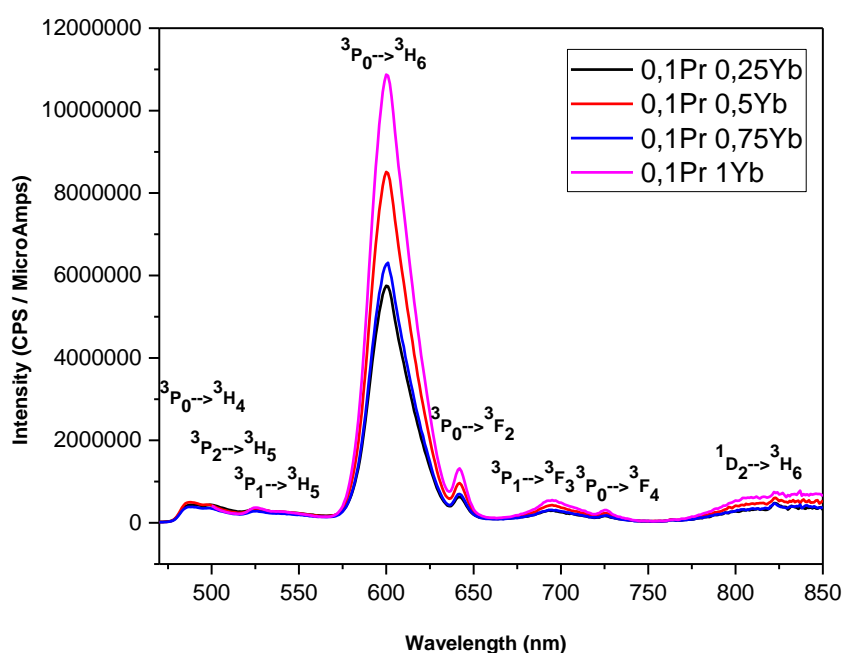


Figure IV.7: Fluorescence decay time of $^3P_0 \rightarrow ^3H_6$ transition of SNW Pr³⁺ glasses.

It is through the latter, we observe the increase in an experimental lifetime (τ_{exp}) and decrease of quantum efficiency η (%) with the addition of Pr₆O₁₁, the height values of the quantum efficiency η (%) correspondent SNW0.05Pr and SNW0.1Pr. This is more evident than for the sample SNW0.05Pr (See tab .10.), where η (%) = 94, which was characterized by the highest quantum efficiency that deserves to be transformed into a good laser. On the other hand, the difference between the experimental and calculated lifetimes is mainly due to the manifestation of non-radiative, the non-radiative contribution is mainly due to the energy transfer between the excited Pr³⁺ ion pairs. The experimental lifetime (τ_{exp}) of the studied glasses doped with xmol.% Pr³⁺ is less than the predicted lifetime (τ_{rad}) obtained by analysis JO. The addition of WO₃ can lead to an increase in the phonon energy of the glasses, which will lead to a decrease in the lifespan of the 3P_0 level. In addition, the decrease in duration with increasing Pr³⁺ concentration is attributed to the effect quenching which corresponds to non-radiative relaxations between Pr³⁺ ions excited at high concentrations [38].

- Case of 47.5 Sb₂O₃ 47.5 NaPO₃ 5 WO₃ 0.1 Pr₆O₁₁ xYb₂O₃, (x= 0.25, 0.5, 0.75, 1) glasses:

The 975 nm band is used to excite the samples to obtain the luminescence of Pr³⁺ ions in the visible by energy transfer. It's the absorption band of Yb³⁺ which correspond to the transition from the ²F_{7/2} fundamental level to the ²F_{5/2} excited level. The absorption band of Pr³⁺ contributions to the absorption spectrum are low in figure (IV.1) due to transition ³H₄ to ¹G₄ [39].



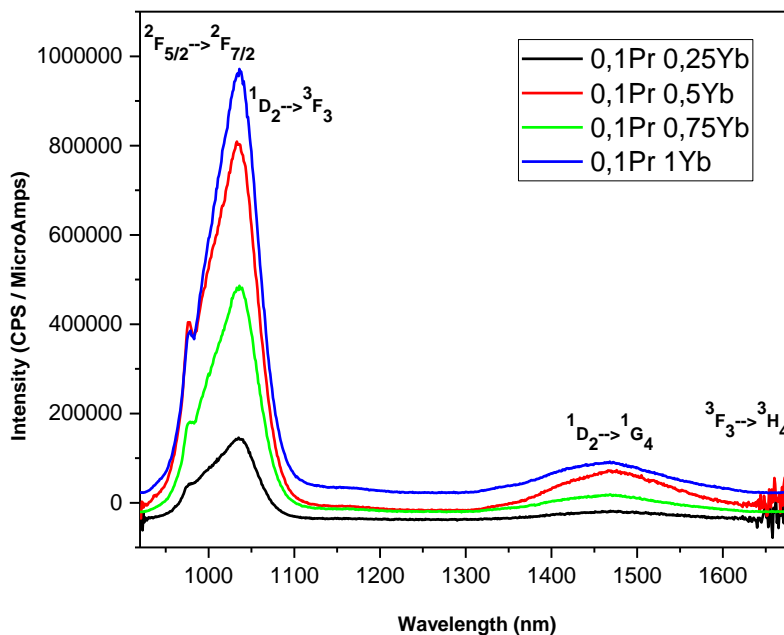


Figure IV.8: Emission spectrum in visible, NIR of SNWPr glasses co doped xYb³⁺ (x = 0.25, 0.5, 0.75, 1 mol. %).

Table IV.12: Emission band position (λ_{max} , nm), radiative transition probability (A_{rad} , s⁻¹), full width at half maximum (FWHM, nm), effective bandwidth ($\Delta\lambda_{eff}$, nm), peak stimulated emission cross-section ($\sigma_{em}^{F-L} \times 10^{-21}$, cm²), Optical gain ($\sigma_{em}^{F-L} \times \tau_{rad} 10^{-23}$ cm³) and the gain bandwidth ($\sigma_{em}^{F-L} \times \Delta\lambda_{eff} \times 10^{-28}$ cm³), of the Pr³⁺/Yb³⁺ co doped SNW glasses.

Transition	Sample	Wavelength	A_{rad}	FWHM	$\Delta\lambda_{eff}$	σ_{em}^{F-L}	$\times \tau_{rad}$	σ_{em}^{F-L}	$\sigma_{em}^{F-L} \times \Delta\lambda_{eff}$
³ P ₂ → ³ H ₅	SNWPr0.25 Yb	499	899,9	7.9966	1,08108	1,05551	240,58333	1,1411	
	SNWPr0. 5Yb	499	682,8	6.4228	0,64388	1,34467	229,15892	0,8658 1	
	SNWPr0.75 Yb	499	460,8	6.8760	0,82715	0,70641	134,37299	0,5843 1	
	SNWPr1Yb	499	404,9	9.2649	3,24224	0,15835	31,98443	0,5134 2	
³ P ₁ → ³ H ₅	SNWPr0.25 Yb	525	1314, 7	8.4433	1,5675	1,30311	297,01833	2,0426 3	
	SNWPr0. 5Yb	525	682,8	8.7921	2,3594	0,44963	76,62582	1,0608 6	

**Chapter IV- Spectroscopic study of the Pr³⁺doped and Pr³⁺/Yb³⁺ co-doped
Sb₂O₃-WO₃-NaPO₃ glasses.**

	SNWPr0.75 Yb	525	467,4	9.2538	2,1204	0,34248	65,1463	0,7261 9
	SNWPr1Yb	525	359,9	11.7759	1,4214	0,39339	79,4578	0,5591 7
→ ³ F ₃	SNWPr0.25 Yb	695	566,7	21.2283	13,3318	0,20283	2134,4905 5	2,7040 7
	SNWPr0. 5Yb	695	294,3	19.7255	14,2638	0,09845	180,10902	1,4042 8
	SNWPr0.75 Yb	695	201,5	20.8807	13,6784	0,07029	195,10532	0,9614 8
	SNWPr1Yb	695	155,1	20.7725	14,7817	0,05007	187,5517	0,7400 8
³ P ₀ → ³ H ₄	SNWPr0.25 Yb	487	5002, 1	23.4944	17,2889	0,33283	123,34456	5,7543 2
	SNWPr0. 5Yb	487	2597, 9	21.0532	16,8597	0,17726	14,19154	2,9885 7
	SNWPr0.75 Yb	487	1778, 5	21.9662	16,7807	0,12192	14,42713	2,0459 5
	SNWPr1Yb	487	1369, 3	21.8779	9,1577	0,17201	26,76818	1,5752 2
³ P ₀ → ³ H ₆	SNWPr0.25 Yb	600	2674, 8	24.6692	25,0814	0,28266	2974,6449 5	7,0896
	SNWPr0. 5Yb	600	1389, 2	25.0894	25,4355	0,14476	264,83216	3,6821
	SNWPr0.75 Yb	600	951	24.6752	24,866	0,10137	281,36478	2,5206 4
	SNWPr1Yb	600	732,2	25.4611	25,5823	0,07586	284,17738	1,9407 1
³ P ₀ → ³ F ₂	SNWPr0.25 Yb	642	2183, 4	6.7938	3,5557	2,13341	790,61935	7,5857 6
	SNWPr0. 5Yb	642	1134	6.9391	3,6876	1,0684	85,53628	3,9398 4
	SNWPr0.75 Yb	642	776,3	7.0284	3,8467	0,70114	82,96629	2,6970 9
	SNWPr1Yb	642	597,7	6.9364	4,1395	0,50165	78,06679	2,0765 8
³ P ₀ → ³ F ₄	SNWPr0.25 Yb	725	1516, 1	6.1424	2,7724	3,08994	1145,0992 2	8,5665 4
	SNWPr0. 5Yb	725	787,4	7.3152	2,9971	1,48447	118,84673	4,4491 1
	SNWPr0.75 Yb	725	539	6.3058	3,1014	0,98199	116,19925	3,0455 5
	SNWPr1Yb	725	415	6.2634	2,7932	0,83951	130,64384	2,3449 1
¹ D ₂ → ³ H ₆	SNWPr0.25 Yb	822	59,4	5.7251	2,1102	0,26283	2765,9268 6	0,5546 2
	SNWPr0. 5Yb	822	29	5.4741	1,2171	0,22248	407,00546	0,2707 8
	SNWPr0.75 Yb	822	18,6	4.3872	1,2563	0,13824	383,70459	0,1736 7
	SNWPr1Yb	822	13,4	6.6586	1,0335	0,12106	453,49861	0,1251 2
¹ D ₂ → ³ F ₃	SNWPr0.25 Yb	1036	29,7	48.0162	37,2202	0,0188	197,83693	0,6997 1
	SNWPr0. 5Yb	1036	14,5	50.7946	37,1884	0,00919	16,80509	0,3416 1
	SNWPr0.75	1036	9,3	51.6518	38,5962	0,01178	32,69634	0,2191

Chapter IV- Spectroscopic study of the Pr³⁺ doped and Pr³⁺/Yb³⁺ co-doped Sb₂O₃-WO₃-NaPO₃ glasses.

	Yb							
	SNWPr1Yb	1036	6,7	52.2887	40,8689	0,00386	14,46822	0,15785
¹ D ₂ → ¹ G ₄	SNWPr0.25 Yb	1474	10,3	153.5568	138,8755	0,00716	75,35154	0,99438
	SNWPr0.5Yb	1474	5	147.7439	147,0636	0,00328	6,00476	0,48271
	SNWPr0.75 Yb	1474	3,2	148.7748	97,8306	0,00316	8,76507	0,30893
	SNWPr1Yb	1474	2,3	145.1927	118,8384	0,00187	6,99931	0,22205
³ F ₃ → ³ H ₄	SNWPr0.25 Yb	1630	8,74	1.4678	3,4559	0,36511	14721,77997	1,26179
	SNWPr0.5Yb	1630	43	1.5042	0,6931	8,95671	65088,30679	6,20789
	SNWPr0.75 Yb	1630	27,9	0.9953	0,03275	122,9897	1,35062E6	4,02791
	SNWPr1Yb	1630	20,3	0.6942	0,03029	96,75482	1,42817E6	2,9307

As shown the Table IV.12 and the Figure IV.8 there is emission bands in the visible luminescence spectrum at 491 nm, 525 nm, 695 nm, 487nm, 600 nm, 642 nm, 725 nm, 822 nm, corresponding to ³P₂ → ³H₅, ³P₁ → ³H₅, ³P₁ → ³F₃, ³P₀ → ³H₄, ³P₀ → ³H₆, ³P₀ → ³F₂, ³P₀ → ³F₄, ¹D₂ → ³H₆, transitions, respectively. and emission bands in near-infrared at 1036 nm, 1474 nm, 1630 nm, corresponding to ¹D₂ → ³F₃, ¹D₂ → ¹G₄, ³F₃ → ³H₄ transitions, respectively.

The higher values of the gain bandwidth and optical gain parameter indicate that the Pr³⁺ doped antimony phosphate glasses may be suitable media for good optical amplification [40]. The highest values for the radiative transition probability (A_{rad}) corresponding to the transitions ³P₀→³H₆ (orange), ³P₀ → ³F₂ (red emission) with ³P₀ → ³H₄ (blue emission) and ³P₁ → ³H₅ [41].

IV. 2. 1. Fluorescence decay (Cas Yb⁺³ ions)

The decline curves (Figure IV.9) for the ³P₀→³H₆ level of Pr³⁺/Yb³⁺ codoped glasses. The difference appearing between τ_{exp} and τ_{rad} clearly indicates that the emissions of level 3P0 are not totally radiative but also contain contributions non-radiative decay. It presents a character of non-radiative decay with a decrease in their lifetime as a function of the concentration of Yb³⁺ due to the interaction with the OH content of the glass or could also be due to non-radiative energy transfer through cross-relaxation channels. We observe the increase in an experimental lifetime (τ_{exp}) with the addition

Chapter IV- Spectroscopic study of the Pr³⁺ doped and Pr³⁺/Yb³⁺ co-doped Sb₂O₃-WO₃-NaPO₃ glasses.

of Pr₆O₁₁, the height values of the quantum efficiency η (%) correspondent the sample SNWPr0.5Yb (tab .IV.11), where η (%) = 100% [42, 43]

Table IV.11: The radiative lifetimes (τ_{rad} , ms), experimental lifetime (τ_{exp} , ms) and quantum efficiency η (%) of Yb³⁺ co doped antimony based glasses (SNWPr).

Composition	τ_{exp} (ms)	τ_{rad} (ms)	η (%)
SNW0.25Yb	0.14	0.15	93
SNW0.5Yb	0.16	0.16	100
SNW0.75Yb	0.17	0.24	70
SNW1Yb	0.21	0.32	65

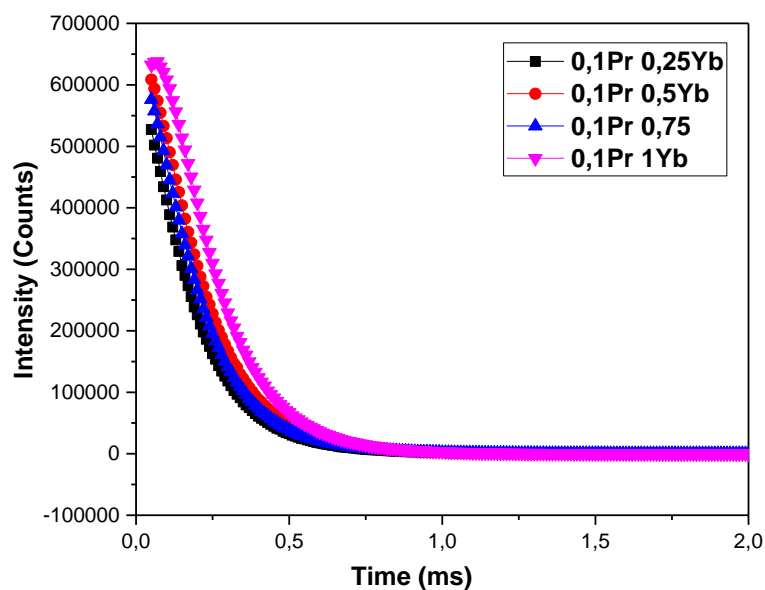


Figure IV.9: Fluorescence decay time of $^3P_0 \rightarrow ^3H_6$ transition of Yb³⁺ co doped SNWPr glasses.

IV. 4. CIE chromaticity coordinates:

➤ **Case of 47.5 Sb₂O₃ 47.5 NaPO₃ 5 WO₃- x Pr₆O₁₁ glasses:**

Using CIE 1931 calculation software [44] from their emission spectra under excitation at 444 nm The chromaticity coordinates of glasses doped with Pr³⁺ ions are shown in the figures (IV.10) and grouped together in the table (IV.13).

Table IV.13: Excitation calorimetric parameters of Pr³⁺ doped antimony based glasses (SNW).

Sample	CIE(x, y)	CCT(K)	Purity(%)	R(O/B)
SNW0.05Pr	(0.5984,0.3834)	1389	94.7	0.4
SNW0.1Pr	(0.6078,0.3793)	1326	96.3	0.29
SNW0.25Pr	(0.6113,0.3785)	1307	97.1	0.30
SNW0.3Pr	(0.6132,0.3773)	1293	97.3	0.30

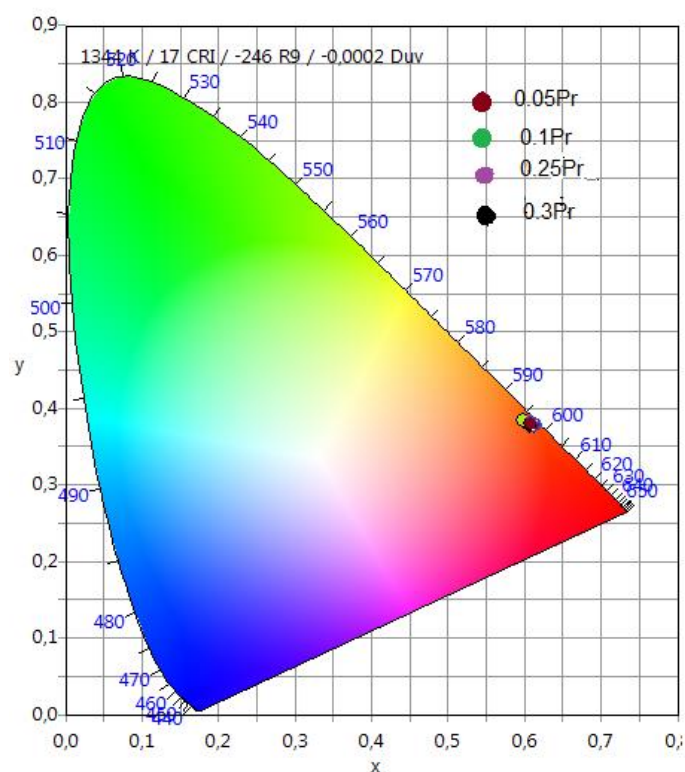


Figure IV.10: Chromaticity Diagram of Pr³⁺ doped SNW glasses.

Chapter IV- Spectroscopic study of the Pr³⁺doped and Pr³⁺/Yb³⁺ co-doped Sb₂O₃-WO₃-NaPO₃ glasses.

The emission peak due to ³P₀→³H₆ transition shifts towards the longer wavelength side; it flaunts an orange shift with the increase of Pr³⁺ concentration. The site distribution of ions in the vicinity of the ligand field is responsible for the appreciable shifts in emission bands [45]. The O/B ratios are found to be 0.4, 0.29, 0.30 and 0.30 for SNWPr0.05, SNWPr0.1, SNWPr0.25 and SNWPr0.3 glasses, respectively. The O / B values described that the Pr³⁺ ions are located in an asymmetric environment exhibiting a high covalent bond between Pr³⁺ and O²⁻. The chromaticity coordinates of glasses doped with Pr³⁺ ions present are mostly passing through the light region reddish orange and orange. The reason is that, at higher concentrations, the distance between Pr³⁺ ions become short, resulting in increased nonradiative energy transfer between them This is also proved by the color purity measurements. For SNWPr0.25 and SNWPr0.3 glass, color purity is 97% .The Commission International de l'Eclairage (CIE) coordinates of these glasses are calculated as (x=0.5984, y=0.3834); (x=0.6078, y=0.3793); (x=0.6113, y= 0.3785)and (x=0.6132, y=0.3773) for SNWPr0.05, SNWPr0.1, SNWPr0.25 and SNWPr0.3 glasses, respectively. The obtained CIE chromaticity coordinates of SNWPr glasses lies in the yellow-orange region as described in Fig. IV.10 [46, 47].

➤ **Case of 47.5 Sb₂O₃ 47.5 NaPO₃ 5 WO₃ 0.1 Pr₆O₁₁ xYb₂O₃, (x= 0.25, 0.5, 0.75, 1) glasses:**

The chromaticity coordinates of Pr³⁺/Yb³⁺ co doped glasses are shown in the figures (IV.11) and grouped together in the table (IV.14).

Table IV.14: Excitation calorimetric parameters of Yb³⁺ co doped antimony based glasses (SNWPr).

Sample	CIE(x, y)	CCT(K)	Purity(%)	R(O/B)
SNWPr0.25Yb	(0.5864,0.3939)	1500	94.2	0.62
SNWPr0.5Yb	(0.5996,0.3858)	1395	95.8	0.46
SNWPr0.75Yb	(0.5963,0.3879)	1421	95.4	0.52
SNWPr1Yb	(0.4691,0.5173)	3279	96.2	-4

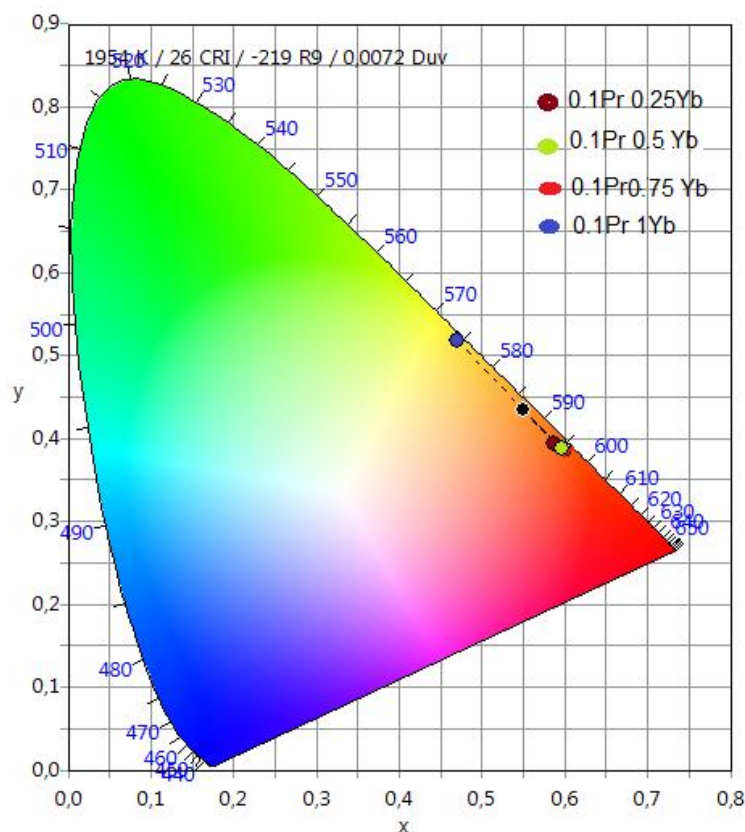


Figure IV.11: Chromaticity Diagram of Yb³⁺ co doped SNW glasses.

The CIE coordinates fall in yellow-orange color regions. The O/B ratios chromaticity coordinates and color purity values support the emission of yellowish-orange fluorescence, the O / B values lead to the Yb³⁺ ion being located in an asymmetric environment with a weak covalent bond between Yb³⁺ and O²⁻, these results suggest that the Pr³⁺/Yb³⁺ co-doped SNW glass is a favorable candidate of yellow-orange light emitting glass for photonic devices. Under other excitation can serve as excellent sources of white light for various photonic applications. It is observed that, for the lowest concentration, the color purity was 94%, whereas on increasing the concentration, its value decreased and reached 96% with a CCT value of 3279, suggesting the applicability of praseodymium-doped antimony phosphate glass (x = 1 mol.%) for near-white-light operation. It is also verified that the sample with the other lowest concentration (x = 0.25, 0.5, 0.75 mol.%) could emit yellow-orange light with purity of about 95% [48, 49].

Conclusion:

In conclusion, Pr⁺³ doped and Pr⁺³/Yb⁺³ co-doped antimony phosphate glasses are studied. The parameters of Judd-ofelt were estimated without consideration of the ³H₄→ ³P₂ hypersensitive transition. The trend $\Omega_4 < \Omega_2 < \Omega_6$ for the SNW_xPr glasses and $\Omega_2 < \Omega_6 < \Omega_4$ for the prepared SNW_{0.1}Pr_xYb glasses, the quality factor $\chi = \Omega_4 / \Omega_6$, obtained in this study are very low and the integrated stimulated cross sections were found to be greater than 10⁻¹⁸ cm²—indicates that these materials could be good desirable candidates for lasing materials. Also, show also predicting that these glasses seem to be for laser applications and optical amplifiers. Using these parameters (J-O), we evaluated different radiative properties such as predicted radiative transition probabilities (A_{rad}), branching ratios (β) and the radiative life (τ_{rad}) of the glasses prepared. SNW_x glasses doped Pr⁺³ give seven emission bands in the visible located at 491 nm, 525 nm, 695 nm, 600 nm, 642 nm, 725 nm, 822 nm, correspond to ³P₂ → ³H₅, ³P₁ → ³H₅, ³P₁ → ³F₃, ³P₀ → ³H₆, ³P₀ → ³F₂, ³P₀ → ³F₄, ¹D₂ → ³H₆, transitions, respectively. In the infrared region three emission bands are obtained at 1036 nm, 1474 nm, 1630 nm, corresponding to ¹D₂ → ³F₃, ¹D₂ → ¹G₄, ³F₃ → ³H₄ transitions, respectively, for SNW co-dope Pr⁺³/ Yb⁺³ glasses the same emission bands. Glasses doped only with Pr⁺³ showed a strong orange and red emission under excitation at 444 nm in the visible region. The emission band at 1474 nm corresponds to the transition to ¹D₂ → ¹G₄ which covers the set O, E, S, C, I and the U band which is very important for optical fibres. It has an effective half-line width of 159,153 nm for SNWPr_{0.25} and SNWPr_{0.1}Yb_{0.25} glasses, and the stimulated emission section ($\sigma_{em}^{F-L} = 0,00845 \times 10^{-21} \text{cm}^2$, $\sigma_{em}^{F-L} = 0,00716 \times 10^{-21} \text{cm}^2$) thus favoring the amplification at telecommunications (in the NIR region) bands and tunable lasers. The decrease in lifetime with the increase of Pr⁺³ concentration is attributed to the non-radiative relaxations between the excited Pr⁺³ ions at higher concentrations. The CIE color coordinates under the 444 nm excitation for SNW_xPr glasses were evaluated and found to be in the red orange region with a purity of 97% and for SNW_{0.1}Pr_xYb and in the yellow orange region near to white light with a purity of 96% . Such glasses are suitable for light generation. The large stimulated emission cross-section and high branching ratios are usual characteristics of good materials for laser action. The comparatively higher magnitudes of the experimentally determined radiative and fluorescence properties confirm that the present glasses with Pr³⁺ ions emit intense

Chapter IV- Spectroscopic study of the Pr³⁺ doped and Pr³⁺/Yb³⁺ co-doped Sb₂O₃-WO₃-NaPO₃ glasses.

orange–red luminescence at 600 nm, corresponding to the ³P₀→³H₆ transition. This indicates that the prepared glasses are among the laser host materials with the greatest potential, having wide applications in optoelectronic luminescent display devices.

References:

- [1].M. Çelikbilek Ersundu, A. E. Ersundu, M. T. Soltani, M. Baazouzi, *Ceram. Int.* 43(2017) 491-497.
- [2].K. Srinivasa Rao, Valluri Ravi Kumar, Ya Zhydachevskii, A. Suchocki, M. Piasecki, G.Naga Raju, V. Ravi Kumar, N. Veeraiah, *Journal of Luminescence* 192 (2017) 443-451.
- [3].R. Vijay, L. Pavić, A. Šantić, A. Moguš-Milanković, P. Ramesh Babu, D. Krishna Rao, V. Ravi Kumar, N. Veeraiah, *Journal of Physics and Chemistry of Solids* 107 (2017)108-117.
- [4].Joanna Pisarska, Martyna Kowal, Marcin Kochanowicz, Jacek Zmojda, Jan Dorosz, Dominik Dorosz, and Wojciech A. Pisarski, *Optics Express*, 24 (2016) 2427-2435.
- [5].E. K. Abdel-Khalek, E. A. Mohamed, A. Ratep, Shaaban M. Salem, I. Kashif, *Journal of Non-Crystalline Solids* 441 (2016) 58-65.
- [6].Juqing Di, Xiaodong Xu, Changtai Xia, Dongzhen Li, Dahua Zhou, Qinglin Sai, Lulu Wang, Jun Xu, *Physica B* 408 (2013) 1-5.
- [7].M. Letz, U. Peuchert, B. Schreder, K. Seneschal, R. Sprengard, J. S. Hayden, *NonCryst. Solids* 351 (2005) 1067-1071.
- [8].G.S. Ofelt, *J. Chem. Phys.* 37, (1962), 511-520.
- [9].B.R. Judd, *Phys. Rev.* 127, (1962), 750-761.
- [10]. B. Suresh, N. Purnachand, Ya. Zhydachevskii, M. G. Brik, M. Srinivasa Reddy, A. Suchocki, M. Piasecki, N. Veeraiah, *Journal of Luminescence* 182 (2017) 312-322.
- [11]. W.T.Carnall, P.R.Fields, K.Rajnak, *J.Chem.Phys.*49(1968),4412-4423.
- [12]. A. Herrera, C. Jacinto, A. R. Becerra, P. L. Franzen, N. M. Balzaretta, *Journal of Luminescence* 180 (2016) 341-347.
- [13]. S. Mihi, M. T. Soltani, *Courrier du Savoir* 26 (2018) 457-464.
- [14]. F. Li, S. L. Pan, X. L. Hou, J. Yao, *Cryst. Growth Des.* 9 (2009) 4091-4095.
- [15]. K. Bhargavi, V. Sudarsan, M.G. Brik, M. Sundara Rao, Y. Gandhi, P. Nageswara Rao, N. Veeraiah, *Journal of Non-Crystalline Solids* 362 (2013) 201-206.

Chapter IV- Spectroscopic study of the Pr³⁺doped and Pr³⁺/Yb³⁺ co-doped Sb₂O₃-WO₃-NaPO₃ glasses.

- [16]. T. Satyanarayana, M. G. Brik, N. Venkatramaiah, I.V. Kityk, K. J. Plucinski, V. Ravikumar and N.Veeraiah, *J. Am. Ceram. Soc.* 93.7 (2010) 2004-2011.
- [17]. D.E. Henrie, R.L. Fellows, G.R. Choppin, *Coord. Chem. Rev.* 18 (1976) 199.
- [18]. L. Srinivasa Rao, M. Srinivasa Reddy, M. V. Ramana Reddy, N. Veeraiah, *Physica B* 403 (2008) 2542-2556.
- [19]. Y.M. Yang, B.Q. Yao, B.J. Chen, C. Wang, G.Z. Ren, X.J. Wang, *Opt. Mater.* 29 (2007) 1159.
- [20]. M.P. Hehlen, M.G. Brik, K.W. Kramer, *J. Lumin.* 136 (2013) 221.
- [21]. S. Tanabe, N. Sugimoto, S. Ito, T. Hanada, *J. Lumin.* 87 (2000) 670–672
- [22]. M. Srinivasa Reddy, G. Naga Raju, G. Nagarjuna, N. Veeraiah, *Journal of Alloys and Compounds* 438 (2007) 41-51.
- [23]. G. Lakshminarayana, Kawa M. Kaky, S. O. Baki, Song Ye, A. Lira, I. V. Kityk, M. A. Mahdi, *Journal of Alloys and Compounds* 686 (2016) 769-784.
- [24]. M.V. Vijaya Kumar , K. Rama Gopal , R.R. Reddy , G.V. Lokeswara Reddy , N. Sooraj Hussain , B.C. Jamalaiah, *Journal of Non-Crystalline Solids* 364 (2013) 20–27.
- [25]. B. Suresh, N. Purnachand, Ya. Zhydachevskii, M. G. Brik, M. Srinivasa Reddy, A.Suchocki, M. Piasecki, N. Veeraiah, *Journal of Luminescence* 182 (2017) 312-322.
- [26]. Y.C.Ratnakaram , N.Sudharani and S.Buddhudu, *Indian J.Phys.*70B(5),409-415(1996).
- [27]. D.R. Simons, A.J. Faber, H. De Wall, *Opt. Lett.* 20 (1995) 468.
- [28]. Y.C. Ratnakaram, *Phys. Chem. Glasses* 35 (1994) 182.
- [29]. K.Ouannes, K. Lebbou, , B.M. Walsh, M. Poulain, G.A.Goget, Y. Guyot , *Optical Materials* xxx (2016) 1-7.
- [30]. D. Rajesh, A. Balakrishna, M. Seshadri, Y. C. Ratnakaram, *Spectrochimica Acta Part A: Molecular and Biomolecular Spectroscopy* 97 (2012) 963-974.

Chapter IV- Spectroscopic study of the Pr³⁺doped and Pr³⁺/Yb³⁺ co-doped Sb₂O₃-WO₃-NaPO₃ glasses.

- [31]. A.A. Kaminskii, Laser Crystals, Springer, Berlin, (1981).
- [32]. N.Aryapriya, , G.Subash, T. Krishnapriya, J. Adon, A. C. Saritha, N. V. Unnikrishnan, P. R. Biju, Journal of Electronic Materials, 49.6 (2020) 3624-3633.
- [33]. G. Lakshminarayana, J. Qiu, M. G. Brik, I. V. Kityk. Journal of Physics D: Applied Physics, 41.17 (2008)175106.
- [34]. J. X. Yang, B. J. Chen, E. Y. B. Pun, H. Lin. Applied optics, 57.30 (2018)9022-9031.
- [35]. Y. K.Sharma, S. S. L. Surana, R. K. Singh. (2008)
- [36]. D.E. McCumber, Phys. Rev. 136, (1964), A954-A957.
- [37]. N. Aryapriya, S. Gopi, T. Krishnapriya, A. JOSE, A.C. Saritha, N.V. Unnikrishnan, C. Joseph, and P.R. Biju, Journal of ELECTRONIC MATERIALS, <https://doi.org/10.1007/s11664-020-08053-6>
- [38]. Belkhir. Tioua, Thèse de doctorat, Université de Biskra, (2019).
- [39]. A. Béjaoui, K. Horchani-Naifer, S. Hraiech, M. Férid, Optical Materials 36 (2013) 310-315.
- [40]. M. Seshadri, M. J. V. Bell, V. Anjos, Y. Messaddeq. Journal of Rare Earths, 39.1 (2021) 33-42.
- [41]. K.Biswas, AD.Sontakke, J.Ghosh, K. Annapurna, J Am Ceram Soc 93(2010)1010.
- [42]. Q. J. Chen, W. J. Zhang, X. Y. Huang, G. P. Dong, M. Y. Peng, Q. Y. Zhang. Journal of alloys and compounds 513(2012) 139-144.
- [43]. L. J. Borrero-González, L. A. O. Nunes, J. L. Carmo, F. B. G. Astrath, M. L. Baesso, Journal of Luminescence 145 (2014) 615-619.
- [44]. G. Lakshminarayana, S. O. Baki, A. Lira, I. V. Kityk, U. Caldiño, Kawa M. Kaky and M. A. Mahdi, Journal of Luminescence, [http://dx. doi. org/10.1016/j.jlumin.2017.02.049](http://dx.doi.org/10.1016/j.jlumin.2017.02.049).
- [45]. X.J. Wang, H.R. Zheng, D. Jia, S.H. Huang, R.S. Meltzer, M.J. Dejneka, W.M. Yen, Microelectron. J. 34 (2003) 549–551.
- [46]. V. A. Prathyusha, D.. Rasayan J. Chem., 10.3 (2017) 881-890.
- [47]. Q. Chen, W. Zhang, X. Huang, G. Dong, M. Peng, and Q. Zhang, J. Alloy. Compd., 513(2012)139–44.
- [48]. E. Fred Schubert, Light-Emitting Diodes, second ed. Cambridge University Press,New York, 2006.

**Chapter IV- Spectroscopic study of the Pr³⁺doped and Pr³⁺/Yb³⁺ co-doped
Sb₂O₃-WO₃-NaPO₃ glasses.**

[49]. C. Joshi, S. B. Rai. Solid state sciences, 14.8 (2012)997-1003.

CONCLUSION

Conclusion

The thesis presented was devoted to the elaboration and characterization of antimony oxide-based glasses (SNW) doped with Pr_6O_{11} and co-doped with $\text{Pr}^{+3}/\text{Yb}^{+3}$ for applications in the laser or optical amplification.

Glasses: SNW, SN_xW 0.1 Pr, SNW_xPr , $\text{SNW}0.1\text{Pr}_x\text{Yb}$ mol%. have been prepared using a melt quenching process to investigate their structure and their various properties such as: thermal, mechanical, physical, optical, luminescence properties as well as the radiative study carried out by the theory of Judd ofelt. The FTIR and Raman spectral profiles reveal the existence of SbO_3 , PO_3^{-2} , WO_4 and WO_6 groups with P-O-W, Sb-O-P, P-O-P and W-O-W vibrations.

These glasses have showed interesting characteristics with good transmission and high values of density, refractive index, thermal stability. Furthermore, the Hardness and elastic moduli of these glasses increases with the addition of tungsten, Pr^{+3} , $\text{Pr}^{+3}/\text{Yb}^{+3}$.

Using visible and near-infrared absorption spectra, the Judd-Ofelt analysis was applied to the absorption bands of Pr^{+3} to calculate the three Judd-Ofelt parameters. According to values obtained from Ω_2 , Ω_4 and Ω_6 certain radiative properties have been determined such as predicted radiative transition probabilities (A_{rad}), branching ratios (β) and the radiative life (τ_{rad}) and the integrated cross sections (Σ). Absorption, emission cross-section characteristics of 1474 nm band. Laser parameters (bandwidth gain and optical gain).The experimental lifetime and the quantum efficiency for the transition from $^3\text{P}_0 \rightarrow ^3\text{H}_6$ and CIE chromaticity coordinates.

$\text{SNW}0.05$ Pr glass has the highest values for the radiative transition probability A_{rad} (4188, 2761 and 2253.8 s^{-1}), the emission cross-section σ_e (0.303 , 0.297 and $2,079 \times 10^{-21} \text{ cm}^2$), the gain of the bandwidth $\sigma_{\text{em}}^{\text{F-L}} \times \Delta\lambda_{\text{eff}}$ (5.045 , 7.416 and $7.935 \times 10^{-28} \text{ cm}^3$) and optical gain $\sigma_{\text{em}}^{\text{F-L}} \times \tau_{\text{rad}}$ (0.954 , 20.166 and $141.188 \times 10^{-23} \text{ cm}^2 \text{ s}$) corresponding to the transitions $^3\text{P}_2 \rightarrow ^3\text{H}_5$ (blue emission at 491 nm), $^3\text{P}_0 \rightarrow ^3\text{H}_6$ (intense orange emission at 600 nm), $^3\text{P}_0 \rightarrow ^3\text{F}_2$ (red emission at 642 nm), For co-doped glass, we found the same observation for the sample $\text{SNW}0.1\text{PrYb}0.25$ the highest values for the radiative transition probability (A_{rad}) corresponding to the transitions $^3\text{P}_0 \rightarrow ^3\text{H}_6$, $^3\text{P}_0 \rightarrow ^3\text{F}_2$ with $^3\text{P}_0 \rightarrow ^3\text{H}_4$ and $^3\text{P}_1 \rightarrow ^3\text{H}_5$.

We note that we obtained a significant increase in the intensity of the emissions in all peaks after the addition of Yb_2O_3 , while the emissions of 1474 nm. This is because of the energy transfers between Yb^{+3} and Pr^{+3} .

The study of the near-infrared luminescence of doped and codoped glasses under excitation at 444 nm, shows the broadband emission in the 1300-1700 nm region corresponding to the transition at $^1\text{D}_2 \rightarrow ^1\text{G}_4$, which covers the whole O, E, S, C, l and the U band which is very important for optical fibres. Noting that the strongest luminescence band is $^3\text{P}_0 \rightarrow ^3\text{H}_6$ transition for SNW0.05Pr then SNW0.1Pr1Yb glasses.

We got high quantum efficiency (η) of level $^3\text{P}_0 \rightarrow ^3\text{H}_6$ in doped and co-doped glasses.

The CIE color coordinates under the 444 nm excitation at 600 nm ($^3\text{P}_0 \rightarrow ^3\text{H}_6$) for SNW_xPr glasses were evaluated and found to be in the red-orange region and for SNW0.1Pr_xYb and in the yellow-orange region near to white light.

These results show that the glasses studied doped with Pr^{+3} are a good candidate promising in the development of an orange light source, which contains attractive potential applications in optical amplifiers band and lasers.

Abstract

New glasses based on Sb_2O_3 are elaborated and characterized, the systems studied as follows $60Sb_2O_3-(40-x) NaPO_3-xWO_3$ (where $x = 0$ to 25), $60 Sb_2O_3 (40-x) NaPO_3 x WO_3 0.1 Pr_2O_3$ ($x=0,5,10,15,20,25$), $47.5 Sb_2O_3 47.5 NaPO_3 5 WO_3- x Pr_6O_{11}$ ($x= 0.05, 0.1, 0.25, 0.3$), $47.5 Sb_2O_3 47.5 NaPO_3 5 WO_3 0.1 Pr_6O_{11} xYb_2O_3$, ($x= 0.25, 0.5,0.75,1$) mol%. The results of different physical properties from Raman, FTIR, DSC, UV-V, density, hardness, elastic moduli and refractive index confirm that these glasses studied prove to be potential candidates for optical devices. Also, the results of Judd-Ofelt parameters, the radiative properties, experimental lifetime and CIE chromaticity diagram by applying the theories of Judd-Ofelt, Mc-Cumber and the Fuchtbauer-Ladenburg method and from absorption and emission spectra confirm that these glasses can be used as materials for optical amplification as well as for orange, red and blue emission applications.

Keywords: antimony oxide glasses, Pr_6O_{11} , Judd-Ofelt theory, emission, amplification,

ملخص:

تم اعداد وتوصيف زجاج جديد يعتمد على أكسيد الأنتيمون (Sb_2O_3)، الأنظمة المدروسة على النحو التالي $60Sb_2O_3-(40-x) NaPO_3-xWO_3$ (where $x=0,5,10,15,20,25$), $60 Sb_2O_3 (40-x) NaPO_3 x WO_3 0.1 Pr_2O_3$ ($x=0,5,10,15,20,25$), $47.5 Sb_2O_3 47.5 NaPO_3 5 WO_3- x Pr_6O_{11}$ ($x= 0.05, 0.1, 0.25, 0.3$), $47.5 Sb_2O_3 47.5 NaPO_3 5 WO_3 0.1 Pr_6O_{11} xYb_2O_3$, ($x= 0.25, 0.5,0.75,1$) mol.%

نتائج الخصائص الفيزيائية المختلفة ل FTIR, DSC , UV-V , Raman , الكثافة , الصلابة , معاملات المرونة , معامل الانكسار أكد أن الزجاج التي تمت دراسته يثبت أنه مرشح محتمل للأجهزة البصرية. أيضًا ، تؤكد نتائج معاملات جود-أوفيلت ، والخصائص الإشعاعية ، وفترات الحياة التجريبية ، ومخطط اللونية CIE من خلال تطبيق نظريات Judd Ofelt ، وطريقة MC-Cumber ومن أطيف الامتصاص والانبعاث أنه يمكن استخدام هذه الزجاجات مواد للتضخيم البصري وكذلك لتطبيقات الانبعاث البرتقالي والأحمر والأزرق.

الكلمات المفتاحية: زجاج أكسيد الأنتيمون، البراسيديوم، نظرية جود-أوفلت، الانبعاث، التضخيم.

Résumé :

De nouveaux verres à base de Sb_2O_3 sont élaborés et caractérisés, les systèmes étudiés sont les suivants $60 Sb_2O_3 (40-x) NaPO_3 x WO_3$, $60 Sb_2O_3 (40-x) NaPO_3 x WO_3 0.1 Pr_2O_3$ ($x=0,5,10,15,20,25$), $47.5 Sb_2O_3 47.5 NaPO_3 5 WO_3- x Pr_6O_{11}$ ($x= 0.05, 0.1, 0.25, 0.3$), $47.5 Sb_2O_3 47.5 NaPO_3 5 WO_3 0.1 Pr_6O_{11} xYb_2O_3$, ($x= 0.25, 0.5,0.75,1$) moles % . Les résultats de différentes propriétés physiques de Raman, FTIR, DSC, UV-V, densité, la dureté, modules d'élasticité et l'indice de réfraction confirment que ces verres étudiés s'avèrent être des candidats potentiels pour des dispositifs optiques. Aussi les résultats des paramètres de judd-ofelt, les propriétés radiatives, la durée de vie expérimentale et le diagramme de chromaticité CIE en appliquant les théories de judd-Ofelt, Mc-Cumber et la méthode de Fuchtbauer-Ladenburg et à partir des spectres d'absorption et d'émission confirment que ces verres peuvent être utilisés comme matériaux pour l'amplification optique ainsi que pour les application d'émission orange, rouge et bleue.

MOTS-CLES : Oxyde d'antimoine, Verres, Pr_6O_{11} , la théorie de judd-Ofelt, émission, amplification.